PERFORMANCE OF COOPERATIVE RELAYING SYSTEMS WITH CO-CHANNEL INTERFERENCE

A Thesis
Presented to
The Academic Faculty

by

Hyungseok Yu

In Partial Fulfillment
of the Requirements for the Degree
Doctor of Philosophy in the
School of Electrical and Computer Engineering

Georgia Institute of Technology
December 2012

PERFORMANCE OF COOPERATIVE RELAYING SYSTEMS WITH CO-CHANNEL INTERFERENCE

Approved by:

Professor Gordon L. Stüber, Adviser
School of Electrical and Computer Engineering
Georgia Institute of Technology

Professor John R. Barry
School of Electrical and Computer Engineering
Georgia Institute of Technology

Professor Ye Geoffrey Li
School of Electrical and Computer Engineering
Georgia Institute of Technology

Professor John Papapolymerou
School of Electrical and Computer Engineering
Georgia Institute of Technology

Professor Sung Ha Kang
School of Mathematics
Georgia Institute of Technology

Date Approved: 2 July 2012

To Misun, Sarah, Kate, and Ayden Yu.

ACKNOWLEDGEMENTS

The 5 years spent in Georgia Tech would be the most precious and valuable time in my life. This dissertation is the result of not only my research but also my living for these years. Numerous people have helped and supported me to complete this dissertation. A few words cannot adequately represent all my appreciation for them.

First and foremost, I would like to thank my advisor, Prof. Gordon L. Stüber. I am sincerely grateful and cannot forget his support, inspiration, and insight. He guided and waited for me in difficult times, and encouraged me to reach the goal. It was my good fortune that he allowed me to be his student.

I appreciate the dissertation committee members, Prof. John Barry, Prof. Ye (Geoffrey) Li, Prof. John Papapolymerou, and Prof. Sung Ha Kang for their efforts and time spent on my dissertation. I will remember my lab-mates at the Wiress System Lab at Georgia Tech, Dr. Sami Almalfouh, Seok-Chul Kwon, and Sajid Saleem for the wonderful times we shared together, and thanks go to Dr. In-Ho Lee for intense technical discussions. The financial support of the Samsung Electronics is also gratefully acknowledged.

Finally, this dissertation is dedicated to my wife, Misun Kim, for her love, support, and sacrifice. My children, Sarah, Kate, and Ayden are all I am, and their smile is one reason for all. I am always indebted to my parent and parent-in-law.

TABLE OF CONTENTS

LIST OF FIGURES

SUMMARY

The objectives of this dissertation are to analyze the performance of cooperative decode-and-forward (DF) relaying systems in the presence of multiple interferers and to improve the network throughput for these systems. Since cooperative relaying can gain benefits of spatial diversity and overcome the hardware constraints of existing wireless systems, it is a focus of considerable research. However, from a practical point of view, there are still many unresolved problems of resource allocation in cooperative relaying systems. To get a practical approach for the cooperative relaying system, in this dissertation, we propose and summarize various DF schemes in the view of network topology (multi-branch dual-hop relaying and multi-branch multi-hop relaying), transmission structure (outage-based symbol relaying, outage-based packet relaying, and cyclic-redundancy-check (CRC)-based packet relaying), slot allocation (fixed-slot selection DF, repeated-slot selection DF, and variable-slot selection DF), and network environments (ad-hoc and cellular networks).

We first analyze the outage probability of multi-branch dual-hop DF cooperative relaying systems over Nakagami/Nakagami fading channels, and present an exact closed-form expression for the outage probability with maximum ratio combining considering (MRC) both the effect of co-channel interference and white Gaussian noise. The effect of imbalanced powers of interference received at the relay and the destination is also analyzed to investigate whether the relay or destination is more sensitive to interference. Second, we generalize DF cooperative diversity to multi-branch multi-hop (MBMH) relaying systems over shadowed-Nakagami/shadowed-Nakagami fading channels, and derive closed-form expressions for the outage probability and the average symbol-error-probability of the MBMH DF relaying systems. Against

shadowing as well as fading, the effect of the numbers of both branches and hops is considered over the proposed systems. Next, the cooperative relaying system can be extended from ad-hoc to cellular networks. We compare the outage performances of the fixed-gain amplify-and-forward and DF cooperative relaying systems with selective combining over entire cell area. Fourth, we investigate the performance benefits and tradeoffs between outage probability and spectral efficiency for the DF cellular relaying systems with MRC. The optimal-relay location and the effective region are evaluated for omnidirectional and sectorized cells in both the uplink and the downlink with respect to co-channel reuse factor. Fifth, we propose the DF cooperative systems with packet transmission: outage-based packet relaying and CRC-based packet relaying. In the cellular networks, we evaluate average packet-error-probability for various proposed schemes with respect to co-channel reuse factor in both the uplink and the downlink. Finally, we propose a variable-slot selection DF scheme which uses dynamic slot allocation operating on CRC-based packet relaying.

Our research on the performance analysis and throughput improvement of the generalized DF cooperative relaying systems for both ad-hoc and cellular networks can provide other researchers with practical approach to develop future cooperative relaying systems.

CHAPTER I

INTRODUCTION

Cooperative diversity is an efficient protocol for combating multipath fading in wireless networks. While cooperative diversity increases capacity gain and communication reliability, it can also overcome the physical constraint of putting multiple antennas in a small handset. The basic concept of cooperative diversity is the same as that of spatial diversity, namely, the use of multiple transmit (Tx) or receive (Rx) antennas. However, instead of multiple antennas in a handset, cooperative diversity extends channels to whole systems by regarding relays as antennas; thus a handset with a single antenna can take advantage of spatial diversity.

According to the signal-processing methods used in the relay, cooperative diversity can be classified into two basic schemes: Decode-and-forward (DF) and amplify-and-forward (AF) schemes [1]. Since the AF relay does not require front-end processing, demodulation, and decoding, the AF scheme was considered to be more practical than the DF scheme, which requires front-end processing. However, at present, the DF scheme is nevertheless attractive because the signal-decoding process can be performed by existing digital-signal processing blocks, while in the AF scheme expensive analog components and/or new hardware structures are required to either amplify the analog signals or to retransmit sampled signals.

1.1 Motivation

In the physical layer, cooperative diversity was generally studied with respect to the number, placement, and power allocation of relays, mostly under conditions of additive white Gaussian noise (AWGN). However, co-channel interference (CCI) often dominates AWGN and degrades the performance of wireless systems [2], and since

relaying systems are generally used to increase the coverage under dense-frequency reuse, they are typically exposed to CCI. Moreover, in some cooperative relaying systems such as wireless sensor networks, the interferers transmit signals with a power level similar to the source, and the signal-to-interference-plus-noise ratio (SINR) may not be so large. In such low SINR regime, the performance analysis in terms of signal-to-interference ratio (SIR) and the asymptotic analysis based on high signal-to-noise ratio (SNR) are not accurate[4, 5]. Nevertheless, prior studies on the performance analysis of cooperative relaying systems have examined the effect of CCI in terms of SIR, while neglecting the effect of AWGN [3], and there has been no research considering the effect of both CCI and AWGN.

Besides the spatial diversity provided by multiple branches in cooperative-diversity systems, a multi-hop transmission using multiple relays also provides an efficient way to combat shadowing and path loss, and it improves the power efficiency of wireless communication systems [6, 7, 8]. As a general relay-topology, multi-branch multi-hop (MBMH) cooperative relaying systems can employ low-complexity relays, and only the destination combines the signals from the last-hop relays in multiple branches. In addition, the combination of cooperative diversity and multi-hop transmission can mitigate not only multipath fading but also shadowing and path loss. Even though cooperative relaying networks are known to mitigate the impact of shadowing, most studies focus on only multipath fading. However, in realistic environments both small-scale fading and large-scale fading should be taken into account together, but a performance analysis on the cooperative relaying networks over composite shadowing and fading channels is limited so far.

In cellular networks, frequency reuse is essential, but CCI caused by frequency reuse is the largest performance limiting factor. Therefore, evaluating system performance with respect to CCI has a high importance in the research area of traditional cellular networks. While an increase in the frequency reuse distance will mitigate

CCI, it will also degrade system efficiency. Without an increase in the frequency reuse distance, the cooperative diversity gain can provide an efficient way to alleviate the effect of CCI as well as multipath fading. In this dissertation, the effect of CCI for the cooperative diversity can be applied to cellular network environments, then, the relation between the cooperative diversity and the co-channel reuse factor can be provided.

Extensive studies have analyzed the performance of selection DF relaying systems, but most research assumed symbol-by-symbol decoding. For practical purposes, symbol-by-symbol decoding is not feasible when considering signaling overhead, since the message should be transmitted through multiple packets in packet-based wireless communication systems. In addition, SNR estimation was originally used to make relaying decisions in selection DF relay networks, which is referred as the outage-based relaying. However, a cyclic-redundancy-check (CRC) based relaying employed in [57] can reduce the system complexity and fully exploit the benefit of DF relaying for per-packet error detection in practical cooperative transmission. Therefore, an important metric for evaluating the performance of DF relaying is the average packet-error-probability (APEP) rather than the average symbol-error-probability (ASEP).

The spatial diversity of cooperative relaying by using orthogonal relay transmission requires the cost of decreased spectral efficiency. To alleviate this limitation, the best relay selection scheme, which includes opportunistic relaying, and the distributed space-time-coding (DSTC) scheme were studied in [5, 19, 20, 65, 66, 67, 68]. However, the best relay selection scheme requires global/local channel state information (CSI) for all channels, so that it imposes excessive amount of feedback data as the number of relays is increased [68]. In addition, DSTC design is quire difficult in practice because of distributed and ad-hoc nature of cooperative networks, and the need and availability of global CSI as well [20]. On the other hand, since synchronization across

multiple relay channels is not critical in orthogonal transmission due to the orthogonality between the slots, cooperative relaying with orthogonal transmission does not require additional interference canceling techniques to avoid inter-relay interference. Therefore, cooperative relaying with orthogonal transmission is still attractive for networks composed of numerous, small, low-powered relays such as wireless sensor networks.

1.2 Contributions

The key contributions of this dissertation are

- A closed-form expression for the outage probability of multi-branch dual-hop (MBDH) DF cooperative relaying system with MRC is derived in the presence of CCI and AWGN for non-identical Nakagami/Nakagami fading channels. The outage performance is analyzed for three different environments and the effect of imbalanced powers of CCI received at the relay and the destination is also analyzed with various Nakagami-m factors and different numbers of relays.

- Closed-form expressions are derived for the outage probability, the ASEP, and the probability density function (pdf) of SINR of the MBMH DF cooperative relaying system for non-identical shadowed Nakagami-m channels in the presence of an arbitrary number of non-identical co-channel interferers. The effect of the number of branches and hops is analyzed for a fixed number of relays by considering the effect of shadowing.

- The outage probability is compared to a dual-receive (Rx) antenna system with cooperative relaying systems using fixed-gain AF and selection DF with selective combining (SC) in cellular networks. The effective region where the cooperative relaying systems outperform a dual-Rx antenna system is depicted in the cell area.

- Closed-form expressions for the outage probability and the spectral efficiency of a selection DF relaying system are obtained for non-identical shadowed Nakagami/shadowed Nakagami channels. The performances are evaluated as a function of a co-channel reuse factor and compared to dual-Rx antenna systems for omnidirectional and sectorized cells in both the uplink and the downlink of cellular networks. The effective regions with regard to the spectral efficiency and the outage probability of the proposed system compared the dual-Rx antenna system are also depicted in the cell area.

- The outage probability, the end-to-end ASEP, and the end-to-end APEP are derived for the selection DF cooperative diversity system using MRC in non-identical Nakagami/Nakagami channels. The performances are evaluated as a function of a co-channel reuse factor and relay position for outage-based symbol relaying, outage-based packet relaying, and CRC-based packet relaying in both the uplink and the downlink of cellular networks. The effect of forward error-correction coding (FEC) on the selection DF relaying schemes is also analyzed.

- A variable-slot selection DF (VSDF) scheme is proposed and compared to fixed-slot selection DF (FSDF) and repeated-slot selection DF (RSDF). Closed-form expressions for the outage probability and throughput of the proposed systems are presented for non-identical Nakagami/Nakagami channels.

1.3 Thesis Outline

This dissertation is organized as follows. Chapter 2 provides a background review, including a brief information of the channels, diversity techniques, combining techniques, and cooperative diversity. We also provide a literature review on the topics discussed in this dissertation. Chapter 3 analyzes the outage probability of MBDH DF cooperative relaying systems over non-identical Nakagami/Nakagami fading channels. Chapter 4 studies general MBMH DF cooperative diversity systems over non-identical

shadowed Nakagami-m fading channels in the presence of an arbitrary number of non-identical co-channel interferers. Chapter 5 provides the outage probability for fixed-gain AF and selection DF cooperative diversity systems with SC, for the case of a log-normal Nakagami faded desired signal and log-normal Rayleigh faded co-channel interferers. Chapter 6 investigates user cooperation diversity systems with DF selection relaying over non-identical shadowed Nakagami/shadowed Nakagami channels in cellular networks. Chapter 7 analyze the outage probability and APEP as a function of a co-channel reuse factor and relay position for outage-based symbol relaying, outage-based packet relaying, and CRC-based packet relaying in both the uplink and the downlink. In Chapter 8, we proposes a VSDF scheme which uses dynamic slot allocation operating on CRC-based packet relaying. Finally, Chapter 9 summarizes the research contributions and concludes with future research.

CHAPTER II

BACKGROUND

2.1 Shadowed Nakagami-m Fading Channels

In realistic wireless channels, the radio signal strength is degraded by three components: Multipath fading, shadowing, and path loss. The channels, where the three components occurs simultaneously, are referred to as the shadowed-fading channels.

In the shadowed-fading channels, first, multipath fading is one of the significant impairments in wireless communication systems, and it results from destructive addition of different replicas of a Tx signal. When the source signal is transmitted, it is reflected from local scatterers and has different paths, so the replicas experience different attenuation, delay, distortion, and phase shift. The combined effect of different replicas can occur either constructive or destructive addition of the signal power. When the received signal experiences the destructive addition, the received signal power can be significantly decreased, and this phenomenon is known as fade. Throughout the dissertation, the multipath fading model has a Nakagami-m distribution, because the Nakagami fading model can closely approximate both Rayleigh and Rician fading models, and the fading conditions can be adjusted more or less severe than the Rayleigh fading model.

Second, shadowing is the variation of the received signal power, which can be observed over sufficiently long distances. The averaged value of the received signal power over a spatial distance of 20 to 30 wavelengths is referred to as local mean power, the value of which slowly varies because of large obstacles [2]. Shadowing is generally modeled by using a log-normal distribution.

Finally, the received signal power at a certain point depends on the carrier frequency, the antenna type, antenna heights, and the distance between the transmitter and the receiver. Among these factors, path loss is the decrement of area mean power according to the distance between the transmitter and the receiver. The area mean power can be obtained by averaging the local mean of the receive signal power over relatively long distances, and it decreases with the exponent of the distance.

In the shadowed-fading channel, the channel gain g can be written as $g = f\sqrt{c \cdot s \cdot d^{-\alpha}}$, where c is a constant, d is the distance between the transmitter and the receiver, α is the propagation path-loss exponent, s is the shadow-fading factor that has the log-normal distribution, and the envelope f has the Nakagami distribution; thus, the squared envelope has a Gamma distribution. Thus, the composite distribution of the squared envelope of the received signal has the log-normal Gamma distribution function

$$p_X(x) = \int_0^\infty \left(\frac{m_X}{\omega_X}\right)^{m_X} \frac{x^{m_X-1}}{\sqrt{2\pi}\sigma_X\omega_X\Gamma(m_X)} \exp\left\{-\frac{m_X x}{\omega_X} - \frac{(\ln\omega_X - \ln\Omega_X)^2}{2\sigma_X^2}\right\} \mathrm{d}\omega_\mathrm{X} \ , \tag{1}$$

where m_X is the Nakagami shape factor, w_X is the local mean, σ_X is the shadow standard deviation, and Ω_X is the area mean of X. The log-normal Gamma distribution has no closed-form solution, but it can be closely approximated by applying Hermite-Gauss quadrature integration [16]

$$p_X(x) = \sum_{i=1}^{N_p} \frac{1}{\sqrt{\pi}} H_{x_i} \left[\left(\frac{m_X}{\Phi(x_i)}\right)^{m_X} \frac{x^{m_X-1}}{\Gamma(m_X)} \exp\left(-\frac{m_X}{\Phi(x_i)}x\right) \right] \ , \tag{2}$$

where H_{x_i} is weight factors, x_i is the zeros, N_p is the order of the Hermite polynomial, and $\Phi(x_i) =: \exp(\sqrt{2}\sigma_X x_i + \ln\Omega_X)$. The moment-generating functions (MGF) of $p_X(x)$ can be obtained from (2) as

$$\mathcal{M}_X(s) = \sum_{i=1}^{N_p} \frac{1}{\sqrt{\pi}} H_{x_i} \left\{1 - \alpha_X(x_i)s\right\}^{-m_X} \ , \tag{3}$$

where $\alpha_X(x_i) =: \Phi(x_i)/m_X$.

2.2 Diversity Techniques

The main idea of diversity techniques is to transmit independent replicas of a Tx signal to a receiver so that the probability that all the replicas are in deep fade simultaneously is reduced. To combine the replicas, the received signals of the different paths should be resolved, which decides the performance of diversity. Thus, the performance of diversity can be evaluated by measuring how many independent replicas are available, and it is defined as diversity order D, which is BER $\propto$ (SNR)$^{-\mathrm{D}}$. Therefore, bit-error ratio (BER) is exponentially decayed if the diversity order D, which is the number of independent replicas, is increased at a given SNR.

This section provides a brief discussion on the diversity techniques, which are commonly employed in wireless communication systems: Frequency diversity, time diversity, and spatial diversity. First, frequency diversity uses different frequency channels to transmit different faded replicas. Since each replica should have uncorrelated fading, the frequency channels should be separated by at least the coherence bandwidth of the channel. Thus, frequency diversity can be an efficient way to combat frequency-selective fading, and the system with frequency diversity transmits the same signal simultaneously in multiple channels without any loss of transmission rate. However, since frequency diversity requires additional bandwidth, it is not an efficient solution for bandwidth-constrained networks.

Second, time diversity achieves diversity order by transmitting the same signal in multiple time intervals. In the aspect of repeating redundant information, error-correction coding can be regarded as a kind of time diversity technique. To have uncorrelated fading statistics, the intervals between transmissions of the same signal should be separated by at least the coherence time of the channel. Time diversity can be an efficient way to combat time-selective fading, and additional bandwidth is not required. However, instead of loss of bandwidth, time diversity can be achieved at the cost of transmission rate since redundant data should be repeated.

Finally, as opposed to the above two diversity techniques, spatial diversity does not require any additional bandwidth or reduced transmission rate. The key of spatial diversity is to transmit the same signals by using multi-Tx antennas and / or to receive the replicas of the same signal by using multi-Rx antennas. Distance between multiple antennas should be chosen in order that multipath fading appearing in the diversity branches becomes uncorrelated; thus, the distance should be at least half of the wavelength. Since spatial diversity can be implemented simply and economically, it has been widely used in wireless systems. However, spatial diversity is limited by the physical constraint of putting multiple antennas in small handset. For such reasons, in cellular networks, the base station (BS) generally employs multiple antennas while the mobile station (MS) has only one or two antennas.

2.3 Diversity-Combining Techniques

Diversity combining is a technique that combines multiple, independent replicas of a Tx signal to one enhanced signal. Among the three components of the channel, which are mentioned earlier, path loss and shadowing can be approximated as constant and dealt with power control for long period. Thus, multipath fading is the target of diversity combining, and diversity combining improves the reliability of the received signal by minimizing the channel power fluctuations. Generally, there are three common techniques in diversity combining: SC, equal-gain combining (EGC), and MRC. These diversity-combining techniques are classified according to how to decide weights of diversity branches.

As shown in Fig. 1, in the SC scheme, the selective combiner chooses the diversity branch with the largest instantaneous SNR. Since the selective combiner compares only signal powers, it does not require continuous monitoring of CSI; thus, it has low complexity. For this reason, SC is often suggested for macro-diversity systems in cellular networks. However, SC gives the worst performance among the three

diversity-combining techniques, because it ignores the information of other branches.

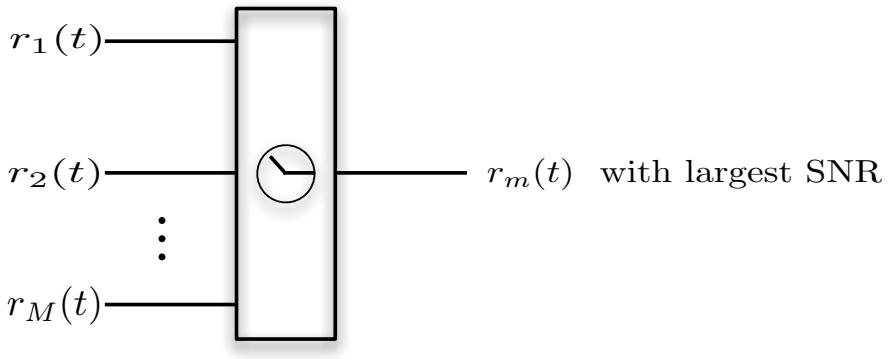

Figure 1: Illustration of selective combining.

MRC provides the optimal performance in terms of maximizing output SNR. In Fig. 2, since all the diversity branches are co-phased ($e^{j\theta_M}$) and summed with the optimal weights (α_M) that are proportional to the respective signal amplitudes, strong signals are more amplified, whereas weak signals are attenuated. Thus, signals with larger received power have larger influence on the output signal.

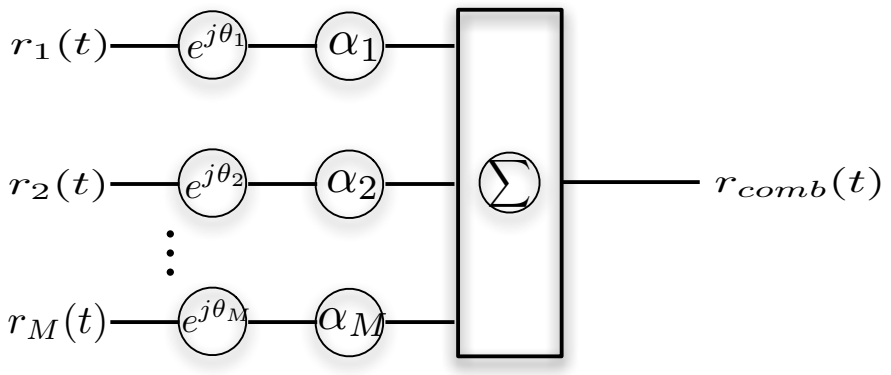

Figure 2: Illustration of maximal-ratio combining.

However, the MRC combiner requires accurate signal amplitude and phase information to find the optimal-weight values with the fading signals. To estimate the channels, the complexity of the MRC system increases. Compared to MRC, EGC

can be simply implemented, but the performance of EGC is comparable to that of MRC, because the weight of EGC is a unit gain and adjusted for every received signal to be co-phased as shown in Fig. 3; thus, EGC gives weights for respective diversity branches similarly to MRC, but the branches are not weighted. Since EGC gives the same weight to both the signals with weak received power and strong received power, the signal with weak received power may attenuate the information of the signal with strong received power.

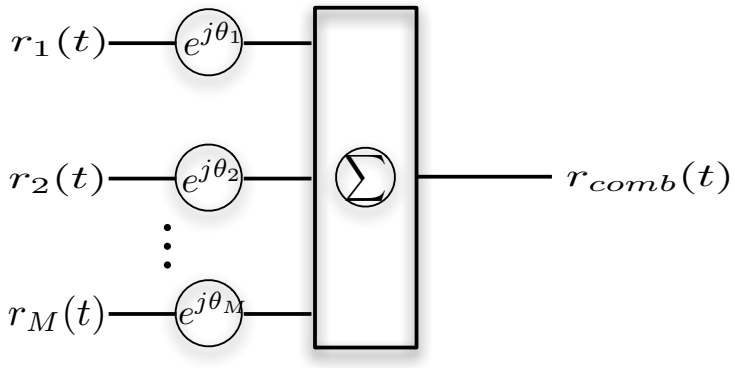

Figure 3: Illustration of equal-gain combining.

The three diversity techniques mentioned above basically target to maximize SNR without interference, but in the presence of interference, optimum combining (OC) can attain the maximum SINR. However, since OC requires the inverse of a square matrix whose dimension is equal to the number of branches, it is not usually employed in practical systems for more than two branches because of excessive complexity.

2.4 Cooperative Diversity

Although the spatial diversity schemes are obviously beneficial on wireless networks in that they do not require any additional bandwidth or reduced transmission rate, most of them may not be practical because of their hardware constraints such as size, cost, and complexity. To overcome these limitations by allowing mobiles with a single antenna to gain the benefits of spatial diversity, cooperative diversity employs virtual

multi-Tx/Rx antennas by extending the channels to the entire systems by regarding relays as antennas. The first research on spatial diversity using the virtual, multiple antennas was introduced as the relay channel in [17, 18]. However, this information-theoretical research has two impractical constraints [9]. First, the terminals should be able to receive and transmit simultaneously on the same channel. Second, all the signals that are simultaneously transmitted from the relays should be co-phased. Since these two constraints was removed by using half-duplex mode and orthogonal transmission, cooperative diversity could be regarded as feasible. As described in Fig. 4, the cooperative relaying protocols have two phases.

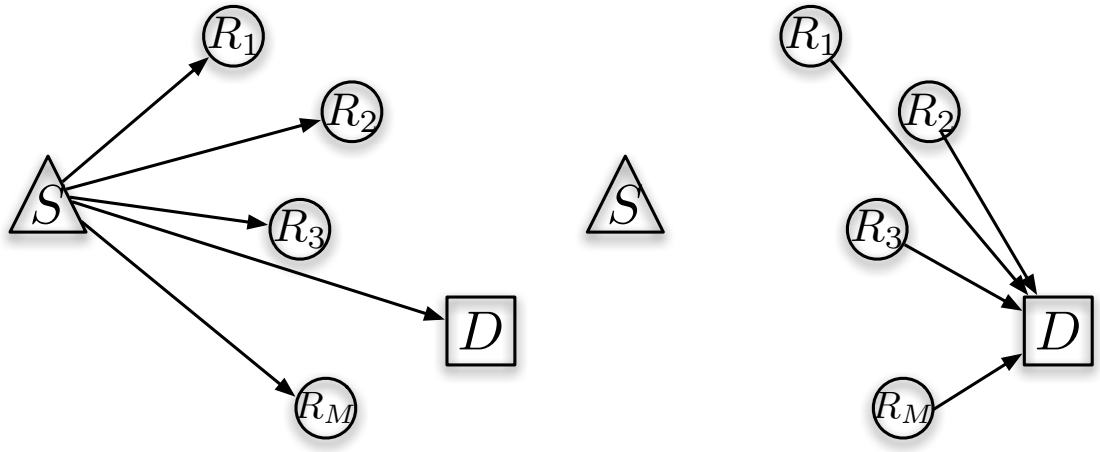

(a) Phase I (b) Phase II

Figure 4: Two phases of cooperative-diversity systems.

The first phase is the broadcasting step, where a source (S) transmits the original signals to relays (R) and a destination (D). During this phase, the relays manipulate the received signals. The second phase denotes the multi-access step, where the relays retransmit the manipulated signals to the destination. To combine all of the received signals in the destination, a variety of combining techniques can be employed.

According to how a relay manipulates the received signals, cooperative diversity is basically classified into two schemes: AF and DF. In addition, according to how the relayed signals are assigned to the channels, each scheme can use orthogonal or

non-orthogonal transmission.

2.4.1 Orthogonal and Non-Orthogonal Transmissions

In cooperative diversity, the destination should be able to separate the relayed signals with a single antenna. The simplest method to separate the relayed signals is to transmit the signals by using channel orthogonality, which is referred to as orthogonal transmission. In orthogonal transmission, to satisfy the half-duplex constraint, all terminals operate on a time-division duplexing (TDD) or frequency-division duplexing (FDD) mode, and time-division multiple access (TDMA) or frequency-division multiple access (FDMA) is used in the second phase of the cooperative relaying protocol, respectively. Thus, since the original signal from the source consumes one slot in the first phase of the cooperative relaying protocol, and the Tx signals of respective relays consume M-slots, assigning the signals to their corresponding orthogonal slots requires $(M + 1)$ phases in the case of M-relays. All the signals in the orthogonal slots are independent, so the destination can receive independent replicas of the source signal and perform diversity combining.

Orthogonal transmission is less efficient than non-orthogonal transmission in terms of spectral resources as the number of relays increases. To improve spectral efficiency, another approach based on space-time codes (STC) was proposed in [19]. In the approach, since the relays use a suitable STC in the second phase, which is called DSTC, the relayed signals can be transmitted simultaneously on the same channel. Thus, without additional bandwidth, non-orthogonal transmission using DSTC can achieve $(M+1)$ diversity order.

However, since non-orthogonal transmission allows for all relays to transmit on the same time or frequency slot, inter-relay interference can be introduced. The cancellation of inter-relay interference is essential for non-orthogonal transmission because of coherent reception between the multiple relays and the destination [9,

20]. Even though orthogonal transmission employs signal combining techniques that require coherent reception as well, it can avoid inter-relay interference as the result of orthogonality between the slots. Thus, in orthogonal transmission, the destination receiver can have a low complexity [1, 21, 70]. So as to isolate the effect of the inter-relay interference and to analyze the effect of CCI without any interference-cancellation technique, we focuse on orthogonal transmission.

2.4.2 Amplify-and-Forward Cooperative Diversity

AF cooperative diversity can be referred to as non-regenerative or analog relaying. The AF relays amplify the received signal and re-transmit to the destination. Since the AF relays do not require front-end processing, demodulation, and decoding, it has less complexity than DF relays. However, since the AF relays do not perform any decision operation on the received signal, noise along the transmission path can be accumulated and propagated.

According to how the relay obtains the amplifying gain, the AF relays can be classified into three subcategories: CSI-assisted relays, blind relays, and semi-blind relays. The CSI-assisted relays use the instantaneous CSI of the previous hop to obtain the amplifying gain. Since the gain can be obtained adaptively according to the previous channel state, the relays can transmit the signals with fixed power. The disadvantage of the CSI-assisted relays is heavy complexity in that the closed loop should be established between the source and the relays. Compared to the CSI-assisted relays, the blind relays do not require any information of the previous hop, and the gain is fixed. Therefore, the relays transmit the signals with variable power, which can make the saturation of the signal power. The semi-blind relays use the average of the CSI over a time period, so they do not need the instantaneous CSI. Even though the semi-blind relays has much lower complexity than the CSI-assisted relays, they show comparable performance to the CSI-assisted relays.

2.4.3 Decode-and-Forward Cooperative Diversity

DF cooperative diversity can be referred to as regenerative or digital relaying. During the first phase of cooperative relaying protocols, the DF relays can decode the received signal, re-encode it, and then retransmit it to the destination. The advantage of DF cooperative diversity is that the relays can impede error propagation, if the relay can successfully decode the source signal. According to whether error detection is employed or not, the DF relays can be categorized into two schemes: Fixed DF relays and selection DF relays. The fixed DF relays do not use the error detection, and retransmit the relayed signal although it has errors; thus, full diversity order cannot be achieved [1]. While the fixed DF relays always forwards the signals received at the relay to the destination, the selection DF relays only retransmit the successfully decoded signals. For error detection methods, the selection DF relays can check a CRC code of the source packets, or the signals can be regarded to be successfully decoded when the SNR of the source-to-relay link is above a specified threshold.

2.5 Literature Review on Cooperative Diversity

Prior studies on the performance analysis of cooperative relaying systems have focused on the effect of CCI in terms of SIR, while neglecting the effect of AWGN [3], and there has been no research considering the effect of both CCI and AWGN. However, the performance analysis in terms of SIR and the asymptotic analysis based on high SNR are not accurate in the low SINR regime [4, 5].

In single-hop multiple antenna systems, the outage probability performance of MRC with CCI has been evaluated in [23] for Nakagami/Nakagami fading channels with identically distributed interfering signals and identically distributed desired signals. The outage probabilities of MRC for Rician/Rayleigh and Nakagami/Rayleigh

fading channels were analyzed in [4, 24], where the interfering signals have non-identical local mean power, and the desired signals are assumed to be identically distributed. The case of Nakagami/Nakagami fading channels with non-identically distributed interfering signals was studied in [25], but the desired signals still have identically distributed Nakagami-m fading. In all single-hop multiple antenna systems, the desired signals were assumed to be identically distributed in [4, 23, 24, 25, 26], where the performance of MRC was analyzed in terms of SINR in [4, 23, 25] while AWGN was neglected in [24, 26].

Dual-hop relaying systems have a similar source-relay-destination path compared to the cooperative relaying systems in this work, but signal combining is not required since a source-to-destination path does not exist. Thus, the performance analysis of cooperative relaying systems can be more general than that of dual-hop relaying systems. The authors in [27, 28] presented an insight on CCI in dual-hop AF relaying systems over non-identical Rayleigh/Rayleigh fading channels. In dual-hop DF relaying systems, the outage probability was analyzed in [29] under the specific scenario in which the destination is corrupted by CCI while the relay is only perturbed by AWGN. A more general scenario was studied in [30], where all nodes are affected by CCI, and the all signals have Rayleigh fading with different local mean, but the effect of AWGN was not studied.

The dual-hop DF cooperative relaying system using MRC was analyzed for links affected by AWGN in [31], where all the desired signals experience Rayleigh fading with different local mean power. The analysis was extended to Nakagami-m fading channels that have non-identical local mean power and non-identical Nakagami-m factor in [27, 32], but they still do not consider CCI. With the consideration of CCI, the dual-hop DF cooperative relaying system using MRC was analyzed in [3], in the case of Nakagami/Nakagami fading where both the desired and interfering signals have a Nakagami-m distribution with different local mean power and m-factor.

However, the analysis neglected AWGN and the outage probability was expressed in terms of a hypergeometric function. Moreover, there was no comprehensive study of the effect of CCI on the outage performance in [3]. The performance analysis of DF cooperative relaying systems in the presence of both CCI and AWGN is very limited, and most expressions for the outage probability involve special functions or infinite series.

The MBMH cooperative relaying systems with the combination of cooperative diversity and multi-hop transmission can mitigate not only multipath fading but also shadowing and path loss. The end-to-end performance analysis of MBMH cooperative relaying systems was studied in [7, 11, 34, 35, 36], but most studies focused on the AF relay, and most prior work considers thermal noise-limited conditions without interference. A few studies have investigated CCI in dual-hop relaying systems [5, 29, 30, 37], but these systems are not generalized to the MBMH relaying scenario. Moreover, a performance analysis on the cooperative relaying networks is limited over the effect of both shadowing and fading so far. Renzo *et al.* presented a good framework for the performance analysis of the MBMH cooperative relaying system over composite log-normal Nakagami-m fading channels [34, 35], but they studied the AF scheme without CCI. Moreover, most existing literature evaluates the bit-error probability by taking upper bound [10, 38], using the Gaussian Q-function [8, 35], or an approximation of Gaussian Q-function [34]. A closed-form expression for ASEP of the MBMH cooperative relaying system has not been evaluated yet.

For the cellular networks, several statistical models have addressed the effect of CCI, for example, Nakagami/Nakagami, shadowed-Rayleigh/shadowed-Rayleigh, and shadowed-Rician/shadowed-Rayleigh fading channels in [39, 43, 44]. While an increase in the frequency reuse distance will mitigate CCI, it will also degrade system efficiency. Such tradeoff between frequency reuse distance and spectral efficiency was characterized by Alouini *et al.* in [45]. In [46], the outage probability as a function of

the co-channel reuse factor was derived on the downlink of cellular networks, but SC was studied over shadowed-Nakagami/shadowed-Rayleigh fading channels. In [3, 37], the outage probability for the DF cooperative-diversity system was obtained for non-identical Nakagami/Nakagami fading channels with MRC; however, this research did not consider cellular network environments.

Most studies assumed symbol-by-symbol decoding [1, 5, 20, 31, 32, 65, 68, 69, 70]. However, for practical purposes, symbol-by-symbol decoding is not feasible when considering signaling overhead. In [42], packet-based cooperative relaying system was investigated. In addition, SNR estimation was originally used to make relaying decisions in selection DF relaying networks. However, in [57], the CRC code approach was introduced and showed it can reduce the system complexity and fully exploit the benefit of DF relaying for per-packet error detection.

Throughput is affected by symbol rate, modulation alphabet size, packet length, the maximum number of retransmissions, and power level. Among the design parameters, to maximize throughput, power level and symbol rate in [69], retransmission by using automatic repeat request (ARQ) in [57], and the modulation alphabet size in [70] were considered in cooperative relaying networks. Throughput performance can be further improved by using dynamic slot allocation operating on CRC-based relaying. Dynamic slot allocation was proposed for efficient resource scheduling in the cellular systems [71, 72], but there are still many unresolved problems of resource scheduling in cooperative relaying systems with packet transmission.

CHAPTER III

COOPERATIVE DIVERSITY SYSTEMS WITH MULTI-BRANCH DUAL-HOP RELAYING

3.1 Overview

Cooperative diversity has generally been studied with respect to the number and placement of relays, and allocation of power, mostly under conditions of AWGN [1, 13, 27, 28, 31, 32]. However, CCI often dominates AWGN in wireless networks with dense frequency reuse. Moreover, cooperative diversity schemes can be vulnerable to CCI, because all relays may use the same carrier frequency and, hence, CCI may exist on every link in the cooperative relaying network.

Some studies on the performance analysis of cooperative relaying systems have focused on the effect of CCI in terms of SIR, while neglecting the effect of AWGN [3], and there has been no research considering the effect of both CCI and AWGN. However, the performance analysis in terms of SIR and the asymptotic analysis based on high SNR are not accurate in the low SINR regime [4, 5]. This issue can be critical in some cooperative relaying systems such as wireless sensor networks, where the interferers transmit signals with a power level similar to the source, and the SINR may not be so large. For these systems, a more general analysis is needed based on the SINR.

This chapter studies the outage probability of DF cooperative relaying systems using MRC in the presence of CCI and AWGN for non-identical Nakagami/Nakagami faded links, i.e., all links have different local mean power and Nakagami-m factor for both the desired and interfering signals. First, an exact and closed-from expression is derived for the outage probability. Second, the outage performance is analyzed

for three different environments: i) an interference dominant environment where the interference power dominates the noise power; ii) an equal interference and noise environment, i.e., the interference power is equal to the noise power; iii) a noise dominant environment where the noise power dominates the interference power. Finally, the effect of imbalanced powers of CCI received at the relay and the destination is analyzed with various Nakagami-m factors and different numbers of relays, to gain insight as to whether the relay or destination is more sensitive to CCI and, hence, more critical in the end-to-end outage performance.

Our results show that a DF cooperative relaying system is more vulnerable to noise than interference for low and moderate SINR, whereas it is more susceptible to interference than noise for high SINR and high-diversity order. Moreover, our results show that the robustness of the destination against CCI is more important than that of the relay. The results are verified by Monte Carlo simulations.

3.2 System and Channel Models

We investigate the MBDH cooperative relaying network shown in Fig. 5. The system consists of a source $\mathbf{S}$, a destination $\mathbf{D}$, and multiple relays $\mathbf{R}_m,\ m = 1, 2, \cdots, M$ where M denotes the maximum number of relays. All the relays and the destination are affected by co-channel interferers $\mathbf{I}_l,\ l = 1, 2, \cdots, L$ where L is the number of interferers.

In this chapter, all the relays use the selection DF scheme, which was proposed by Laneman *et al.* [1]. The selection DF relays only retransmit the successfully decoded packets. If the relays fail to decode the source packet, the relays do not transmit in their corresponding slots. Also, since the relays themselves decide whether or not each packet is forwarded, a feedback channel between the relays and the source is not necessary. The source, the relays, and the destination have a single-Tx/Rx antenna, and use orthogonal transmission through a TDD mode.

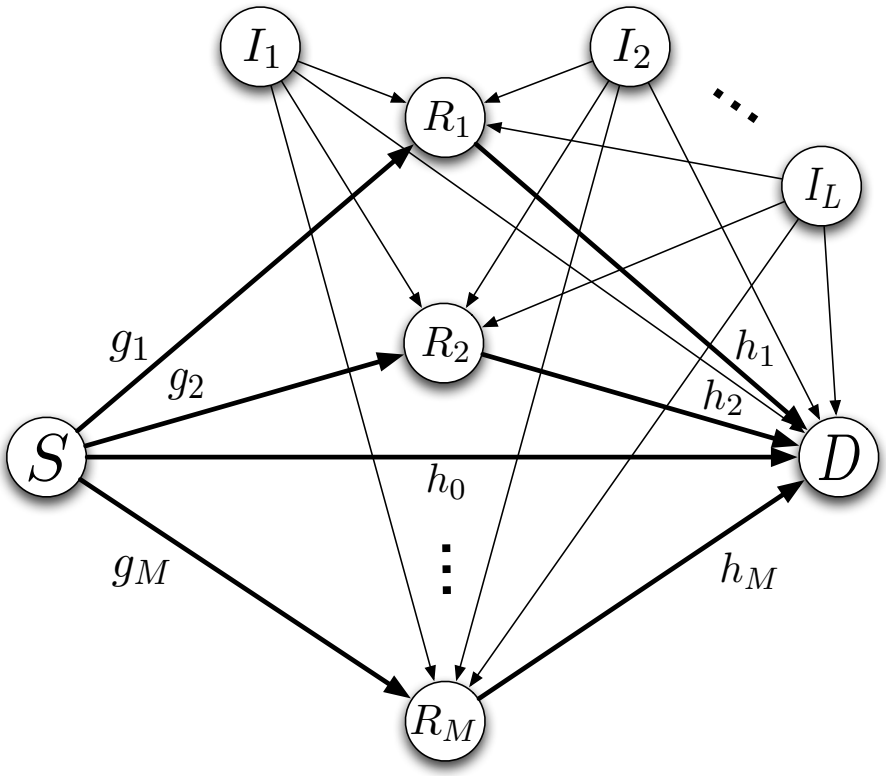

Figure 5: DF MBDH cooperative relaying network.

In cooperative relaying networks, the nodes, including the interferers, are assumed to have sufficient distance between each another and the destination so as to have independently faded links to the destination. To combine all of the received signals at the destination, MRC is employed in the proposed system, and the receivers at the destination are assumed to have perfect channel knowledge for the desired signals and no channel knowledge for the interfering signals. Throughout this dissertation, frequency and time synchronizations are assumed to be perfect, and all terminals are assumed to employ the same modulation scheme.

The links for both desired signals and interfering signals in the proposed system are affected by quasi-static flat-Nakagami fading, such that the fades remain constant over a packet duration. In addition, all links have mutually-independent and

non-identical Nakagami-m fading. Therefore, the received signals of the source-to-destination, source-to-relay, and relay-to-destination paths are,

$$
\begin{aligned}
y_{SD} &= h_0\, c_S \sqrt{P_S} + n_D + \sum_{l=1}^{L} h_{lD}\, c_l \sqrt{P_l} \ , \\
y_{SR_m} &= g_m\, c_S \sqrt{P_S} + n_{R_m} + \sum_{l=1}^{L} g_{lR_m}\, c_l \sqrt{P_l} \ , \\
y_{R_m D} &= h_m\, (c_{R_m} \sqrt{P_{R_m}}) + n_D + \sum_{l=1}^{L} h_{lD}\, c_l \sqrt{P_l} \ ,
\end{aligned} \tag{4}
$$

where P_S, P_{R_m}, and P_l represent the Tx powers of the source, the m-th relay, and the l-th interferer, respectively. The Tx powers may not be equal. The AWGN n has a zero mean and a variance σ^2 in all links, and c is the transmitted symbol with unit power. The channel gain h (or g) can be denoted as

$$
h = f\ \sqrt{k\, d^{-\alpha}} \ , \tag{5}
$$

where k is a constant; $|f|$ has a Nakagami-m distribution ($|f|^2$ has a Gamma density); d is the distance between the transmitter and the receiver, and α is the path-loss exponent.

Throughout this chapter, X_0, X_m^g, X_m^h, and X_m indicate the instantaneous SNR of the source-to-destination, the source-to-m-th relay, the m-th relay-to-destination, and the source-m-th relay-destination links, respectively. Likewise, the instantaneous interference-to-noise ratios (INRs) of the l-th interferer-to-m-th relay and l-th interferer-to-destination links are denoted as Y_l^m and Y_l, respectively. Therefore, the instantaneous SNR of the source-to-destination link can be written as $X_0 = |h_0|^2 P_S/\sigma^2$, and the instantaneous INR of the l-th interferer-to-m-th relay link can be written as $Y_l^m = |g_{lR_m}|^2 P_l/\sigma^2$.

In this chapter, to isolate the effect of power allocation for nodes, the Tx powers of the source, the relays, and the interferers assume to be the same as $P_S = P_{R_m} = P_l$. The local mean of Rx SNR of the desired signal can be expressed as $\omega_X = E\{|h|^2\}\, \Omega_t$,

where Ω_t is the Tx SNR, and $E\{\cdot\}$ is the statistical long-term average operator. To compare the effect of network geometry fairly and generally, the distance between nodes can be normalized by the length of the source-to-destination link. By assuming the normalized channel gain of the source-to-destination link is $E\{|h_0|^2\} = 1$, the normalized local mean of Rx SNR of the source-to-m-th relay and that of the m-th relay-to-destination can be expressed by

$$\omega_{X_m^g} = \left(\frac{d_{S,D}}{d_{S,R_m}}\right)^{\alpha} \Omega_t \,, \;\; \omega_{X_m^h} = \left(\frac{d_{S,D}}{d_{R_m,D}}\right)^{\alpha} \Omega_t \;\; . \tag{6}$$

Likewise, local mean of Rx INR of the l-th interferer-to-m-th relay and that of the l-th interferer-to-destination can be expressed as

$$\omega_{Y_l^m} = \left(\frac{d_{S,D}}{d_{I_l,R_m}}\right)^{\alpha} \Omega_t \,, \;\; \omega_{Y_l} = \left(\frac{d_{S,D}}{d_{I_l,D}}\right)^{\alpha} \Omega_t \;\; , \tag{7}$$

respectively.

3.3 Exact Closed-Form of Outage Probability

In this section, an exact closed-form of the outage probability is derived for DF cooperative relaying systems operating on Nakagami/Nakagami channels. To obtain the outage probability, different approaches can be used. One method uses the MGF of the SINR of the source-relay-destination path [31, 32, 27]. Another method uses the conditional outage probability of the individual relay-to-destination paths along with the corresponding probability that the relay belongs to the decoding set, defined as the set of relays having successfully decoded packets [3, 5, 47]. However, the exact closed-form of the outage probability obtained from the latter approach is generally very difficult to compute when links are non-identically distributed, as stated in [31]. Therefore, we obtain the outage probability by using the MGF-based approach.

Since the proposed system is perturbed by both CCI and AWGN, the output SINR with MRC is the sum of the individual SINRs of the diversity branches. The

output SINR is given by [23]

$$Z_{out} = \frac{\sum_0^M P_{X_m}}{\sum_1^L P_{Y_l} + \sigma^2} = \frac{\sum_0^M X_m}{\sum_1^L Y_l + 1} = \frac{X}{Y+1} \ , \tag{8}$$

where P_{X_m} and P_{Y_l} are the received powers for the m-th desired signal and the l-th interfering signal, respectively. Since both the SNR and INR are proportional to the squared envelope of their respective received signals, the pdfs of the SNR X_m^g (or X_m^h) and INR Y_l (or Y_l^m) for a single-hop link are,

$$\begin{aligned} p_{X_m^g}(x) &= \left(\frac{m_{X_m^g}}{\omega_{X_m^g}}\right)^{m_{X_m^g}} \frac{x^{m_{X_m^g}-1}}{\Gamma(m_{X_m^g})} \exp\left(-\frac{m_{X_m^g} x}{\omega_{X_m^g}}\right) \ , \\ p_{Y_l}(y) &= \left(\frac{m_{Y_l}}{\omega_{Y_l}}\right)^{m_{Y_l}} \frac{y^{m_{Y_l}-1}}{\Gamma(m_{Y_l})} \exp\left(-\frac{m_{Y_l} y}{\omega_{Y_l}}\right) \ , \end{aligned} \tag{9}$$

where $m_{X_m^g}$ and m_{Y_l} are the Nakagami shape factors, and $\omega_{X_m^g}$ and ω_{Y_l} are the local means of X_m^g and Y_l, respectively. The MGF of these pdfs can be written as

$$\begin{aligned} \mathcal{M}_{X_m^g}(s) &= (1 - \alpha_{X_m^g} s)^{-m_{X_m^g}} \ , \\ \mathcal{M}_{Y_l}(s) &= (1 - \alpha_{Y_l} s)^{-m_{Y_l}} \ , \end{aligned} \tag{10}$$

where $\alpha_{X_m^g} =: \omega_{X_m^g}/m_{X_m^g}$, and $\alpha_{Y_l} =: \omega_{Y_l}/m_{Y_l}$.

The outage probability is defined as the probability that the output SINR is below a specified threshold λ_{th}. Therefore, the outage probability at the destination can be expressed as

$$P_{out}(\lambda_{th}) = 1 - Pr\left(\frac{X}{\lambda_{th}} \geq Y + 1\right) = 1 - P \ , \tag{11}$$

where

$$P = \int_0^\infty p_Y(y) \int_{Y+1}^\infty p_U(u) \, \mathrm{d}u \, \mathrm{d}y \ , \tag{12}$$

and $U = X/\lambda_{th}$. To solve (12), the pdfs of the combined SNR $p_X(x)$ and the combined INR $p_Y(y)$ are required.

3.3.1 Pdf of the Combined SNR

By using the MGF-based approach the MGF of the combined SNR, which is the sum of independent random variables, is equal to the product of the individual MGFs, and the pdf of the combined SNR can be obtained from the inverse Laplace transform of the MGF of the combined SNR as follows:

$$p_X(x) = \mathcal{L}^{-1}\left[\prod_{m=0}^{M} \mathcal{M}_{X_m}(s)\right] \quad , \tag{13}$$

where $\mathcal{M}_{X_m}(s)$ is the MGF of X_m, and $\mathcal{L}^{-1}[\ \cdot\ ]$ is the inverse Laplace transform.

In [31], Hu and Beaulieu presented the pdf of the SNR of the source-relay-destination path for a selection DF relaying scheme. In practical selection DF relay systems, to forward successfully decoded packets, the relay will check a cyclic-redundancy-check code of the packets received from the source. However, to isolate the coding performance from the outage probability analysis, the packets that a relay receives are assumed to be successfully decoded when the SINR of the source-to-relay link is above a specified threshold λ_{th}, as in Laneman *et al.* [1]. Hence, the pdf of the SNR of the source-m-th relay-destination path, $p_{X_m}(x)$, is as follows:

$$p_{X_m}(x) = P_{out,z_m^g}(\lambda_{th})\delta(x) + \{1 - P_{out,z_m^g}(\lambda_{th})\}p_{X_m^h}(x), \ \ (m \geq 1) \ , \tag{14}$$

where $\delta(x)$ is the dirac delta function. For convenience, let $P_{o,m} = P_{out,Z_m^g}$, which is derived in Section 3.3.3, for the remainder of this chapter.

The MGF of X_m can be expressed as

$$\mathcal{M}_{X_m}(s) = P_{o,m} + (1 - P_{o,m})\mathcal{M}_{X_m^h}(s) = P_{o,m}\left\{1 + \frac{(1 - P_{o,m})}{P_{o,m}}\mathcal{M}_{X_m^h}(s)\right\} \ . \tag{15}$$

Since X_m's are independent, and X_0 is the SNR of the source-to-destination path, the MGF of X is given by

$$\mathcal{M}_X(s) = \prod_{m=0}^{M} \mathcal{M}_{X_m}(s) = \mathcal{M}_{X_0}(s)\prod_{m=1}^{M} P_{o,m}\left\{1 + \frac{(1 - P_{o,m})}{P_{o,m}}\mathcal{M}_{X_m^h}(s)\right\} \ . \tag{16}$$

By virtue of the multinomial formula which is derived in [32], the product terms can be changed into summation terms as follows:

$$\prod_{m=1}^{M}(1+B_m) = 1+\sum_{m=1}^{M}\sum_{\lambda_1=1}^{(M-m)+1}\sum_{\lambda_2=\lambda_1+1}^{(M-m)+2}\cdots\sum_{\lambda_{m-1}=\lambda_{m-2}+1}^{M+1}\sum_{\lambda_m=\lambda_{m-1}+1}^{M}\prod_{n=1}^{m}B_{\lambda_n} \ , \quad (17)$$

where $\lambda_0 = 0$. With the formula in (17), (16) can be rewritten as

$$\begin{aligned}\mathcal{M}_X(s) =& \mathcal{M}_{X_0}(s)\left(\prod_{m=1}^{M}P_{o,m}\right)\left\{1+\sum_{m=1}^{M}\sum_{\lambda_1=1}^{M-m+1}\cdots\right. \\ &\left.\times\sum_{\lambda_m=\lambda_{m-1}+1}^{M}\left(\prod_{n=1}^{m}\frac{1-P_{o,\lambda_n}}{P_{o,\lambda_n}}\right)\prod_{n=1}^{m}\mathcal{M}_{X^h_{\lambda_n}}(s)\right\} \ . \end{aligned} \quad (18)$$

Taking the inverse Laplace transform of (18) yields the pdf of X as

$$p_X(x) = \left(\prod_{m=1}^{M}P_{o,m}\right)\left\{p_{X_0}(x)+\sum_{m=1}^{M}\sum_{\lambda_1=1}^{M-m+1}\cdots\sum_{\lambda_m=\lambda_{m-1}+1}^{M}\left(\prod_{n=1}^{m}\frac{1-P_{o,\lambda_n}}{P_{o,\lambda_n}}\right)p_{X^h}(x)\right\} \ . \quad (19)$$

In (19), since $p_{X_0}(x)$ is the pdf of the SNR of the source-to-destination path, it has the Gamma distribution

$$p_{X_0}(x) = \left(\frac{1}{\alpha_{X_0}}\right)^{m_{X_0}}\frac{x^{m_{X_0}-1}}{\Gamma(m_{X_0})}\exp\left(-\frac{x}{\alpha_{X_0}}\right) \ . \quad (20)$$

To obtain the pdf of the combined SNR of the relay-to-destination paths, $p_{X^h}(x)$, the product of the individual MGFs of the SNRs of the relay-to-destination paths is required. When the Nakagami shape factor is assumed to be an integer value, the product of the MGFs of P Gamma distributed random variables can be further derived in [24] as follows:

$$\prod_{i=1}^{P}(1-\alpha_i z)^{-m_i} = \sum_{i=1}^{P}\sum_{j=1}^{m_i}\frac{\beta_{i,j}}{(z-1/\alpha_i)^j} \ , \quad (21)$$

where m_i is the shape factor of the i-th Gamma distribution,

$$\beta_{i,j} = \left(\frac{-1}{\alpha_i}\right)^{m_i}\sum_{\tau(i,j)}\prod_{k=1,k\neq i}^{P}\binom{m_k+q_k-1}{q_k}\frac{(\alpha_k)^{q_k}}{(1-\alpha_k/\alpha_i)^{m_k+q_k}} \ , \quad (22)$$

and where $\tau(i,j)$ denotes a set of P-tuples such that $\tau(i,j) = \{(q_1, \cdots, q_P) : \ q_i = 0, \sum_{k=1}^{P} q_k = (m_i - j)\}$, and the q are nonnegative integers. Since (22) uses a partial fraction sum, the normalized local mean α_i should be distinct for all i. This assumption is reasonable since the point where the α_i's are equal only exists in the joint pdf and has no probability mass. The Nakagami shape factor is assumed to be an integer value in this chapter, which is not a major limitation since the accuracy of the channel measurement usually corresponds to integer arithmetic, or it bounds to lower and upper integer values in practice [48].

By using (21) and inverse Laplace transform, the pdf $p_{X^h}(x)$ can be obtained as

$$p_{X^h}(x) = \mathcal{L}^{-1}\left[\prod_{n=0}^{m} \mathcal{M}_{X^h_{\lambda_n}}(s)\right] = \sum_{a=0}^{m} \sum_{b=1}^{m_{X^h_{\lambda_a}}} \frac{(-1)^b}{(b-1)!} \beta^X_{a,b}\, x^{b-1} \exp\left(-\frac{x}{\alpha_{X^h_{\lambda_a}}}\right) \ , \quad (23)$$

where

$$\beta^X_{a,b} = \left(\frac{-1}{\alpha_{X^h_{\lambda_a}}}\right)^{m_{X^h_{\lambda_a}}} \sum_{\tau(i,j)} \prod_{k=1, k\neq i}^{m} \binom{m_{X^h_k} + q_k - 1}{q_k} \frac{(\alpha_{X^h_k})^{q_k}}{\left(1 - \frac{\alpha_{X^h_{\lambda_k}}}{\alpha_{X^h_{\lambda_a}}}\right)^{m_{X^h_k} + q_k}} \ . \quad (24)$$

The pdf of the combined SNR $p_X(x)$ can be obtained by substituting (20) and (23) into (19) as follows:

$$p_X(x) = \left(\prod_{m=1}^{M} P_{o,m}\right) \Bigg\{ \left(\frac{1}{\alpha_{X_0}}\right)^{m_{X_0}} \frac{x^{m_{X_0}-1}}{\Gamma(m_{X_0})} \exp\left(-\frac{x}{\alpha_{X_0}}\right) + \sum_{m=1}^{M} \sum_{\lambda_1=1}^{M-m+1} \cdots$$
$$\times \sum_{\lambda_m=\lambda_{m-1}+1}^{M} \left(\prod_{n=1}^{m} \frac{1 - P_{o,\lambda_n}}{P_{o,\lambda_n}}\right) \sum_{a=0}^{m} \sum_{b=1}^{m_{X^h_{\lambda_a}}} \frac{(-1)^b}{(b-1)!} \beta^X_{a,b}\, x^{b-1} \exp\left(-\frac{x}{\alpha_{X^h_{\lambda_a}}}\right) \Bigg\} \ . \quad (25)$$

3.3.2 Pdf of the Total INR

We now derive the pdf, $p_Y(y)$, of the sum of INRs, Y, in (8). Since the individual pdfs of the INR, $p_{Y_l}(y)$, are mutually independent Gamma distributions in the l-th interferer-to-destination link, the pdf of the total INR is similar to (23) as follows:

$$p_Y(y) = \mathcal{L}^{-1}\left[\prod_{l=1}^{L} \mathcal{M}_{Y_l}(s)\right] = \sum_{a=1}^{L} \sum_{b=1}^{m_{Y_a}} \frac{(-1)^b}{(b-1)!} \beta^Y_{a,b}\, y^{b-1} \exp\left(-\frac{y}{\alpha_{Y_a}}\right) \ , \quad (26)$$

where

$$\beta_{a,b}^{Y} = \left(\frac{-1}{\alpha_{Y_a}}\right)^{m_{Y_a}} \sum_{\tau(i,j)} \prod_{k=1,k\neq i}^{L} \binom{m_{Y_k}+q_k-1}{q_k} \frac{(\alpha_{Y_k})^{q_k}}{\left(1-\frac{\alpha_{Y_{\lambda_k}}}{\alpha_{Y_{\lambda_a}}}\right)^{m_{Y_k}+q_k}} \quad . \tag{27}$$

3.3.3 Outage Probability of the Relay

Similarly to (11), the outage probability of the m-th relay can be obtained, but the SINR of the m-th relay is denoted as

$$Z_m^g = \frac{X_m^g}{Y^m+1} \quad . \tag{28}$$

Compared to (11), X_m^g is not the output SNR with MRC but rather the SNR of the source-to-m-th relay path. Therefore, X_m^g has the Gamma distribution

$$p_{X_m^g}(x) = \left(\frac{1}{\alpha_{X_m^g}}\right)^{m_{X_m^g}} \frac{x^{m_{X_m^g}-1}}{\Gamma(m_{X_m^g})} \exp\left(-\frac{x}{\alpha_{X_m^g}}\right) \quad . \tag{29}$$

However, Y^m is the combined INR from L-interferers to the m-th relay, so the pdf of the INR can be obtained from (23) as

$$p_{Y^m}(y) = \sum_{a=1}^{L} \sum_{b=1}^{m_{Y_a^m}} \frac{(-1)^b}{(b-1)!} \beta_{a,b}^{Y^m} \; y^{b-1} \exp\left(-\frac{y}{\alpha_{Y_a^m}}\right). \tag{30}$$

With (11), the outage probability of the m-th relay, $P_{o,m}$, can be obtained by substituting (29) and (30) into (12), and the integral terms can be solved by using *Lemma 1* in the Appendix A, as follows:

$$\begin{aligned} P_{o,m} =& 1 - \left(\frac{\lambda_{th}}{\alpha_{X_m^g}}\right)^{m_{X_m^g}} \sum_{a=1}^{L} \sum_{b=1}^{m_{Y_a^m}} \frac{(-1)^b \beta_{a,b}^{Y^m}}{\Gamma(m_{X_m^g})\Gamma(b)} \int_0^\infty y^{b-1} e^{-\frac{y}{\alpha_{Y_a^m}}} \int_{y+1}^\infty u^{m_{X_m^g}-1} e^{-\frac{\lambda_{th}\, u}{\alpha_{X_m^g}}} \, \mathrm{d}u \, \mathrm{d}y \\ =& 1 - \sum_{a=1}^{L} \sum_{b=1}^{m_{Y_a^m}} \sum_{n=0}^{m_{X_m^g}-1} \frac{(-1)^b \beta_{a,b}^{Y^m}}{\Gamma(n+1)} \left(\frac{\lambda_{th}}{\alpha_{X_m^g}}\right)^n \exp\left(-\frac{\lambda_{th}}{\alpha_{X_m^g}}\right) \sum_{k=0}^{n} \binom{n}{k} \\ & \times \left(\frac{1}{\alpha_{Y_a^m}} + \frac{\lambda_{th}}{\alpha_{X_m^g}}\right)^{-(b+k)} \frac{\Gamma(b+k)}{\Gamma(b)} \quad , \end{aligned} \tag{31}$$

where $U' = X_m^g/\lambda_{th}$.

3.3.4 End-to-end Outage Probability

The end-to-end outage probability in (11) can be obtained by substituting $p_X(x)$ in (25) and $p_Y(y)$ in (26) into (12). Hence, P in (12) becomes

$$P = \left(\prod_{m=1}^{M} P_{o,m}\right)\left[\sum_{a=1}^{L}\sum_{b=1}^{m_{Y_a}} \frac{(-1)^b \beta_{a,b}^{Y}}{\Gamma(b)} \left\{ \left(\frac{\lambda_{th}^{m_{X_0}}}{\alpha_{X_0}}\right)^{m_{X_0}} \int_0^{\infty} y^{b-1} e^{-\frac{y}{\alpha_{Y_a}}} \right.\right.$$
$$\times \int_{y+1}^{\infty} \frac{u^{m_{X_0}-1}}{\Gamma(m_{X_0})} e^{-\frac{\lambda_{th}}{\alpha_{X_0}}u} \,\mathrm{d}u\,\mathrm{d}y + \sum_{m=1}^{M}\sum_{\lambda_1=1}^{M-m+1}\cdots\sum_{\lambda_m=\lambda_{m-1}+1}^{M}\left(\prod_{n=1}^{m}\frac{1-P_{o,\lambda_n}}{P_{o,\lambda_n}}\right)$$
$$\left.\left. \times \sum_{c=0}^{m}\sum_{d=1}^{m_{X_{\lambda_c}^h}} \frac{(-1)^d}{\Gamma(d)} \beta_{c,d}^{X}\, \lambda_{th}^{d} \int_0^{\infty} y^{b-1} e^{-\frac{y}{\alpha_{Y_a}}} \int_{y+1}^{\infty} u^{d-1} e^{-\frac{\lambda_{th}}{\alpha_{X_{\lambda_c}^h}}u} \,\mathrm{d}u\,\mathrm{d}y \right\}\right] . \quad (32)$$

Using *Lemma 1* in the Appendix A, the integral terms in (32) can be solved to an exact-closed form as

$$P = \left(\prod_{m=1}^{M} P_{o,m}\right)\sum_{a=1}^{L}\sum_{b=1}^{m_{Y_a}}\sum_{n=0}^{m_{X_0}-1} \frac{(-1)^b \beta_{a,b}^{Y}}{\Gamma(n+1)} \left(\frac{\lambda_{th}}{\alpha_{X_0}}\right)^{n} e^{-\frac{\lambda_{th}}{\alpha_{X_0}}} \sum_{k=0}^{n}\binom{n}{k}\left(\frac{1}{\alpha_{Y_a}}+\frac{\lambda_{th}}{\alpha_{X_0}}\right)^{-(b+k)}$$
$$\times \frac{\Gamma(b+k)}{\Gamma(b)} + \left(\prod_{m=1}^{M} P_{o,m}\right)\sum_{m=1}^{M}\sum_{\lambda_1=1}^{M-m+1}\cdots\sum_{\lambda_m=\lambda_{m-1}+1}^{M}\left(\prod_{n=1}^{m}\frac{1-P_{o,\lambda_n}}{P_{o,\lambda_n}}\right)$$
$$\times \sum_{c=0}^{m}\sum_{d=1}^{m_{X_{\lambda_c}^h}} (-1)^d \beta_{c,d}^{X} (\alpha_{X_{\lambda_c}^h})^d \sum_{a=1}^{L}\sum_{b=1}^{m_{Y_a}}\sum_{n=0}^{d-1} \frac{(-1)^b \beta_{a,b}^{Y}}{\Gamma(n+1)} \left(\frac{\lambda_{th}}{\alpha_{X_{\lambda_c}^h}}\right)^{n} e^{-\frac{\lambda_{th}}{\alpha_{X_{\lambda_c}^h}}}$$
$$\times \sum_{l=0}^{n}\binom{n}{l}\left(\frac{1}{\alpha_{Y_a}}+\frac{\lambda_{th}}{\alpha_{X_{\lambda_c}^h}}\right)^{-(b+l)} \frac{\Gamma(b+l)}{\Gamma(b)} . \quad (33)$$

Equation (33) can be separated into two terms having similar form, such that the end-to-end outage probability, P_{out}, can be written as

$$P_{out} = 1 - P$$
$$= 1 - \left(\prod_{m=1}^{M} P_{o,m}\right)\left[G(\lambda_{th}; m_{X_0}, m_{Y_a}, \alpha_{X_0}, \alpha_{Y_a}) + \sum_{m=1}^{M}\sum_{\lambda_1=1}^{M-m+1}\cdots\sum_{\lambda_m=\lambda_{m-1}+1}^{M}\right.$$
$$\left. \times \left(\prod_{n=1}^{m}\frac{1-P_{o,\lambda_n}}{P_{o,\lambda_n}}\right)\sum_{c=0}^{m}\sum_{d=1}^{m_{X_{\lambda_c}^h}} (-1)^d \beta_{c,d}^{X}\, (\alpha_{X_{\lambda_c}^h})^d G(\lambda_{th}; d, m_{Y_a}, \alpha_{X_{\lambda_c}^h}, \alpha_{Y_a})\right], \quad (34)$$

where

$$G(\lambda_{th}; m_X, m_Y, \alpha_X, \alpha_Y)$$
$$\triangleq \sum_{a=1}^{L} \sum_{b=1}^{m_Y} \sum_{n=0}^{m_X-1} \frac{(-1)^b \beta_{a,b}^Y}{\Gamma(n+1)} \left(\frac{\lambda_{th}}{\alpha_X}\right)^n \exp\left(-\frac{\lambda_{th}}{\alpha_X}\right) \sum_{k=0}^{n} \binom{n}{k} \left(\frac{1}{\alpha_Y} + \frac{\lambda_{th}}{\alpha_X}\right)^{-(b+k)} \frac{\Gamma(b+k)}{\Gamma(b)} \ , \tag{35}$$

and L is the number of interferers. Similarly, $P_{o,m}$ in (31) and (34) can also be expressed as

$$P_{o,m} = 1 - G(\lambda_{th}; m_{X_m^g}, m_{Y^m}, \alpha_{X_m^g}, \alpha_{Y^m}) \ . \tag{36}$$

In the case of a single interferer ($L = 1$), $p_{Y^m}(y)$ and $p_Y(y)$ have a Gamma distribution. In this case, the end-to-end outage probability is given by

$$P_{out}^1 = 1 - \left(\prod_{m=1}^{M} P_{o,m}^1\right) \Bigg[G^1(\lambda_{th}; m_{X_0}, m_Y, \alpha_{X_0}, \alpha_Y) + \sum_{m=1}^{M} \sum_{\lambda_1=1}^{M-m+1} \cdots \sum_{\lambda_m=\lambda_{m-1}+1}^{M}$$
$$\times \left(\prod_{n=1}^{m} \frac{1 - P_{o,\lambda_n}^1}{P_{o,\lambda_n}^1}\right) \sum_{a=0}^{m} \sum_{b=1}^{m_{X_{\lambda_a}^h}} (-1)^b \beta_{a,b}^X \, (\alpha_{X_{\lambda_a}^h})^b G^1(\lambda_{th}; b, m_Y, \alpha_{X_{\lambda_a}^h}, \alpha_Y) \Bigg] \ , \tag{37}$$

where

$$\begin{aligned} P_{o,m}^1 =& 1 - \left(\frac{1}{\alpha_{Y^m}}\right)^{m_{Y^m}} \frac{(\lambda_{th}/\alpha_{X_m^g})^{m_{X_m^g}}}{\Gamma(m_{Y^m})\Gamma(m_{X_m^g})} \int_0^\infty y^{m_{Y^m}-1} e^{-\frac{y}{\alpha_{Y^m}}} \int_{y+1}^\infty u^{m_{X_m^g}-1} e^{-\frac{\lambda_{th}}{\alpha_{X_m^g}} u} \, \mathrm{d}u \, \mathrm{d}y \\ =& 1 - \left(\frac{1}{\alpha_{Y^m}}\right)^{m_{Y^m}} e^{-\frac{\lambda_{th}}{\alpha_{X_m^g}}} \sum_{n=0}^{m_{X_m^g}-1} \frac{1}{n!} \left(\frac{\lambda_{th}}{\alpha_{X_m^g}}\right)^n \sum_{k=0}^{n} \binom{n}{k} \\ & \times \left(\frac{1}{\alpha_{Y^m}} + \frac{\lambda_{th}}{\alpha_{X_m^g}}\right)^{-(m_{Y^m}+k)} \frac{\Gamma(m_{Y^m}+k)}{\Gamma(m_{Y^m})} \\ =& 1 - G^1(\lambda_{th}; m_{X_m^g}, m_{Y^m}, \alpha_{X_m^g}, \alpha_{Y^m}) \ , \end{aligned} \tag{38}$$

and

$$G^1(\lambda_{th}; m_X, m_Y, \alpha_X, \alpha_Y)$$
$$\triangleq \left(\frac{1}{\alpha_Y}\right)^{m_Y} e^{-\frac{\lambda_{th}}{\alpha_X}} \sum_{n=0}^{N-1} \frac{1}{n!} \left(\frac{\lambda_{th}}{\alpha_X}\right)^n \sum_{k=0}^{n} \binom{n}{k} \left(\frac{1}{\alpha_Y} + \frac{\lambda_{th}}{\alpha_X}\right)^{-(m_Y+k)} \frac{\Gamma(m_Y+k)}{\Gamma(m_Y)} \ . \tag{39}$$

3.4 Performance Analysis

We evaluate the outage performance of DF cooperative relaying systems when MRC is employed over Nakagami/Nakagami channels with various conditions: The number of relays and interferers, noise variances, Nakagami shape factors, and the distance between nodes. The analytic results in this section are verified by Monte Carlo simulations, which are performed with 10^8 trials to achieve the accuracy of 10^{-6} in outage probability.

Numerical results assume that the threshold SINR is $\lambda_{th} = 12$ dB, and the path-loss exponent is $\alpha = 3$. In Figs. 6 and 7, to exclude the effect of the placement of relays, the normalized distances between nodes are assumed to be symmetrical such that $d_{S,R_m}/d_{S,D} = d_{R_m,D}/d_{S,D} = 1$. For multiple interferers, the normalized distances between interferers and other nodes, $d_{I_l,R_m}/d_{S,D}$ and $d_{I_l,D}/d_{S,D}$, are assumed to be uniformly distributed on the interval (0.5, 1.5) so that interferers are placed near the relays and the destination. The effect of varying the relative placement of nodes will be treated later in Figs. 8, 9, and 10.

Figure 6 shows the outage performance comparison when the number of relays increases from one to five, and the Nakagami shape factor of the desired channels changes from one to two. The number of interferers is five, and individual interferers have the same as two, so the total interference power is fixed as ten. The total INR, $\sum_{l=1}^{L=5} P_{Y_l}/\sigma^2$, is 10 dB with $\sigma^2 = 1$ for all curves. As the number of relays increases, the slope of outage probability curve is steep, which means the cooperative-diversity order increases. Moreover, Fig. 6 shows that an increase in the Nakagami shape factor of desired signals provides an additional diversity gain on top of the cooperative-diversity gain. Note that the markers in this plot describe the simulation results, which perfectly match the analytic results of (34). Thus, since all parameters in (34) are verified in Fig. 6 by the simulations, the analytic results after Fig. 6 are not necessary to be verified again.

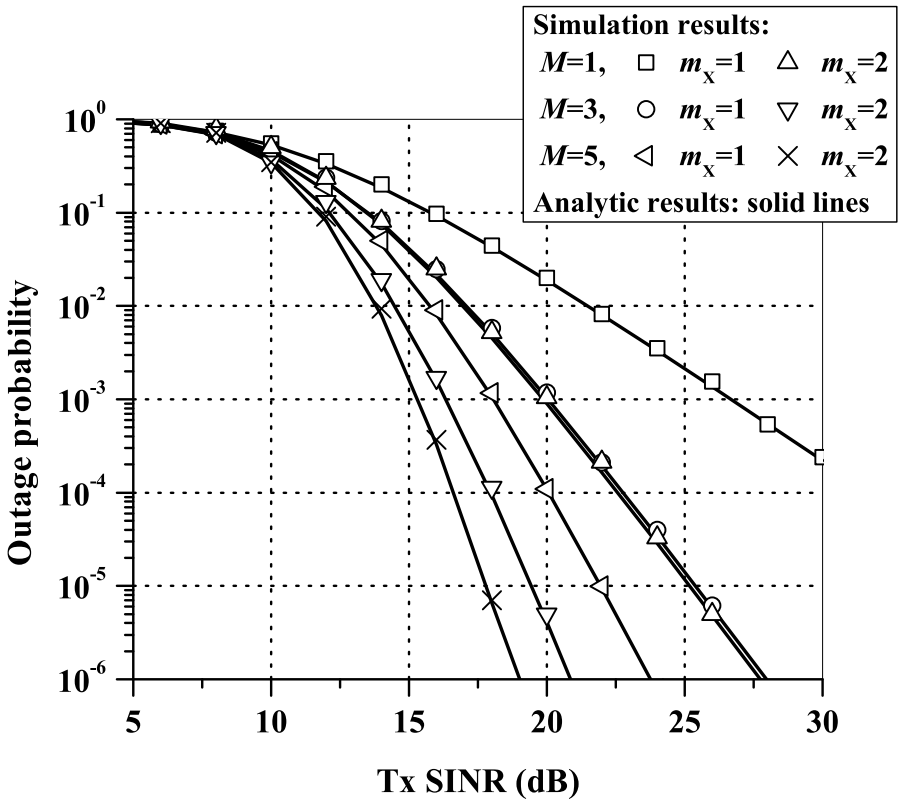

Figure 6: Outage probability for various number of relays and Nakagami shape factors when INR = 10 dB, $L = 5$, $m_Y = 1$, and $\sigma^2 = 1$.

Figure 7 describes the effects of relative mixture of noise and interference power on the outage probability. In the literature on DF cooperative relaying systems, most papers neglect noise power and investigate the outage probability in terms of SIR. However, this figure points out the importance of SINR on the outage probability performance. In Fig. 7, all curves have the same total-interference-plus-noise-power as $\sigma^2 + P_Y = 10$. However, three mixtures are set for the different number of relays and the Nakagami shape factor: the interference-dominant environment ($\sigma^2 = 1$, $P_Y = 9$), the equal-interference-and-noise environment ($\sigma^2 = 5$, $P_Y = 5$), and the noise-dominant environment ($\sigma^2 = 9$, $P_Y = 1$). In the low and moderate SINR, the noise-dominant configuration shows the worst outage performance among the configurations for any number of relays and channel conditions.

As the diversity order increases, the performance gaps among these configurations

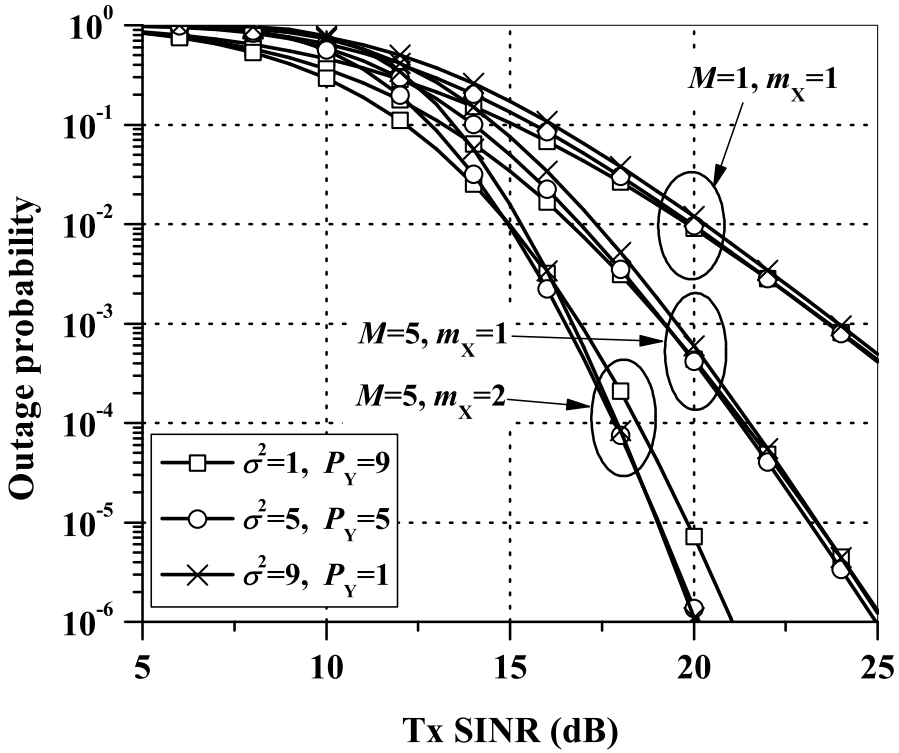

Figure 7: Outage probability for various number of relays and Nakagami shape factors with different noise and interference configurations when $L = 1$, and $m_Y = 1$.

become large in the low-SINR region, and the interference-dominant configuration has the worst performance among the configurations in the high-SINR region. Therefore, from Fig. 7, it is observed that the DF cooperative relaying system is more vulnerable to noise than to interference for low and moderate SINR, whereas it is more susceptible to interference than to noise for high SINR and high-diversity order.

Figure 8 shows the outage performance of DF cooperative relaying systems for two scenarios: The interferer is located close to the relay but far away from the destination (i.e., $d_{I,R_m}/d_{S,D} = 1$ and $d_{I,D}/d_{S,D} = 5$), which is referred to as the interfered relay, and the interferer is located close to the destination but far away from the relay (i.e., $d_{I,R_m}/d_{S,D} = 5$ and $d_{I,D}/d_{S,D} = 1$), which is referred to as the interfered destination.

When $M = 2$ and $m_X = 1$, the system with the interfered relay shows better performance than that with the interfered destination. However, as the number of relays increases to five (i.e., $M = 5$), the system with the interfered relay works better than that with the interfered destination in the low-SINR region, but in the high-SINR region the outage performances become similar. Moreover, when the Nakagami shape factor of desired channels increases to two (i.e., $m_X = 2$), the system with the interfered destination provides better performance than that with the interfered relay. This is because the source-to-destination path is less perturbed than the source-to-relay path in the interfered relay, while all paths are corrupted in the interfered destination. In addition, the destination achieves more diversity order than the relay as the numbers of relays and the Nakagami shape factor increase. As a result, interference at the destination causes a large performance degradation when the destination attains a low-diversity order, whereas interference at the relay causes a performance loss when the destination achieves a high-diversity order.

Figure 9 shows the outage probability for the DF cooperative relaying system with a single interferer in terms of the position of the relay. In this figure, it is assumed that the relay is located between the source and the destination, the interferer is equally distant from the relay and the destination, i.e., $d_{I,R} = d_{I,D}$, and the interference power is ten. Thus, the same interference power is applied to both the relay and the destination. For $d_{I,R}/d_{S,D} = d_{I,D}/d_{S,D} = 5$, the relaying position that minimizes the outage probability is a little bit closer to the source as 0.445. However, as the distance from the interferer decreases (i.e., the interference power increases), the optimal-relaying position moves toward the destination. The reason is that the destination requires higher SINR than the relay as the interference power increases, since the destination is more vulnerable to the interference than the relay when a low-diversity order is achieved at the destination, as seen in Fig. 8. The figure also demonstrates

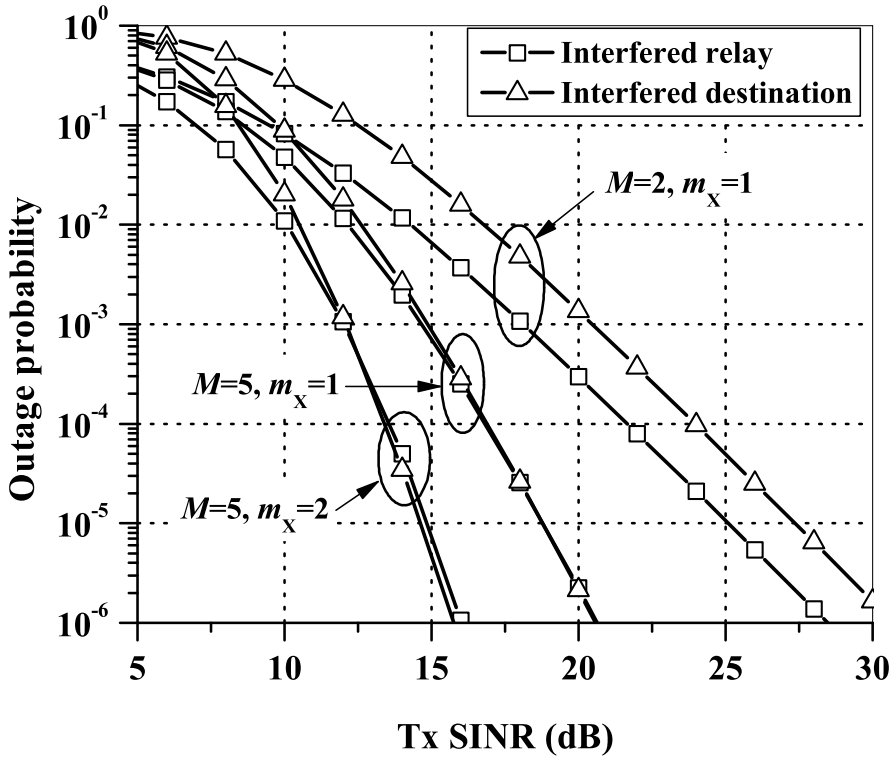

Figure 8: Outage probability comparison of interfered relay and interfered destination when $L = 1$, $m_Y = 1$, INR = 10 dB, and $\sigma^2 = 1$.

that the outage performance for a short source-to-relay distance (i.e., the source-to-relay link is much better than the relay-to-destination link) is worse than that for a long source-to-relay distance (i.e., the relay-to-destination link is much better than the source-to-relay link).

In Fig. 9, it is shown that the outage performance is Improved as the Nakagami shape factor of the interference increases. However, compared to the performance improvement caused by increasing the Nakagami shape factor of the desired signals in Fig. 6, the outage performance is relatively insensitive to the Nakagami shape factor of the interfering signals.

Figure 10 shows the effect of imbalanced interference powers at the relay and the destination on the outage probability of the DF cooperative relaying systems. In the figure, it is assumed that a single interferer is located between the relay and the

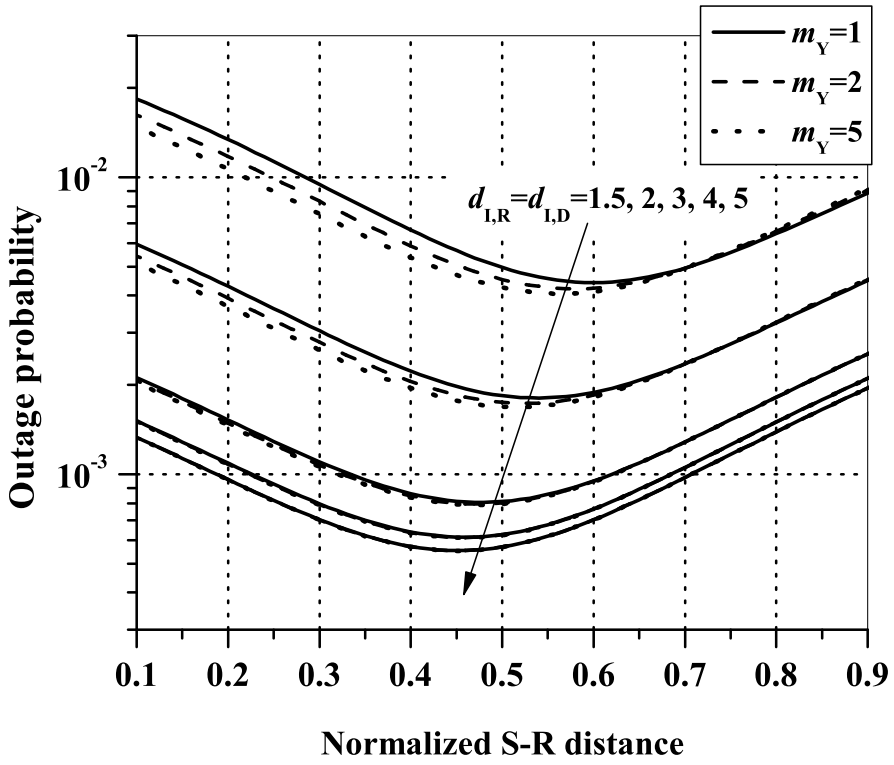

Figure 9: Outage probability versus normalized source-to-relay distance for the location of the interferer when SINR = 15 dB, $L = 1$, $m_X = 1$, and $\sigma^2 = 1$.

destination, and the interference power is ten. When the number of relays increases, the best position of the interferer moves from the relay to the destination as the diversity order of the destination increases, but the best position of the interferer is still closer to the relay than the destination. This result is the same as the Fig. 9 in that the destination is susceptible to interference.

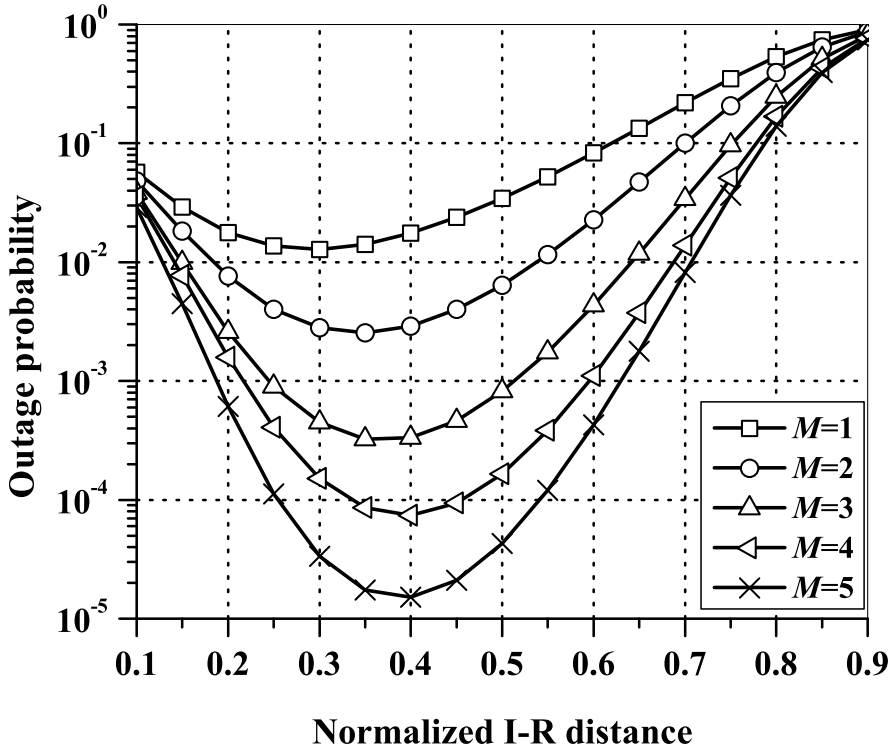

Figure 10: Outage probability versus normalized interferer-to-relay distance for the various number of relays when SINR = 15 dB, $L = 1$, $m_Y = 1$, and $\sigma^2 = 1$.

CHAPTER IV

COOPERATIVE DIVERSITY SYSTEMS WITH MULTI-BRANCH MULTI-HOP RELAYING

4.1 Overview

Besides the spatial diversity provided by multiple relays in cooperative diversity systems [1], a multi-hop transmission using multiple relays also provides an efficient way to combat shadowing and path loss, and it improves the power efficiency of a system [6, 7, 8]. However, a network constrained to use only point-to-point links has an average throughput that diminishes to zero as the number of relays approaches infinity [9]. To alleviate this limitation, a multi-hop diversity system was proposed, in which each relay can combine the signals from all preceding transmitting relays and re-transmit to the following relays [9, 10, 38]. Although the multi-hop diversity system guarantees a throughput improvement, each relay requires coherent reception from all preceding relays along with a signal combiner. These requirements are impractical for networks composed of numerous, small, low-cost relays such as wireless sensor networks.

As a general relay-topology based on cooperative diversity, a MBMH cooperative relaying systems can employ low-complexity relays, and only the destination combines the signals from the last-hop relays in multiple branches. In addition, the combination of cooperative diversity and multi-hop transmission can mitigate not only multipath fading but also shadowing and path loss [7, 11, 33, 34, 35, 36]. Note that the MBMH cooperative relaying system is not a multi-hop diversity transmission system, but rather a parallel multi-hop transmission system.

The end-to-end performance analysis of MBMH cooperative relaying systems was

studied in [7, 34, 35, 11, 36], but most studies focused on systems using AF relays. Moreover, most prior work considers thermal noise-limited conditions without interference. However, CCI often limits the performance of wireless systems, and since relaying systems are usually used to increase the coverage under dense frequency reuse, they are typically exposed to CCI.

Even though cooperative relaying networks are known to mitigate the impact of shadowing, most studies examined only multipath fading. However, in realistic environments, both small-scale and large-scale fading should be taken into account together, but the performance of cooperative relaying networks on composite shadowing and fading channels has so far been limited. Renzo *et al.* presented a workable framework for the performance analysis of the MBMH cooperative relaying system over shadowed Nakagami fading channels [34, 35], but they considered the AF scheme without CCI. Moreover, most existing literature evaluates the bit-error probability by taking an upper bound [10, 38], by using the Gaussian Q-function [35, 8], or an approximation of the Gaussian Q-function [34]. A closed-form expression for average symbol-error probability (ASEP) for selection DF MBMH cooperative relaying systems has not yet been obtained.

In this chapter, we provide closed-form expressions for the pdf of the SINR and the outage probability of a selection DF MBMH cooperative relaying system operating on composite shadowed Nakagami/shadowed Nakagami channels. Based on the statistical analysis, ASEPs with $\mathcal{M}$-ary phase shift keying (PSK) and $\mathcal{M}$-ary quadrature amplitude modulation (QAM) for the proposed system are also derived.

4.2 System and Channel Models

This section considers the general MBMH cooperative relaying network shown in Fig. 11. The system consists of a source $\mathbf{S}$, a destination $\mathbf{D}$, and multiple relays $\mathbf{R}_n^m$, where $m = 1, 2, \cdots, M$ denotes the m-th cooperating branch with the maximum number of

branches being M, and $n = 1, 2, \cdots, N(m)$ denotes the n-th cooperating hop with the maximum number of hops of the m-th branch being $N(m)$. Each branch can have a different number of hops. The n-th hop relay in the m-th branch is affected by co-channel interferers $\mathbf{I}_{l,n}^{m}$, $l = 1, 2, \cdots, L_n^m$ where L_n^m is the number of interferers. All interfering signals are assumed to add incoherently.

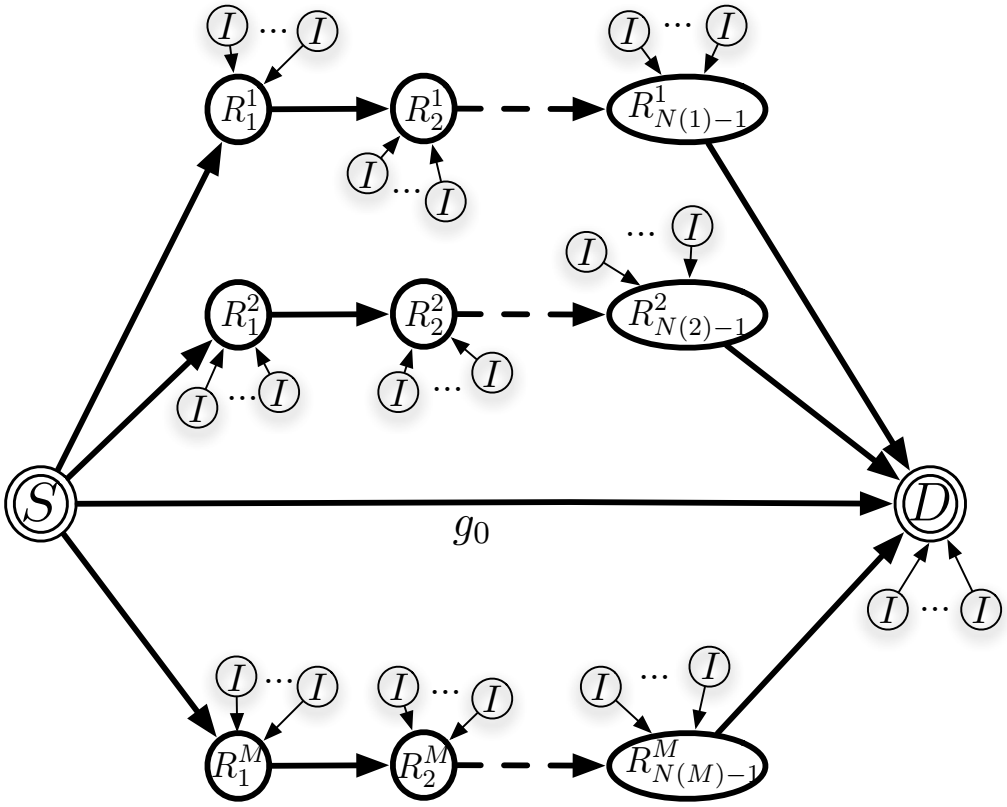

Figure 11: DF MBMH cooperative relaying system.

All terminals have a single Tx and Rx antenna, and the relays use a selection DF scheme as mentioned in Section 3.2. Note that in the selection DF relaying system proposed in [1, 38], the source retransmits the packet to the destination when the relay fails to decode the packet by allowing the relay to send feedback information to the source. However, in the proposed system, the source does not transmit the packet again. As a result, feedback channels are not necessary between the relays and

the source, so that the proposed system can reduce system complexity. The multiple-access protocol in the system uses an orthogonal transmission based on time-division multiple access.

Likewise to Section 3.2, in our cooperative relaying network, all terminals, including co-channel interferers, are assumed to be located at a sufficient distance between each another and the destination such that they have independently faded links to the destination. To combine the multiple received signals at the destination, the proposed system employs MRC. Note that the MRC scheme requires knowledge of the CSI of all links between the destination and its preceding relays. Therefore, in the DF MBMH cooperative relaying network, the destination is assumed to have perfect CSI for the desired signals and no channel knowledge for the interfering signals.

Each link in the system is affected by path loss, fading, and shadowing. Shadowing is assumed to have a log-normal distribution, and flat Nakagami fading that is quasi-static over a packet duration is assumed. In addition, all links are mutually independent and statistically non-identical. Therefore, the received signal from the $(n-1)$th hop relay to the n-th hop relay in the m-th branch is

$$S_{R_{n-1}^m, R_n^m} = g_n^m \, x_R \sqrt{P_{R_{n-1}^m}} + n + \sum_{l=1}^{L_n^m} h_{l,n}^m \, x_l \sqrt{P_l} \ , \tag{40}$$

where P_R and P_l represent the Tx powers of the relay and interferer, respectively, and the Tx powers may not be equal. The AWGN n has a zero mean and a variance σ^2 in all links, and x_R and x_l are the transmitted symbols with unit power in the relay and the interferer, respectively. The channel gain of the n-th hop desired signal in the m-th branch is g_n^m, and the channel gain of the l-th interfering signal to the n-th hop relay in the m-th branch is $h_{l,n}^m$. Source **S** can be denoted as R_0, destination **D** can be denoted as $R_{N(m)}$, and the channel gain of the source-to-destination link is g_0. The channel gain g (or h) can be written as $g = f\sqrt{c \cdot s \cdot d^{-\alpha}}$, where c is a constant, d is the distance between the transmitter and the receiver, α is the propagation path-loss exponent, s is the shadow-fading factor that has a log-normal distribution,

and the envelope f has a Nakagami distribution, thus, the squared envelope has a Gamma distribution. The relation of the area mean power to the path loss between the terminals will be provided in Section 4.2.2.

Throughout the chapter, X_n^m indicates the instantaneous received SNR of the n-th hop link in the m-th branch, which can be written as $X_n^m = |g_n^m|^2 P_{R_{n-1}^m}/\sigma^2$. Also, $Y_{l,n}^m$ denotes the instantaneous received INR from the l-th interferer to the n-th hop relay in the m-th branch, which can be written as $Y_{l,n}^m = |h_{l,n}^m|^2 P_l/\sigma^2$.

4.2.1 Power Allocation

For end-to-end performance, the allocation of power is an important factor because the received SINR is proportional to the Tx power. The increased power because of a larger number of relays undoubtedly indicates enhanced performance. Thus, to fairly compare the performance of different DF MBMH cooperative relaying systems, the total end-to-end Tx power should be fixed. We assume that the source and all the relays transmit at the same power. The fixed total end-to-end Tx power is

$$P_{tot} = P_S + \sum_{k=1}^{K} P_k \ , \tag{41}$$

where P_k is the Tx power of the k-th relay assumed equal to P_S, and K is the total number of relays, which can be expressed as $K = M \times (N-1)$ for the M-branch and N-hop cooperative relaying system.

4.2.2 Geometrical Topology

The proposed system assumes that all relays are located in a two dimensional plane, and uniformly distributed between the source and the destination. For the purpose of simplicity, we consider the system that has M branches and N hops in each branch. Thus, the distance between the adjacent terminals in the n-th hop link of the m-th branch is given by $d_n^m = d_0/N$, where d_0 is the distance between the source and the destination. Based on this geometric information and the path-loss model in

Section 4.2, the area mean power of the desired signal in the n-th hop link of the m-th branch, $\Omega_{X_n^m}$, can be normalized with respect to the area mean power of the received signal over the source-to-destination link, Ω_0, as follows:

$$\Omega_{X_n^m} = \left(\frac{d_0}{d_n^m}\right)^{\alpha} \Omega_0 = N^{\alpha} \frac{P_{tot}}{(K+1)} \ , \tag{42}$$

where $\Omega_0 = E\{|g_0|^2\}P_S$, and the average channel gain of the source-to-destination link is assumed to be unity, i.e., $E\{|g_0|^2\} = 1$. Likewise, if the Tx power of each interferer is assumed to be the same as that of the relays and source, the area mean power of the l-th interfering signal to the n-th hop relay in the m-th branch, $\Omega_{Y_{l,n}^m}$, is

$$\Omega_{Y_{l,n}^m} = \left(\frac{d_0}{d_{l,n}^m}\right)^{\alpha} \frac{P_{tot}}{(K+1)} \ . \tag{43}$$

4.2.3 Signal Representation

Both the desired and the interfering signals are assumed to experience log-normal shadowing and Nakagami-m fading. Their composite pdfs can be expressed as a closed form by applying Hermite-Gauss quadrature integration as in Section 2.1.

Since both the SNR and INR are proportional to the squared envelope of their respective received signals, the pdfs of SNR X_n^m and INR $Y_{l,n}^m$, which have a composite log-normal Gamma distribution, can be expressed as

$$\begin{aligned} p_{X_n^m}(x) &= \sum_{i=1}^{N_p} \frac{1}{\sqrt{\pi}} H_{x_i} \left[\left(\frac{m_{X_n^m}}{\Phi_n^m(x_i)} \right)^{m_{X_n^m}} \frac{x^{m_{X_n^m}-1}}{\Gamma(m_{X_n^m})} \exp\left(-\frac{m_{X_n^m}}{\Phi_n^m(x_i)} x \right) \right], \\ p_{Y_{l,n}^m}(y) &= \sum_{j=1}^{N_p} \frac{1}{\sqrt{\pi}} H_{x_j} \left[\left(\frac{m_{Y_{l,n}^m}}{\Phi_{l,n}^m(x_j)} \right)^{m_{Y_{l,n}^m}} \frac{y^{m_{Y_{l,n}^m}-1}}{\Gamma(m_{Y_{l,n}^m})} \exp\left(-\frac{m_{Y_{l,n}^m}}{\Phi_{l,n}^m(x_j)} y \right) \right], \end{aligned} \tag{44}$$

where H_{X_i} and H_{X_j} are weight factors, x_i and x_j are the zeros, N_p is the order of the Hermite polynomial, which is 16 as in [2, Table 3.1], $m_{X_n^m}$ and $m_{Y_{l,n}^m}$ are the Nakagami shape factors, and σ_X and σ_Y are the shadow standard deviations of the channels for the desired and interfering signals, respectively. In (44), $\Phi_n^m(x_i) =: \exp(\sqrt{2}\sigma_{X_n^m} x_i + \ln \Omega_{X_n^m})$, and $\Phi_{l,n}^m(x_j) =: \exp(\sqrt{2}\sigma_{Y_{l,n}^m} x_j + \ln \Omega_{Y_{l,n}^m})$. The moment

generating functions (MGFs), $M_{X_n^m}$ and $M_{Y_{l,n}^m}$, can be obtained from (44) as

$$\mathcal{M}_{X_n^m}(s) = \sum_{i=1}^{N_p} \frac{1}{\sqrt{\pi}} H_{x_i} \left\{1 - \alpha_{X_n^m}(x_i)s\right\}^{-m_{X_n^m}} \quad ,$$
$$\mathcal{M}_{Y_{l,n}^m}(s) = \sum_{j=1}^{N_p} \frac{1}{\sqrt{\pi}} H_{x_j} \left\{1 - \alpha_{Y_{l,n}^m}(x_j)s\right\}^{-m_{Y_{l,n}^m}} \quad , \tag{45}$$

where $\alpha_{X_n^m}(x_i) =: \Phi_n^m(x_i)/m_{X_n^m}$, and $\alpha_{Y_{l,n}^m}(x_j) =: \Phi_{l,n}^m(x_j)/m_{Y_{l,n}^m}$.

4.3 Probability Density Function Analysis

In this section, we derive a closed-form for the pdf of the SINR of the proposed system. First, we obtain the pdf of the SINR between the terminals for multiple interferers. Then, the end-to-end pdf of the SINR is derived.

4.3.1 Pdf per Hop

The relays in our system cannot combine the signals from the preceding relays because they have no signal combiner. Thus, a single branch for the desired signal is affected by the interferers. Since this chapter considers both CCI and AWGN, the SINR of the n-th hop relay in the m-th branch is expressed as

$$Z_n^m = \frac{P_{X_n^m}}{\sum_{l=1}^{L_n^m} P_{Y_{l,n}^m} + \sigma^2} = \frac{X_n^m}{\sum_{l=1}^{L_n^m} Y_{l,n}^m + 1} = \frac{X_n^m}{Y_n^m + 1} \quad , \tag{46}$$

where $P_{X_n^m}$ and $P_{Y_{l,n}^m}$ are the received power of the desired signal and that of the l-th interfering signal in the n-th hop of m-th branch respectively. The pdf of SINR Z can be expressed in terms of the pdfs of SNR X and INR Y as

$$p_Z(z) = \int_0^\infty (1+y) p_X\{z(1+y)\} p_Y(y)\, \mathrm{d}y \quad . \tag{47}$$

In the case of multiple interferers ($L_n^m \geq 1$), the pdf of the sum of INRs, $p_{Y_n^m}$, is required in (47). Since the individual pdfs of the INRs, $p_{Y_{l,n}^m}(y)$, are mutually independent composite log-normal Gamma distributions, the pdf of the total INR, $p_{Y_n^m}(y)$, can be obtained by taking the inverse Laplace transform of the product of

the MGFs of INRs. With such a method, the pdf of the sum of Gamma distributions was derived in [24, 37]. However, to obtain the pdf of the sum of the composite log-normal Gamma distributions, taking the inverse Laplace transform of the product of L_n^m-MGFs of INRs in (45) yields

$$p_{Y_n^m}(y) = \sum_{a=1}^{L_n^m} \sum_{b=1}^{m_{Y_{a,n}^m}} \sum_{j_a=1}^{N_p} \frac{1}{\sqrt{\pi}} H_{x_{j_a}} \frac{(-1)^b}{\Gamma(b)} \beta_{a,b}^{Y}(x_{j_a}) y^{b-1} \exp\left(-\frac{y}{\alpha_{Y_{a,n}^m}(x_{j_a})}\right) \ , \tag{48}$$

where

$$\beta_{a,b}^{Y}(x_{j_a}) = \sum_{\tau(a,b)} \prod_{k=1,k\neq a}^{L_n^m} \binom{m_k + q_k - 1}{q_k} \sum_{j_k=1}^{N_p} \frac{1}{\sqrt{\pi}} H_{x_{j_k}} \left(\frac{-1}{\alpha_a(x_{j_a})}\right)^{m_a} \times \frac{\{\alpha_k(x_{j_k})\}^{q_k}}{\{1 - \alpha_k(x_{j_k})/\alpha_a(x_{j_a})\}^{m_k+q_k}} \ ,$$

where $\tau(a,b)$ denotes a set of L_n^m-tuples such that $\tau(a,b) = \{(q_1, \cdots, q_{L_n^m}) : \ q_a = 0, \sum_{k=1}^{L_n^m} q_k = (m_a - b)\}$, and the q's are nonnegative integers. As mentioned in (22), the normalized area mean α_a should be distinct for all a's, and the Nakagami fading factor m is assumed to be integer valued. Thus, the pdf of the SINR of the n-th hop relay in the m-th branch is obtained by substituting (44) and (48) into (47), and the integral term can be solved by using *Lemma 2* in Appendix A and the $\hat{H}$-function in Appendix B as follows:

$$p_{Z_n^m}(z) = \sum_{a=1}^{L_n^m} \sum_{b=1}^{m_{Y_{a,n}^m}} \sum_{i=1}^{N_p} \sum_{j_a=1}^{N_p} \frac{1}{\pi} H_{x_i} H_{x_{j_a}} \{-\alpha_{Y_{a,n}^m}(x_{j_a})\}^b \beta_{a,b}^{Y}(x_{j_a}) \times \hat{H}(z; m_{X_n^m}, b, \alpha_{X_n^m}(x_i), \alpha_{Y_{a,n}^m}(x_{j_a})) \ . \tag{49}$$

4.3.2 End-to-End Pdf

The output SINR of MRC in the destination is the sum of the individual SINRs of the branches. Compared to (46), the output SINR is written as

$$Z_{out} = \frac{\sum_{m=0}^{M} P_{X^m}}{\sum_{l=1}^{L_D} P_{Y_{l,D}} + \sigma^2} = \frac{\sum_{m=0}^{M} X^m}{\sum_{l=1}^{L_D} Y_{l,D} + 1} = \frac{X}{Y+1} \ , \tag{50}$$

where P_{X^m} and X^m are the end-to-end received power and the end-to-end SNR of the desired signal in the m-th branch, respectively; $P_{Y_{l,D}}$ and $Y_{l,D}$ are the received

power and the INR of the l-th interfering signal to the destination, respectively; L_D is the number of interferers at the destination.

In the selection DF relaying system, each hop is independent of the previous hops, and if the relay fails to decode the received packet because of low SINR, the relay does not transmit it. Therefore, for the selection DF relaying with dual-hop, Hu and Beaulieu in [31] showed that the pdf of the SNR of the source-relay-destination link can be expressed by the probability that the relay can forward the source packet and the pdf of the SNR of the relay-to-destination link [31, eq. 6]. Similarly to dual-hop relaying, for the selection DF relaying with multi-hops, the pdf of the SNR of the m-th branch, $p_{X^m}(x)$, is given by

$$p_{X^m}(x) = \bar{P}_{o_{N(m)-1}}^{\ m}(\lambda_{th})\delta(x) + \{1 - \bar{P}_{o_{N(m)-1}}^{\ m}(\lambda_{th})\}p_{X^m_{N(m)}}(x) \ \ , (m \geq 1) \ \ , \tag{51}$$

where $\delta(x)$ is the dirac delta function, $\bar{P}_{o_{N-1}}^{\ m}$ is the outage probability of the $(N-1)$th hop in the m-th branch, and λ_{th} is the outage threshold. In the multi-hop relaying transmission, $\bar{P}_{o_{N-1}}^{\ m}$ is the probability that an outage event will occur at any relay along from the first hop to the $(N-1)$th hop as in [10, 38]. The probability can be written as

$$\bar{P}_{o_{N-1}}^{\ m}(\lambda_{th}) = 1 - \prod_{i=1}^{N-1}\{1 - P_{o_i}^{\ m}(\lambda_{th})\} \ \ , \tag{52}$$

where $P_{o_i}^{\ m}$ is the outage probability of the i-th hop relay in the m-th branch, which is obtained in (59) of Section 4.4.1. For convenience, let $P_o^m = \bar{P}_{o_{N-1}}^{\ m}$ for the remainder of this chapter.

In the cooperative diversity system, the relayed signals from multiple branches are combined by MRC in the destination. For Nakagami-m channels, the pdf of the combined SNR of MRC was derived in Chapter 3, and it can be re-expressed as

$$p_X(x) = \left(\prod_{m=1}^{M} P_o^m\right)\left\{p_{X^0}(x) + \sum_{m=1}^{M}\sum_{\lambda_1=1}^{M-m+1}\cdots\sum_{\lambda_m=\lambda_{m-1}+1}^{M}\left(\prod_{n=1}^{m}\frac{1-P_o^{\lambda_n}}{P_o^{\lambda_n}}\right)p_{X_N^m}(x)\right\} \ \ , \tag{53}$$

where $p_{X^0}(x)$ is the pdf of the SNR of the source-to-destination link, and $p_{X_N^m}(x)$ is the combined SNR of m branches in the last N hop, which is similar to (48) as

$$p_{X_N^m}(x) = \sum_{a=1}^{m} \sum_{b=1}^{m_{X_N^a}} \sum_{i_a=1}^{N_p} \frac{1}{\sqrt{\pi}} H_{x_{i_a}} \frac{(-1)^b}{\Gamma(b)} \beta_{a,b}^{X}(x_{i_a}) x^{b-1} \exp\left(-\frac{x}{\alpha_{X_N^a}(x_{i_a})}\right) \quad , \tag{54}$$

where

$$\beta_{a,b}^{X}(x_{i_a}) = \sum_{\tau(a,b)} \prod_{k=1,k\neq a}^{m} \binom{m_k + q_k - 1}{q_k} \sum_{i_k=1}^{N_p} \frac{1}{\sqrt{\pi}} H_{x_{i_k}} \left(\frac{-1}{\alpha_a(x_{i_a})}\right)^{m_a} \times \frac{\{\alpha_k(x_{i_k})\}^{q_k}}{\{1 - \alpha_k(x_{i_k})/\alpha_a(x_{i_a})\}^{m_k+q_k}} .$$

By applying (54) to (53) yield the end-to-end pdf of output SNR as follows:

$$\begin{aligned} p_X(x) = \left(\prod_{m=1}^{M} P_o^m\right) \Bigg\{ & \sum_{i_0=1}^{N_p} \frac{1}{\sqrt{\pi}} H_{x_{i_0}} \left(\frac{1}{\alpha_{X_0}(x_{i_0})}\right)^{m_{X_0}} \frac{x^{m_{X_0}-1}}{\Gamma(m_{X_0})} \exp\left(\frac{-x}{\alpha_{X_0}(x_{i_0})}\right) \\ & + \sum_{m=1}^{M} \sum_{\lambda_1=1}^{M-m+1} \cdots \sum_{\lambda_m=\lambda_{m-1}+1}^{M} \left(\prod_{n=1}^{m} \frac{1 - P_o^{\lambda_n}}{P_o^{\lambda_n}}\right) \sum_{a=0}^{m} \sum_{b=1}^{m_{X_N^{\lambda_a}}} \sum_{i_a=1}^{N_p} \frac{1}{\sqrt{\pi}} \\ & \times H_{x_{i_a}} \frac{(-1)^b}{\Gamma(b)} \beta_{a,b}^{X}(x_{i_a}) x^{b-1} \exp\left(-\frac{x}{\alpha_{X_N^{\lambda_a}}(x_{i_a})}\right) \Bigg\} \quad . \end{aligned} \tag{55}$$

The output INR Y is the sum of the INRs of the L_D interferers. Thus, the pdf of Y can be expressed as the sum of multiple independent composite log-normal Gamma distributions, and it can be also written as

$$p_Y(y) = \sum_{a=1}^{L_D} \sum_{b=1}^{m_{Y_{a,D}}} \sum_{j_a=1}^{N_p} \frac{1}{\sqrt{\pi}} H_{x_{j_a}} \frac{(-1)^b}{\Gamma(b)} \beta_{a,b}^{Y}(x_{j_a}) y^{b-1} \exp\left(-\frac{y}{\alpha_{Y_{a,D}}(x_{j_a})}\right) \quad . \tag{56}$$

For the multiple interferers, substituting $p_X(x)$ in (55) and $p_Y(y)$ in (56) into (47) yields the end-to-end pdf of SINR Z. Applying *Lemma 2* in Appendix A to the integral term of (47) and using the $\hat{H}$-function in Appendix B yield the closed-form

of the end-to-end pdf as follows:

$$p_Z(z) = \left(\prod_{m=1}^{M} P_o^m\right)\Bigg[\sum_{c=1}^{L_D}\sum_{d=1}^{m_{Y_{c,D}}}\sum_{i_0=1}^{N_p}\sum_{j_c=1}^{N_p}\frac{1}{\pi}H_{x_{j_c}}\beta_{c,d}^{Y}(x_{j_c})H_{x_{i_0}}\{-\alpha_{Y_{c,D}}(x_{j_c})\}^d$$
$$\times\hat{H}(z;m_{X_0},d,\alpha_{X_0}(x_{i_0}),\alpha_{Y_{c,D}}(x_{j_c})) + \sum_{m=1}^{M}\sum_{\lambda_1=1}^{M-m+1}\cdots\sum_{\lambda_m=\lambda_{m-1}+1}^{M}\left(\prod_{n=1}^{m}\frac{1-P_o^{\lambda_n}}{P_o^{\lambda_n}}\right)$$
$$\times\sum_{a=0}^{m}\sum_{b=1}^{m_{X_N^{\lambda_a}}}\sum_{i_a=1}^{N_p}\frac{1}{\sqrt{\pi}}H_{x_{i_a}}\beta_{a,b}^{X}(x_{i_a})\{-\alpha_{X_N^{\lambda_a}}(x_{i_a})\}^b\sum_{c=1}^{L_D}\sum_{d=1}^{m_{Y_{c,D}}}\sum_{j_c=1}^{N_p}\frac{1}{\sqrt{\pi}}H_{x_{j_c}}\beta_{c,d}^{Y}(x_{j_c})$$
$$\times\{-\alpha_{Y_{c,D}}(x_{j_c})\}^d\hat{H}(z;b,d,\alpha_{X_N^{\lambda_a}}(x_{i_a}),\alpha_{Y_{c,D}}(x_{j_c}))\Bigg]\ . \tag{57}$$

4.4 Outage Probability Analysis

We now derive the end-to-end outage probability for the proposed system. Based on the pdf analysis in Section 4.3, the outage probability is defined as the probability that the output SINR is below a specified threshold λ_{th}. Therefore, the outage probability at the destination can be expressed as

$$P_o(\lambda_{th}) = Pr(Z < \lambda_{th}) = \int_0^{\lambda_{th}} p_Z(z)\,\mathrm{d}z\ . \tag{58}$$

4.4.1 Outage Probability per Hop

In this section, we derive the outage probability between the terminals, the results of which are used in (52) to compute the outage probability of each branch.

By substituting the pdf of the SINR per hop with multiple interferers ($L_n^m \geq 1$) in (49) into (58), the outage probability per hop with multiple interferers can be derived. It can be also expressed with the $\hat{F}$-function in Appendix B as follows:

$$P_{on}^{\ m}(\lambda_{th}) = 1 - \sum_{a=1}^{L_n^m}\sum_{b=1}^{m_{Y_{a,n}^m}}\sum_{i=1}^{N_p}\sum_{j_a=1}^{N_p}\frac{1}{\pi}H_{x_i}H_{x_{j_a}}\{-\alpha_{Y_{a,n}^m}(x_{j_a})\}^b\beta_{a,b}^{Y}(x_{j_a})$$
$$\times\hat{F}(\lambda_{th};m_{X_n^m},b,\alpha_{X_n^m}(x_i),\alpha_{Y_{a,n}^m}(x_{j_a}))\,. \tag{59}$$

4.4.2 End-to-End Outage Probability

As we discussed in Section 4.3.2, the outage probability of the m-th branch, P_o^m, consists of the independent outage probabilities of respective hops, which is derived in (59). The end-to-end outage probability with multiple Interferers is given by substituting (57) into (58) as

$$P_o(\lambda_{th}) = 1 - \left(\prod_{m=1}^{M} P_o^m\right) \left[\sum_{c=1}^{L_D} \sum_{d=1}^{m_{Y_{c,D}}} \sum_{i_0=1}^{N_p} \sum_{j_c=1}^{N_p} \frac{1}{\pi} H_{x_{i_0}} H_{x_{j_c}} \beta_{c,d}^{Y}(x_{j_c}) \{-\alpha_{Y_{c,D}}(x_{j_c})\}^d \right.$$
$$\times \hat{F}(\lambda_{th}, m_{X_0}, d, \alpha_{X_0}(x_{i_0}), \alpha_{Y_{c,D}}(x_{j_c})) + \sum_{m=1}^{M} \sum_{\lambda_1=1}^{M-m+1} \cdots \sum_{\lambda_m=\lambda_{m-1}+1}^{M} \left(\prod_{n=1}^{m} \frac{1 - P_o^{\lambda_n}}{P_o^{\lambda_n}}\right)$$
$$\times \sum_{a=0}^{m} \sum_{b=1}^{m_{X_{\lambda_a}^h}} \sum_{i_a=1}^{N_p} \frac{1}{\sqrt{\pi}} H_{x_{i_a}} \beta_{a,b}^{X}(x_{i_a}) \{-\alpha_{X_N^{\lambda_a}}(x_{i_a})\}^b \sum_{c=1}^{L_D} \sum_{d=1}^{m_{Y_{c,D}}} \sum_{j_c=1}^{N_p} \frac{1}{\sqrt{\pi}} H_{x_{j_c}} \beta_{c,d}^{Y}(x_{j_c})$$
$$\left. \times \{-\alpha_{Y_{c,D}}(x_{j_c})\}^d \hat{F}(\lambda_{th}; b, d, \alpha_{X_N^{\lambda_a}}(x_{i_a}), \alpha_{Y_{c,D}}(x_{j_c})) \right] . \tag{60}$$

4.5 Average Symbol Error Probability Analysis

We present the closed form of ASEP for the selection DF MBMH cooperative relaying system over shadowed Nakagami/shadowed Nakagami channels. The ASEP derived in this section can be applied to $\mathcal{M}$-PSK and $\mathcal{M}$-QAM systems. One of the advantages of the selection DF scheme is that every link can employ different modulation schemes, but all terminals in our system use the same modulation scheme to reduce system complexity.

Generally, the single-hop ASEP can be expressed as

$$P_s = E_z[\alpha Q(\sqrt{2\beta z})] \ , \tag{61}$$

where $Q(\cdot)$ is the Gaussian Q-function, and α and β are modulation-specific constants for modulation order $\mathcal{M}$. In the case of $\mathcal{M}$-PAM, $\alpha = 2(\mathcal{M}-1)/\mathcal{M}$ and $\beta = 3/(\mathcal{M}^2-1)$ [49, eq. 5.2-44]. In the case of $\mathcal{M}$-PSK, $\alpha = 2$ and $\beta = \sin^2(\pi/\mathcal{M})$ [49, eq. 5.2-61]. The ASEP of $\mathcal{M}$-QAM system with $\mathcal{M} = 4^k, k = 1, 2, \ldots,$ can be written

by using that of $\sqrt{\mathcal{M}}$-PAM as in [2, eq. 5.89]

$$P_{\mathcal{M}}(z_s) = 1 - (1 - P_{\sqrt{\mathcal{M}}})^2 \ , \tag{62}$$

where $P_{\sqrt{\mathcal{M}}}$ is the ASEP of $\sqrt{\mathcal{M}}$-PAM system.

To evaluate ASEP in (61), most prior work uses an MGF-based approach, but the integration of the MGF of the MBMH cooperative relaying system is quite involve even for identical shadowed Nakagami-m channels. Therefore, we use another approach proposed in [50, eq. 20], as follows:

$$P_s = \frac{\alpha\sqrt{\beta}}{2\sqrt{\pi}} \int_0^\infty \frac{e^{-\beta\lambda}}{\sqrt{\lambda}} F_Z(\lambda)\, \mathrm{d}\lambda \ , \tag{63}$$

where $F_Z(\lambda)$ is the cumulative density function (cdf). As discussed in Section 4.4.2, the end-to-end outage probability is derived in (60), which consists of the outage probability of the last hop, the source-to-destination link, and the probability that previous relays forward the source packet as mentioned in (52). Since the variable λ in (63) is also related to the outage probability of the last hop and the source-to-destination link, which are a single hop, the end-to-end ASEP can be derived by using (63). Note that the outage probability derived in the chapter is for the signal outage not for the capacity outage. Thus, $F_Z(\lambda)$ is the same as the outage probability for SINR Z in (58). Therefore, the end-to-end ASEP of the proposed system can be obtained by substituting (60) into (63) as

$$\begin{aligned} P_{s,Z} = \alpha/2 - \left(\prod_{m=1}^{M} P_o^m\right) \Bigg[& \sum_{c=1}^{L_D} \sum_{d=1}^{m_{Y_{c,D}}} \sum_{i_0=1}^{N_p} \sum_{j_c=1}^{N_p} \frac{1}{\pi} H_{i_0} H_{j_c} (-\alpha_{Y_c})^d \beta_{c,d}^{Y}(x_{j_c}) \\ & \times \hat{S}(\alpha, \beta, m_{X_0}, d, \alpha_{X_0}(x_{i_0}), \alpha_{Y_c}(x_{j_c})) + \sum_{m=1}^{M} \sum_{\lambda_1=1}^{M-m+1} \cdots \sum_{\lambda_m=\lambda_{m-1}+1}^{M} \left(\prod_{n=1}^{m} \frac{1 - P_o^{\lambda_n}}{P_o^{\lambda_n}}\right) \\ & \times \sum_{a=0}^{m} \sum_{b=1}^{m_{X_N^{\lambda_a}}} \sum_{i_a=1}^{N_p} \frac{1}{\sqrt{\pi}} H_{x_{i_a}} \beta_{a,b}^{X}(x_{i_a}) \{-\alpha_{X_N^{\lambda_a}}(x_{i_a})\}^b \sum_{c=1}^{L_D} \sum_{d=1}^{m_{Y_{c,D}}} \sum_{j_c=1}^{N_p} \frac{1}{\sqrt{\pi}} H_{x_{j_c}} \beta_{c,d}^{Y}(x_{j_c}) \\ & \times \{-\alpha_{Y_{c,D}}(x_{j_c})\}^d \hat{S}(\alpha, \beta, b, d, \alpha_{X_N^{\lambda_a}}(x_{i_a}), \alpha_{Y_{c,D}}(x_{j_c})) \Bigg] \ . \end{aligned} \tag{64}$$

4.6 Performance Analysis

In this section, outage probabilities and the ASEPs are evaluated in various scenarios for general DF MBMH cooperative systems over shadowed-Nakagami/shadowed-Nakagami channels. The analytic results in this section are verified by Monte Carlo simulations, which are performed with 10^8 trials to achieve the accuracy of 10^{-6} in the outage probability. Our results assume that the Nakagami shape factor of the desired signals $m_X = 2$, and that of the interfering signals $m_Y = 1$. The threshold SINR is $\lambda_{th} = 12$ dB, and the path-loss exponent is $\alpha = 3$. The number of co-channel interferers at each relay is four with the Tx powers of the individual interferers $P_{Y_{l,n}^m} = 2.5$. Thus, the total Tx power of the interferers is fixed as ten, and the total Tx INR is 10 dB with $\sigma^2 = 1$ for all curves. However the normalized distances between the relays and the interferers, $d_{l,n}^m/d_0$, are assumed to be uniformly distributed over the interval (0.5, 1.5) such that interferers are placed near relays. In particular, this section considers 16-QAM scheme, but the type of modulation is not limited according to Section 4.5.

Figures 12, 13, 14, and 15 show the end-to-end outage performance comparisons. Note that the markers in these figures describe the simulation results, and the solid lines are analytically obtained from (60). These figures show that the analytic results are in perfect agreement with simulation results.

Figure 12 shows that the end-to-end outage performance is improved by increasing the number of branches over Nakagami/Nakagami channels. A single-hop system provides a reference in terms of the outage probability versus the total Tx SINR. As expected, the outage performances of all the DF MBMH cooperative relaying systems outperform those of the single-hop system. As the number of branches increases, the slope of the outage probability curve becomes steeper, which indicates that the cooperative-diversity order also increases. The diversity gain is the largest when the number of branches increases from one to two, but the performance gap decreases

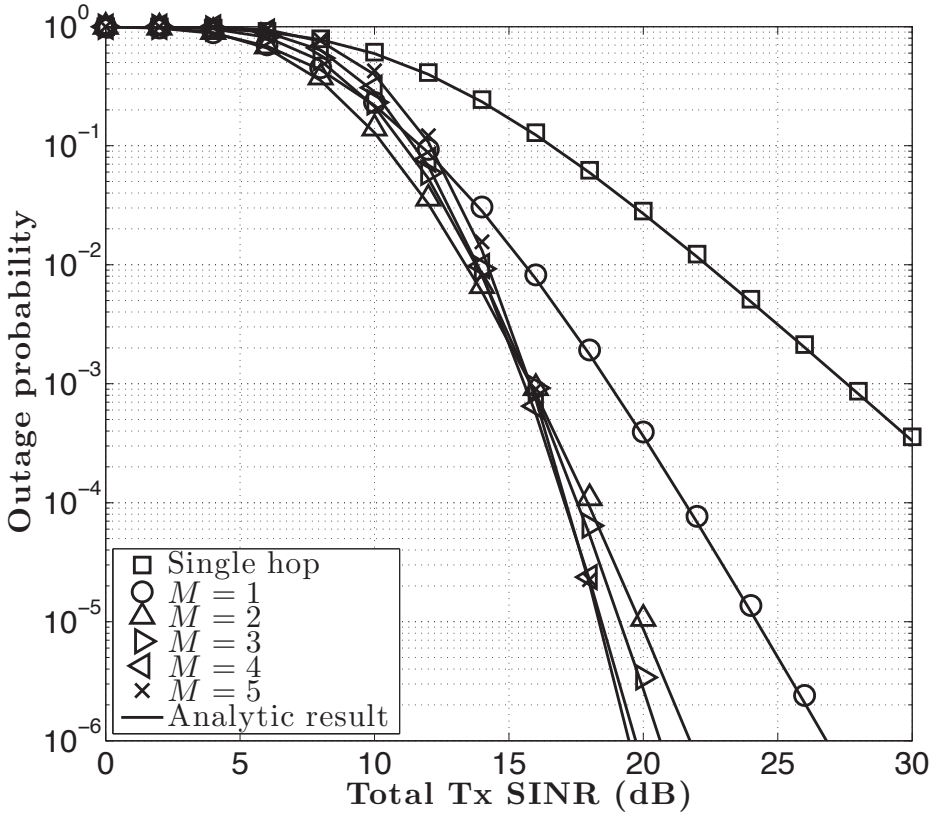

Figure 12: Outage probability for various number of branches without shadowing when $N = 2$, INR = 10 dB, $L = 4$, $m_X = 2$, $m_Y = 1$, and $\sigma^2 = 1$.

as the number of branches increases. The interesting result is that as the number of branches increases, the outage performance worsens in the low SINR region and a cooperative-diversity gain occurs in the high SINR region. The reason for this behavior is that as the number of relays increases under the fixed total power constraint, the individual Tx powers decrease, and the impact of the decreased Tx power dominates the cooperative-diversity gain in the low SINR region.

Figure 13 describes the effect of the number of hops without shadowing, in which the number of hops increases from two to five, but the number of cooperating branches is fixed at one. Since the destination combines the signals of the source-to-destination link with the cooperating branch, the cooperative-diversity order is two. A single-hop MRC system with two Rx antennas provides a reference with the same diversity

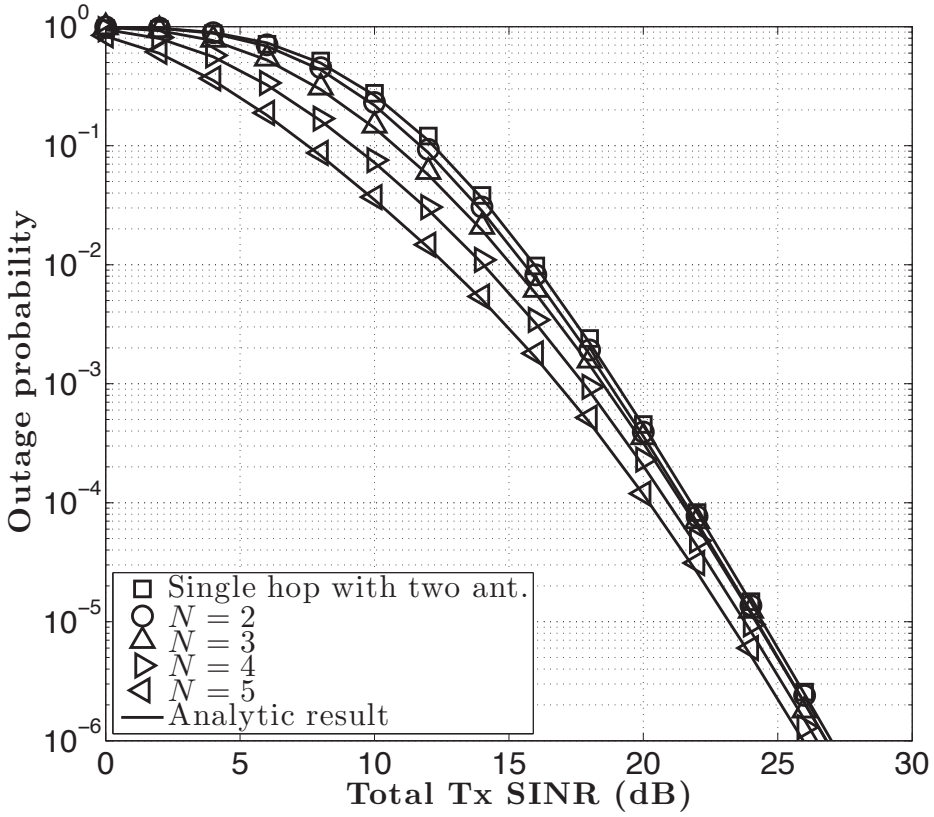

Figure 13: Outage probability for various number of hops without shadowing when $M = 1$.

order as two. As expected, the outage probability is improved when the number of hops increases because the reduced distance between terminals decreases the impact of path loss. It can be observed that the impact of path loss is relatively insensitive in the high SINR region, so that the outage performance improvement is more salient in the low SINR region than in the high SINR region. In addition, unlike the result in Fig. 12, the performance gap increases as the number of hops increases because the impact of path loss is not proportional to the reduced distance due to the path-loss exponent. If the path-loss exponent is increased, the performance gap is increased exponentially. The figure indicates that the multi-hop transmission is more power efficient in the low SINR than in the high SINR when shadowing is not considered.

Figures 14 and 15 show the effects of the numbers of branches and hops when

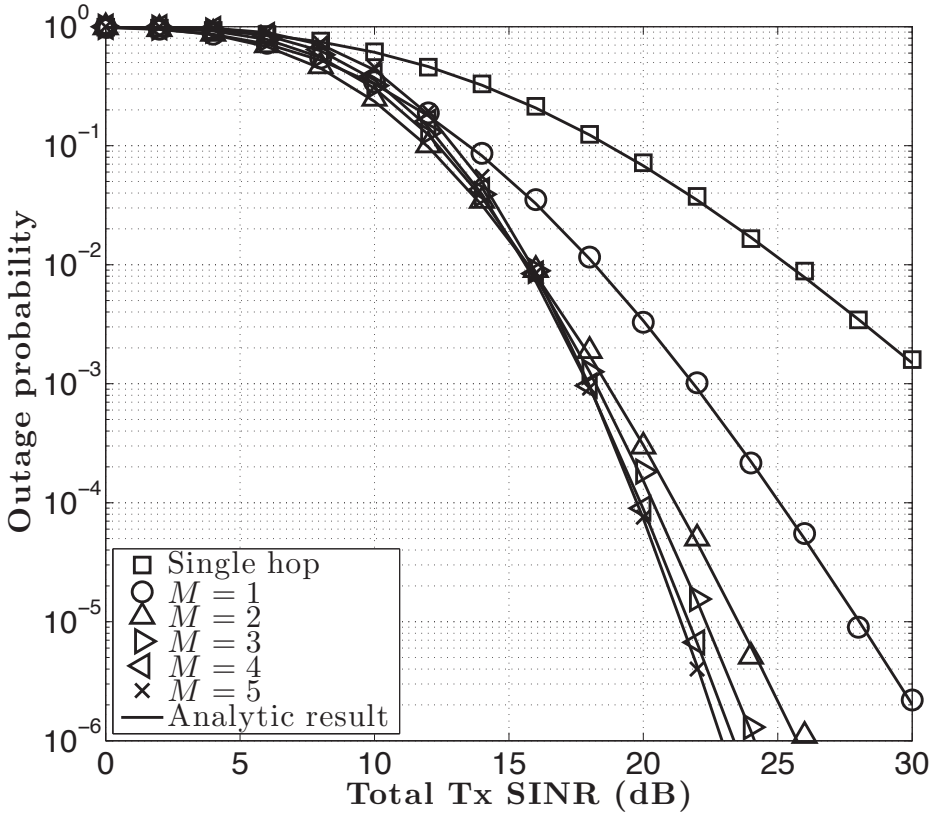

Figure 14: Outage probability for various number of branches with shadowing when N=2, $\sigma_X = 3$ dB, and $\sigma_Y = 3$ dB.

shadowed-Nakagami/shadowed-Nakagami channels are considered. The shadow standard deviations for all the desired signals, σ_X, and for all the interfering signals, σ_Y, are also 3 dB. Compared to the curves in Fig. 12, those in Fig. 14 are degraded because of shadowing, but the cooperative-diversity gain also improves the outage performance when the number of branches increases.

Compared to Fig. 13, Figure 15 depicts the performance improvement against shadowing, which is provided by increasing the number of hops, holds for not only the low SINR region but also the high SINR region.

Figure 16 evaluates the end-to-end ASEP, which is analytically obtained from (64), with and without shadowing in the Nakagami-m fading channels. Note that since (64) is obtained from (60), which is verified in Figs. 12, 13, 14, and 15 by the simulations,

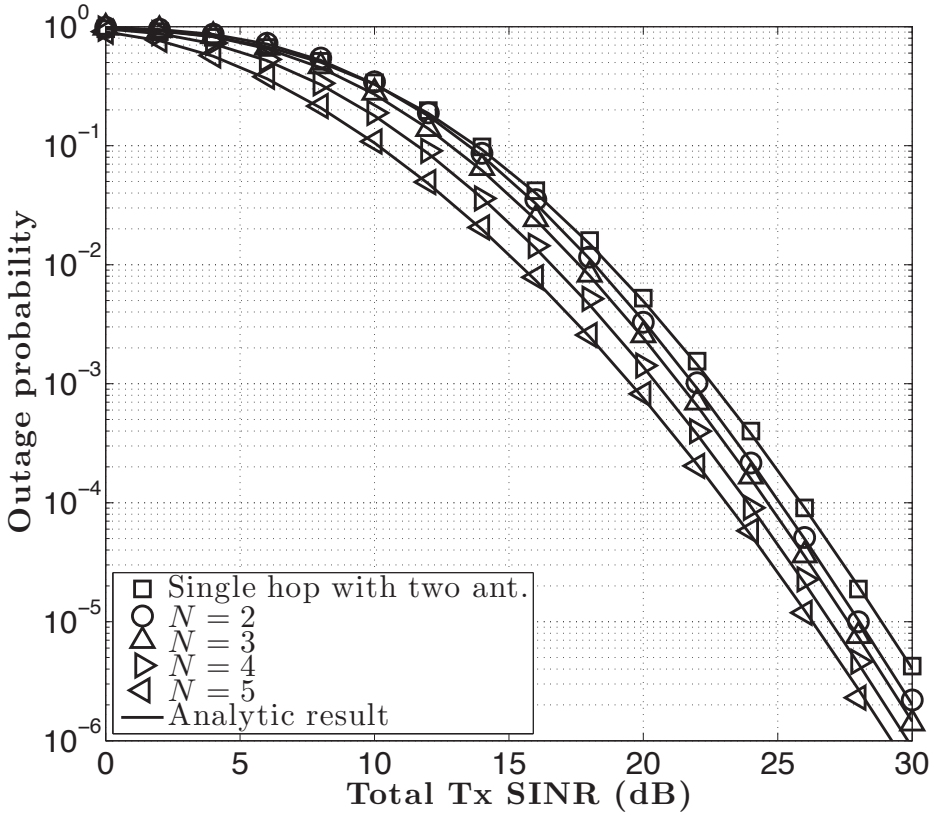

Figure 15: Outage probability for various number of hops with shadowing when M=1, $\sigma_X = 3$ dB, and $\sigma_Y = 3$ dB.

the analytic results after Fig. 15 are not necessary to be verified again. The figure shows a comparison of various relay topologies, but the total number of relays is fixed as $K = 4$, which includes three topologies: $M = 1$ and $N = 5$, $M = 2$ and $N = 3$, and $M = 4$ and $N = 2$. With only Nakagami-m fading channels, the system with $N = 5$ outperforms the other systems in the low SINR region, but this system shows the worst performance in the high SINR region. However, the system with $M = 4$ exhibits the best performance in the high SINR region, but worse performance than that of the other systems in the low SINR region. We can observe that the outage and error performances in the low SINR region can be improved by increasing the number of hops, while increasing the number of branches can improves the performances in the high SINR. However, when shadowing is considered with the shadow standard

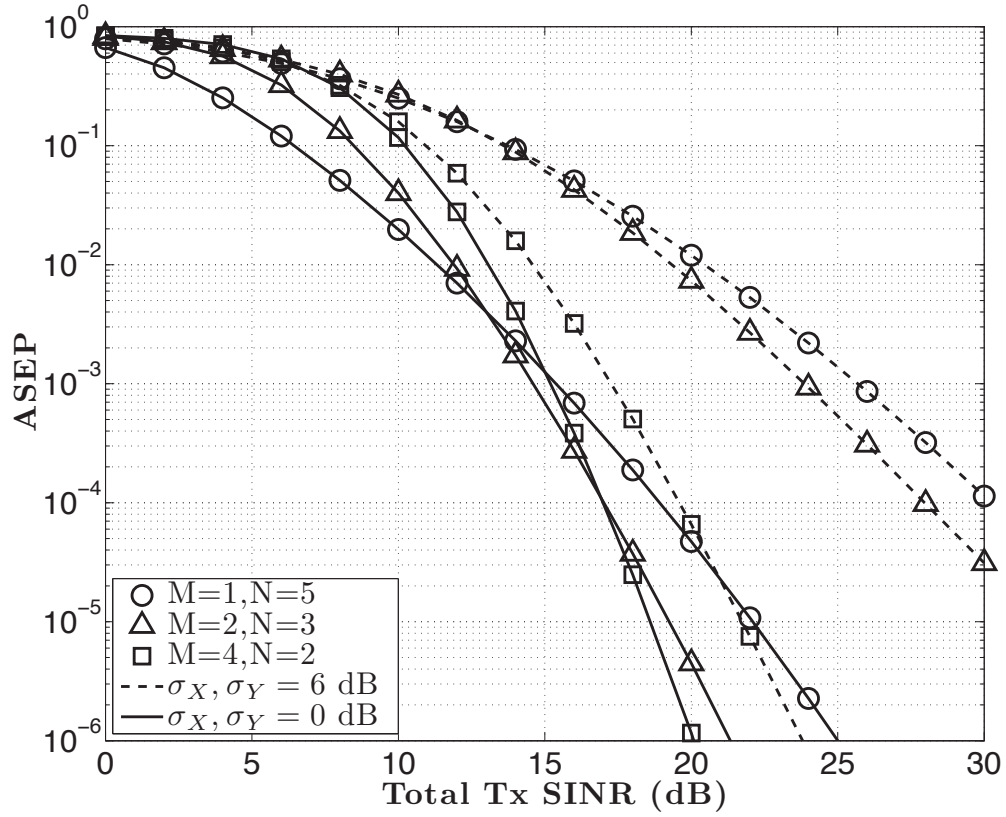

Figure 16: ASEP of 16-QAM for the MBMH cooperative relaying systems with $K = 4$ when $\sigma_X = \sigma_Y = 0$ dB and $\sigma_X = \sigma_Y = 6$ dB.

deviations for all signals $\sigma_X = \sigma_Y = 6$ dB, the behavior of the systems changes. In particular, the system with $N = 5$ exhibits the worst performance, and the system with $M = 4$ outperforms the other systems in the entire SINR region. The result demonstrates that the cooperative-diversity gain achieved by increasing the number of branches improves the outage and error performances against shadowing more efficiently than the multi-hop transmission.

Figure 17 presents the impact of the placement of co-channel interferer for the system with $M = 4$ and $N = 3$ over Nakagami/Nakagami channels. In the figure, a single co-channel interferer with 10 dB Tx INR is considered at each relay. The figure shows a comparison of ASEPs in three scenarios: First, the interferer is located in the first hop, which is referred to as "interfered first relays" such that the first hop

relays are affected mainly by CCI. Second, the interferer is placed in the second hop, which is referred to as "interfered middle relays" such that the relays in the middle of hops are interfered largely. Third, the interferer is placed in the last hop, which is referred to as "interfered destination." As a reference, the system with equally distant interferers is provided, in which all the terminals are corrupted by an interferer with the normalized distance $d_{l,n}^{m}/d_0 = 1$. As the normalized distance becomes 0.5, all the curves are degraded since the interferers are closely placed. Significant results are that as the SINR increases, the system with the interfered destination shows the worst performance, and the system with interfered middle relays outperforms the other systems. Although the normalized distance changes to 0.25, the order of the performance curves remains the same. In the multi-hop diversity system with regenerative relaying, a weak link is the hop between the source and the first relay, thus, the outage and error performances are better when the first relay is close to the source than when the last relay is close to the destination [10]. However, the DF MBMH cooperative relaying system shows that the weak link of the multi-hop diversity system can be made up by multiple branches, thus the outage and error performances depend on the diversity combining in the destination.

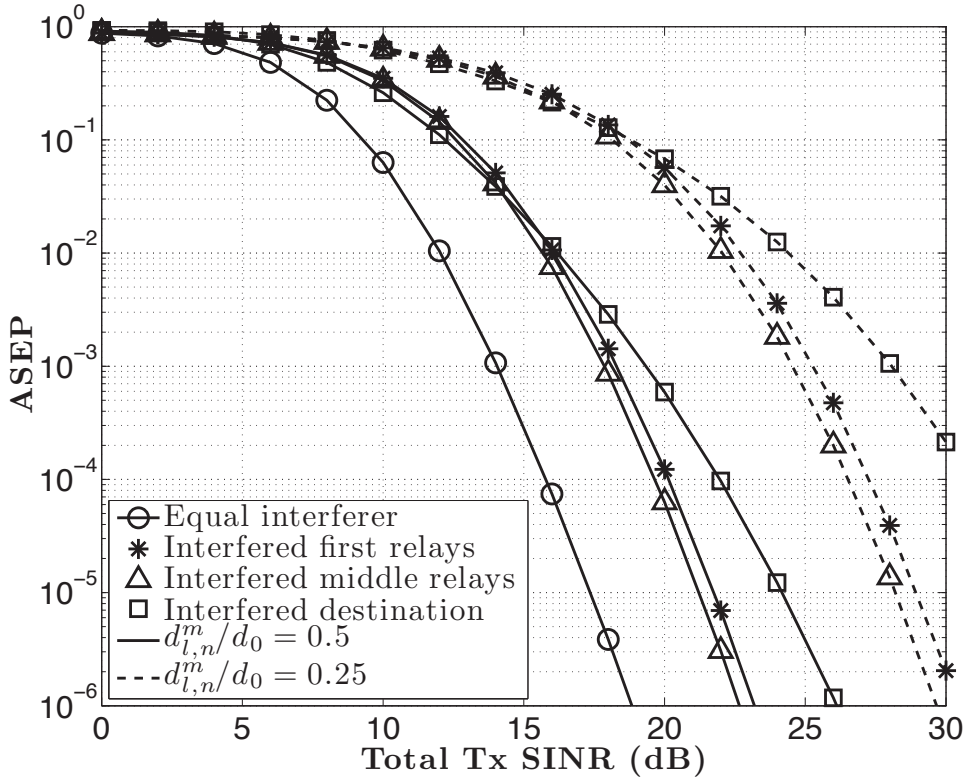

Figure 17: ASEP comparison of the placement of interferers when $M = 4$, $N = 3$, $L = 1$ and $\sigma_X = \sigma_Y = 0$ dB.

CHAPTER V

COOPERATIVE DIVERSITY SYSTEMS WITH SELECTION COMBINING IN CELLULAR NETWORKS

5.1 Overview

In general, the performance of cooperative diversity schemes depends on the number of relays, the placement of relays, and the allocation of power. In addition, it is well known that cellular networks are interference limited rather than noise limited [23]. Hence, the cooperative diversity schemes can be vulnerable to CCI, because the relays may all use the same frequency, and CCI might exist on every link in the cellular relay network.

We investigate and compare the outage probability on the forward channel of a DF cooperative diversity system and an AF cooperative diversity system to that of a dual-Rx antenna system, where the system uses selective combining in the presence of CCI. The cooperative diversity systems in this chapter employ dual-branch diversity, which is applied to a traditional three-node-relay system [1], and was originally proposed to increase the capacity of cellular networks [13].

The systems in this chapter use SC because it does not require continuous monitoring of CSI. Thus SC has low complexity and is often suggested for macro-diversity systems in cellular networks. This chapter assumes shadowed Nakagami faded desired signals on their respective paths in the presence of multiple shadowed Rayleigh faded co-channel interferers.

5.2 System and Channel Models

This chapter considers a traditional cooperative-diversity scheme consisting of a source S, a destination D, and a relay R. Each radio path is affected by N_I co-channel interferers. A system model of this work in cellular networks is depicted in Fig. 18. The destination employs SC to combine the received signals at the mobile station.

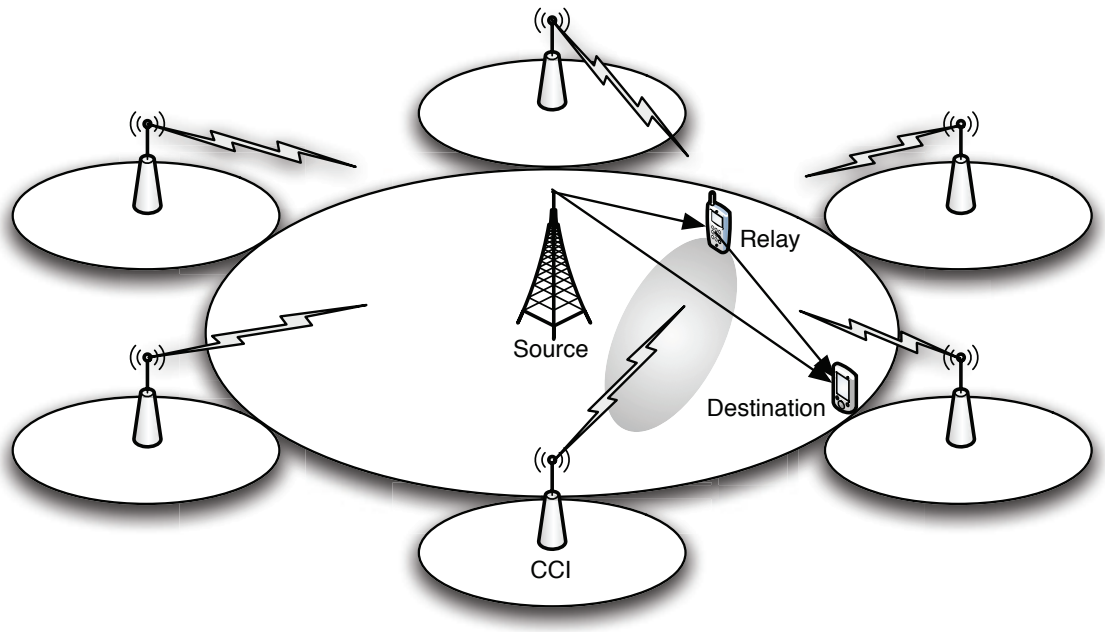

Figure 18: Cooperative cellular relaying system

The channels in this chapter are affected by path loss, shadowing, and fading. Path loss and shadowing are significant factors that determine the connectivity between nodes. In addition, the desired signal is affected by quasi-static flat Nakagami fading, and the interfering signals are affected by quasi-static flat Rayleigh fading.

Therefore, the received signals of the source-to-destination, source-to-relay, and relay-to-destination paths are,

$$y_{S,D} = x_S \cdot g_{S,D}\sqrt{P_S} + n_D + \sum_{l=1}^{N_I} I_l \ ,$$
$$y_{S,R} = x_S \cdot g_{S,R}\sqrt{P_S} + n_R + \sum_{l=1}^{N_I} I_l \ ,$$
$$y_{R,D} = g_{R,D} \cdot \mathbf{S} + n_D + \sum_{l=1}^{N_I} I_l \ , \tag{65}$$

respectively, where x is the transmitted symbol with unit power, P is the transmit power, and n is AWGN with zero mean and a variance σ^2. In the DF scheme, $\mathbf{S} = x_R \cdot \sqrt{P_R}$ for the regenerated signals, but $\mathbf{S} = A \cdot y_{S,R}$ in the AF scheme, where A is the amplification factor [51]. The relay is placed in the same cell as the source and the destination, and they are fixed during a time slot. The channel gain of the source-to-destination path can be written as $g_{S,D} = \sqrt{(c \cdot s_{S,D} \cdot p_{S,D})} f_{S,D}$, where c is a constant representing the transmit and receive antenna gains; $p_{S,D}$ is the path loss between the source and the destination; $s_{S,D}$ is the log-normal shadow-fading factor; and $|f_{S,D}|$ has a Nakagami distribution, and $|f_{S,D}|^2$ has a Gamma distribution. The channel gains of the source-to-relay and relay-to-destination paths can be similarly defined. A two-slope path-loss model [44] is used to describe the path loss, $p_{S,D}$, as shown below.

$$\frac{P_r}{P_t} = \frac{1}{d^a \left(1 + \frac{d}{g}\right)^b} \ , \tag{66}$$

where P_t is the transmitted power, P_r is the received power, and d is the distance between the transmitter and the receiver, g is the turning point, a is the basic attenuation coefficient, and b is the additional attenuation coefficient.

The allocation of transmit power is an important factor because the received SINR is proportional to the transmit power. However, to compare the performance of cooperative diversity and dual-Rx diversity fairly, the total end-to-end transmit

power should be fixed [52]. The cooperative power ratio, denoted by ζ, is defined as follows:

$$P_{\text{tot}} = P_S + P_R \ , \quad \frac{P_R}{P_S} = \zeta \ , \tag{67}$$

where P_{tot} is the total end-to-end transmit power.

To geometrically describe the location of the relay and the destination, the length of the source-destination path is set to $d_{S,D}$; the length of the source-relay path, $d_{S,R}$, is $k \cdot d_{S,D}$, where $0 < k \leq 1$. Thus, the length of the relay-destination path, $d_{R,D}$, is $d_{S,D}\sqrt{k^2 - 2k\cos\theta + 1}$, where θ is the angle between the source-relay and source-destination paths.

5.3 Per-hop Statistical Distribution

The channels between the nodes can be modeled by a composite distribution due to shadowing and fading. The channel for the desired signal is Nakagami-m faded with log-normal shadowing, since a line-of-sight may exist between the nodes. In contrast, the interferers are Rayleigh faded with log-normal shadowing since the interferers are usually located in the distance with non-line-of sight conditions [44]. The composite pdf for the incoherent power sum of multiple Rayleigh faded co-channel interferers with log-normal shadowing can be approximated by a log-normal distribution [44]. Therefore, the joint pdf for a composite log-normal Nakagami-m distribution and a log-normal distribution leads to the outage probability for each path, and the overall outage probability with selective combining can be determined as a function of the outage probabilities of the individual paths.

In this chapter, both co-channel interference and Gaussian noise are considered so that the outage probability is

$$P_o(\lambda_{th}) = \mathrm{P}_r\left(\frac{P_X}{P_Y + \sigma^2} < \lambda_{\text{th}}\right) \ , \tag{68}$$

where P_X and P_Y are the signal power of the desired signal and interfering signals, respectively, σ^2 is the Gaussian noise power, and λ_{th} is the threshold.

Let X be the SNR of the desired signal, and Y be the total INR of N_I co-channel interferers. Thus, Y can be expressed as

$$Y = \sum_{i=1}^{N_I} Y_i \ , \tag{69}$$

where Y_i is the i-th INR.

The SINR Z is given by

$$Z = \frac{P_X}{P_Y + \sigma^2} = \frac{P_X/\sigma^2}{P_Y/\sigma^2 + 1} = \frac{X}{Y+1} \ . \tag{70}$$

Since both SNR and INR are proportional to the squared envelope of the received signal, the composite pdf for the log-normal Nakagami-m distributed SNR is given by

$$p_X(x) = \int_0^\infty \left(\frac{m_X}{\omega_X}\right)^{m_X} \frac{x^{m_X-1}}{\sqrt{2\pi}\sigma_X\omega_X\Gamma(m_X)} \exp\left\{-\frac{m_X x}{\omega_X} - \frac{(\ln\omega_X - \ln\Omega_X)^2}{2\sigma_X^2}\right\} d\omega_X, \tag{71}$$

where m_X is the Nakagami shape factor, w_X is the local mean, σ_X is the shadow standard deviation, and Ω_X is the area mean of X [53]. The composite pdf for multiple log-normal Rayleigh distributed INRs conditioned on the number of interferers N_I is approximated by the log-normal distribution

$$p_Y(y|N_I) = \frac{1}{\sqrt{2\pi}\sigma_Y y} \exp\left\{-\frac{(\ln y - \ln\Omega_Y)^2}{2\sigma_Y^2}\right\} \ , \tag{72}$$

where σ_Y is the standard deviation and Ω_Y is the area mean of Y as described in [43].

Since the pdf of the SINR Z is defined in (47), Substituting (71) and (72) into (47) yields

$$\begin{aligned} p_Z(z) = \int_0^\infty \int_0^\infty & \frac{(1+y)}{2\pi\sigma_X\omega_X\sigma_Y y} \left(\frac{m_X}{\omega_X}\right)^{m_X} \frac{\{z(y+1)\}^{m_X-1}}{\Gamma(m_X)} \\ & \times \exp\left\{-\frac{m_X}{\omega_X} z(y+1) - \frac{(\ln\omega_X - \ln\Omega_X)^2}{2\sigma_X^2} - \frac{(\ln y - \ln\Omega_Y)^2}{2\sigma_Y^2}\right\} d\omega_X dy. \end{aligned} \tag{73}$$

Using a change in the variables of integration $t_1 = (\ln \omega_X - \ln \Omega_X)/\sqrt{2}\sigma_X$, $t_2 = (\ln y - \ln \Omega_Y)/\sqrt{2}\sigma_Y$, (73) can be computed by using Gauss-Hermite quadrature integration as follows:

$$\begin{aligned} p_Z(z) &= \int_{-\infty}^{\infty}\int_{-\infty}^{\infty} \frac{1}{\pi}\Phi(t_1,t_2)^{m_X}\frac{z^{m_X-1}}{\Gamma(m_X)}\exp\left\{-\Phi(t_1,t_2)z\right\}\exp(-t_1^2-t_2^2)\ dt_1dt_2 \\ &= \sum_{i=1}^{N_p}\sum_{j=1}^{N_p} H_{x_i}H_{x_j}G(x_i,x_j) + R_m \ , \end{aligned} \tag{74}$$

where H_{x_i} and H_{x_j} are the weight factors, x_i and x_j are the zeros of the Hermite polynomial, N_p is the order of the Hermite polynomial, R_m is a very small value, and

$$G(x_i,x_j) = \frac{1}{\pi}\Phi(x_i,x_j)^{m_X}\frac{z^{m_X-1}}{\Gamma(m_X)}\exp(-\Phi(x_i,x_j)z), \tag{75}$$

where

$$\Phi(x_i,x_j) = m_X\frac{\exp(\sqrt{2}\sigma_Y x_j + \ln\Omega_Y)+1}{\exp(\sqrt{2}\sigma_X x_i + \ln\Omega_X)} \ . \tag{76}$$

Therefore, by using (74), the outage probability becomes

$$\begin{aligned} P_o(\lambda_{th}) &= \mathrm{P}_r\left(\frac{P_X}{P_Y+\sigma^2} < \lambda_{th}\right) \\ &= \int_{-\infty}^{\infty}\frac{1}{\pi}\exp(-t_1^2)\int_{-\infty}^{\infty}\exp(-t_2^2)\frac{\Phi(t_1,t_2)^{m_X}}{\Gamma(m_X)}\int_0^{\lambda_{th}}\exp\{-\Phi(t_1,t_2)z\}z^{m_X-1}dzdt_1dt_2 \\ &= \int_{-\infty}^{\infty}\int_{-\infty}^{\infty}\frac{1}{\pi\Gamma(m_X)}\gamma\{m_X,\lambda_{th}\Phi(t_1,t_2)\}\exp(-t_1^2)\exp(-t_2^2)\ dt_1dt_2 \\ &= \sum_{i=1}^{N_p}\sum_{j=1}^{N_p} H_{x_i}H_{x_j}F(x_i,x_j) + R_m \ , \end{aligned} \tag{77}$$

where

$$F(x_i,x_j) = \frac{1}{\pi\Gamma(m_X)}\gamma\{m_X,\lambda_{th}\Phi(x_i,x_j)\} \ , \tag{78}$$

and $\gamma(\cdot,\cdot)$ is the incomplete Gamma function.

5.4 Outage Probability of DF Cooperative Diversity

The overall outage probability of DF cooperative diversity can be expressed as a function of the outage probabilities of the respective paths, since the DF scheme

exhibits independent performance for each path. Based on the geometric information in Section 5.2, area mean power of the signal-to-interference ratio (SIR) between the nodes can be expressed in terms of path loss in (66) and the cooperative power ratio in (67) as follows:

$$\begin{aligned}
\frac{\Omega_{S,D}}{\Omega_Y} &= \frac{R_u^a (G+R_u)^b}{(1+\zeta)(G+1)^b} = \epsilon_{S,D} \ , \\
\frac{\Omega_{R,D}}{\Omega_Y} &= \frac{\zeta (R_u/K)^a (G+R_u/K)^b}{(1+\zeta)(G+1)^b} = \epsilon_{R,D} \ , \\
\frac{\Omega_{S,R}}{\Omega_Y} &= \frac{(R_u/k)^a (G+R_u/k)^b}{(1+\zeta)(G+1)^b} = \epsilon_{S,R} \ ,
\end{aligned} \tag{79}$$

where $R_u = D/R$ is the co-channel reuse factor (D is the co-channel reuse distance and R is the cell radius), $K = \sqrt{k^2 - 2k\cos\theta + 1}$, and $G = g/R$. We assume that the transmitted power of the co-channel interferers is the same as P_{tot},and D is the co-channel reuse distance. Although link imbalance exists in different directions between a relay/destination and interferers [2], we assume that all interferers are situated at distance D from the relay and destination.

From (70) and (79), the area mean power of the source-to-relay path and the relay-to-destination path can be expressed in terms of the average SINR of the source-to-destination path, path loss, and the average INR as follows:

$$\begin{aligned}
\Omega_{S,R} &= \frac{\epsilon_{S,R}}{\epsilon_{S,D}} Z_{S,D} (\Omega_Y + 1) \ , \\
\Omega_{R,D} &= \frac{\epsilon_{R,D}}{\epsilon_{S,D}} Z_{S,D} (\Omega_Y + 1) \ ,
\end{aligned} \tag{80}$$

where $Z_{S,D}$ is the average SINR of the source-to-destination path.

The outage probability of the source-to-destination path in the DF scheme is denoted by $P_{o,DF}(\lambda_{th}|\Omega_{S,D})$, that of the source-to-relay path by $P_{o,DF}(\lambda_{th}|\Omega_{S,R})$, and that of the relay-to-destination path by $P_{o,DF}(\lambda_{th}|\Omega_{R,D})$. Then, for the DF scheme,

the outage probability of the source-relay-destination path is given by

$$\begin{aligned} P_{o,DF}(\lambda_{th}|\Omega_{S,R},\Omega_{R,D}) &= 1 - Pr(z_{S,R} > \lambda_{th})Pr(z_{R,D} > \lambda_{th}) \\ &= 1 - (1 - P_{o,DF}(\lambda_{th}|\Omega_{S,R}))(1 - P_{o,DF}(\lambda_{th}|\Omega_{R,D})). \end{aligned} \tag{81}$$

For the special case of $m_X = 1$ (Rayleigh fading), the per-hop outage probability is calculated from (77) as

$$P_{o,DF}(\lambda_{th}|\Omega) = \sum_{i=1}^{N_p}\sum_{j=1}^{N_p} H_{x_i}H_{x_j}\frac{1}{\pi}\Big[1 - \exp\{-\lambda_{th}\Phi(x_i,x_j)\}\Big]. \tag{82}$$

Thus, the overall outage probability of SC is obtained by the product of the outage probabilities of each branch, i.e.,

$$P_{o,DF}(\lambda_{th}|SC) = P_{o,DF}(\lambda_{th}|\Omega_{S,D})P_{o,DF}(\lambda_{th}|\Omega_{S,R},\Omega_{R,D}) \ . \tag{83}$$

Substituting (77), (79), and (81) into (83) yields the overall outage probability of DF cooperative diversity with SC.

5.5 Outage Probability of AF Cooperative Diversity

In this chapter, the AF cooperative diversity scheme employs semi-blind fixed-gain relaying as in [51]. Semi-blind relaying shows comparable performance to CSI-assisted relaying, and it has low complexity since the instantaneous CSI is not needed. Moreover, the semi-blind method, which averages the CSI over a time period, follows the slow fading in a shadowed channel.

From (65), the SINR of the source-relay-destination path in AF cooperative diversity can be described as [51]

$$z_{S,R,D} = \frac{|g_{S,R}|^2|g_{R,D}|^2A^2P_S}{(|g_{R,D}|^2A^2+1)(\sigma^2+I)} = \frac{z_{S,R}z_{R,D}}{z_{R,D}+C} \ , \tag{84}$$

where P_S is the signal power of the source, and I is the total interference power of N_I co-channel interferers, and $z_{S,R}$, $z_{R,D}$ are the SINRs of the source-to-relay and

relay-to-destination paths, respectively, and C is expressed as [51]

$$C = \frac{P_R}{A^2(\sigma^2 + I)} \ , \tag{85}$$

where P_R is the signal power of the source.

For the semi-blind relay, the amplification factor A is defined as [51]

$$A^2 = \mathbf{E}\left[\frac{P_R}{P_S|g_{S,R}|^2 + (\sigma^2 + I)}\right] = \frac{P_R}{\mathbf{E}\{\sigma^2 + I\}}\mathbf{E}\left[\frac{1}{z_{S,R} + 1}\right] \ . \tag{86}$$

With the per-hop pdf in (74), the second term of (86) can be obtained as

$$\begin{aligned}\mathbf{E}\left[\frac{1}{z_{S,R} + 1}\right] &= \sum_{i=1}^{N_p}\sum_{j=1}^{N_p} H_{x_i}H_{x_j}\frac{\Phi(x_i, x_j)^{m_X}}{\pi\Gamma(m_X)}\int_0^\infty \frac{z_{S,R}^{m_X - 1}\exp\{-\Phi(x_i, x_j)z_{S,R}\}}{z_{S,R} + 1}dz_{S,R} \\ &= \sum_{i=1}^{N_p}\sum_{j=1}^{N_p} H_{x_i}H_{x_j}\frac{\Phi(x_i, x_j)}{\pi}\Psi(1, 2 - m_X; \Phi(x_i, x_j)),\end{aligned} \tag{87}$$

where $\Psi(\cdot, \cdot; \cdot)$ is the confluent hypergeometric function of the second kind [54].

With these results, the outage probability of the source-relay-destination path can be obtained from the outage probability by conditioned on $z_{R,D}$ as follows:

$$\begin{aligned}P_{o,AF}(\lambda_{th}|\Omega_{S,R}, \Omega_{R,D}) &= \int_0^\infty Pr\left[\frac{z_{S,R}z_{R,D}}{z_{R,D} + C} < \lambda_{th}|z_{R,D}\right] p_{Z_{R,D}}(z_{R,D})\ dz_{R,D} \\ &= \int_0^\infty Pr\left[\psi \cdot z_{S,R} < \lambda_{th}|z_{R,D}\right] p_{Z_{R,D}}(z_{R,D})\ dz_{R,D} \ ,\end{aligned} \tag{88}$$

where $z_{S,R,D} = \psi \cdot z_{S,R}$, and $\psi = \frac{z_{R,D}}{z_{R,D}+C}$. Since $\psi > 0$, the probability term inside integral can be written as the outage probability of $z_{S,R}$, which is given in (77), viz.,

$$Pr\left[z_{S,R} < \frac{\lambda_{th}}{\psi}\right] = \sum_{i=1}^{N_p}\sum_{j=1}^{N_p} H_{x_i}H_{x_j}F'(x_i, x_j) + R_m, \tag{89}$$

where

$$F'(x_i, x_j) = \frac{1}{\pi\Gamma(m_X)}\gamma\left\{m_X, \lambda_{th}\left(1 + \frac{C}{z_{R,D}}\right)\Phi(x_i, x_j)\right\} \ , \tag{90}$$

and

$$\Phi(x_i, x_j) = m_X\frac{\exp(\sqrt{2}\sigma_Y x_j + \ln\Omega_Y) + 1}{\exp(\sqrt{2}\sigma_{S,R}x_i + \ln\Omega_{S,R})} \ . \tag{91}$$

In (88), the pdf of $z_{R,D}$ is given by

$$p_{Z_{R,D}}(z_{R,D}) = \sum_{k=1}^{N_p}\sum_{l=1}^{N_p} H_{x_k}H_{x_l}G(x_k,x_l) + R_m \ , \tag{92}$$

where

$$G(x_k,x_l) = \frac{\Phi(x_k,x_l)^{m_X} z_{R,D}^{m_X-1}}{\pi\Gamma(m_X)} \exp\{-\Phi(x_k,x_l)z_{R,D}\} \tag{93}$$

and

$$\Phi(x_k,x_l) = m_X \frac{\exp(\sqrt{2}\sigma_Y x_l + \ln\Omega_Y) + 1}{\exp(\sqrt{2}\sigma_{R,D}x_k + \ln\Omega_{R,D})} \ . \tag{94}$$

Therefore, the outage probability of the source-relay-destination path in AF cooperative diversity can be obtained by the integration of the product between (89) and (92) as follows:

$$\begin{aligned}
&P_{o,AF}(\lambda_{th}|\Omega_{S,R},\Omega_{R,D}) \\
&= \int_0^\infty \left\{\sum_{i=1}^{N_p}\sum_{j=1}^{N_p} H_{x_i}H_{x_j}F'(x_i,x_j)\right\}\left\{\sum_{k=1}^{N_p}\sum_{l=1}^{N_p} H_{x_k}H_{x_l}G(x_k,x_l)\right\} dz_{R,D} \\
&= \sum_{i=1}^{N_p}\sum_{j=1}^{N_p}\sum_{k=1}^{N_p}\sum_{l=1}^{N_p} H_{x_i}H_{x_j}H_{x_k}H_{x_l}\frac{\Phi(x_k,x_l)^{m_X}}{\{\pi\Gamma(m_X)\}^2}\int_0^\infty \gamma\left\{m_X,\lambda_{th}\left(1+\frac{C}{z_{R,D}}\right)\Phi(x_i,x_j)\right\} \\
&\quad \times z_{R,D}^{m_X-1}\exp\{-\Phi(x_k,x_l)z_{R,D}\}dz_{R,D} \ .
\end{aligned} \tag{95}$$

For convenience, the variables in (95) are simplified as $z = z_{R,D}, \Phi_1 = \Phi(x_i,x_j), \Phi_2 = \Phi(x_k,x_l)$. Then, the integral term in (95) can be manipulated by using a series expression of the incomplete Gamma function as follows:

$$\begin{aligned}
&\int_0^\infty \gamma\left\{m_X,\lambda_{th}\left(1+\frac{C}{z}\right)\Phi_1\right\} z^{m_X-1}\exp(-\Phi_2 z)dz \\
&= (m_X-1)!\Big[\int_0^\infty z^{m_X-1}\exp(-\Phi_2 z)dz - \exp(-\lambda_{th}\Phi_1)\sum_{m=0}^{m_X-1}\frac{(\lambda_{th}\Phi_1)^m}{m!}\int_0^\infty\left(1+\frac{C}{z}\right)^m \\
&\quad \times \exp\left(-\lambda_{th}\Phi_1\frac{C}{z} - \Phi_2 z\right) z^{m_X-1}dz\Big] \ ,
\end{aligned} \tag{96}$$

where the second integral term can be written as

$$\int_0^\infty \exp\left(-\lambda_{th}\Phi_1\frac{C}{z}-\Phi_2 z\right)\left(1+\frac{C}{z}\right)^m z^{m_X-1}dz$$
$$=\sum_{n=0}^{m}\binom{m}{n}2C^n\left(\frac{\Phi_2}{\lambda_{th}\Phi_1 C}\right)^{\frac{1}{2}(n-m_X)}K_{n-m_X}\left(2\sqrt{\lambda_{th}\Phi_1\Phi_2 C}\right)\ , \qquad (97)$$

and where $K_n(z)$ is the modified Bessel function of the second kind [54].

Finally, substituting (96) and (97) into (95) leads to the outage probability of the AF relaying path as follows:

$$P_{o,AF}(\lambda_{th}|\Omega_{S,R},\Omega_{R,D})$$
$$=\sum_{i=1}^{N_p}\sum_{j=1}^{N_p}\sum_{k=1}^{N_p}\sum_{l=1}^{N_p}H_{x_i}H_{x_j}H_{x_k}H_{x_l}\ \frac{1}{\pi^2}\Big[1-\frac{\exp\{-\lambda_{th}\Phi(x_i,x_j)\}\Phi(x_k,x_l)^{m_X}}{\Gamma(m_X)}$$
$$\times\sum_{m=0}^{m_X-1}\frac{\{\lambda_{th}\Phi(x_i,x_j)\}^m}{m!}\sum_{n=0}^{m}\binom{m}{n}2C^n\left\{\frac{\Phi(x_k,x_l)}{\lambda_{th}\Phi(x_i,x_j)C}\right\}^{\frac{1}{2}(n-m_X)}$$
$$\times K_{n-m_X}\left\{2\sqrt{\lambda_{th}\Phi(x_i,x_j)\Phi(x_k,x_l)C}\right\}\Big]\ . \qquad (98)$$

Note that the special case of $m_X = 1$ (98) reduces to the same result in [51], as follows:

$$P_{o,AF}(\lambda_{th}|\Omega_{S,R},\Omega_{R,D})$$
$$=\sum_{i=1}^{N_p}\sum_{j=1}^{N_p}\sum_{k=1}^{N_p}\sum_{l=1}^{N_p}H_{x_i}H_{x_j}H_{x_k}H_{x_l}\frac{1}{\pi^2}\Big[1-\exp\{-\lambda_{th}\Phi(x_i,x_j)\}$$
$$\times 2\sqrt{\lambda_{th}C\Phi(x_i,x_j)\Phi(x_k,x_l)}K_1\Big\{2\sqrt{\lambda_{th}\Phi(x_i,x_j)\Phi(x_k,x_l)C}\Big\}\Big]\ . \qquad (99)$$

Therefore, the overall outage probability of SC in AF cooperative diversity is obtained by the product of the outage probabilities of each branch, $P_{o,AF}(\lambda_{th}|\Omega_{S,D})$ and $P_{o,AF}(\lambda_{th}|\Omega_{S,R},\Omega_{R,D})$ like (83), where $P_{o,AF}(\lambda_{th}|\Omega_{S,D}) = P_{o,DF}(\lambda_{th}|\Omega_{S,D})$ since both are for the direct path.

5.6 Performance Analysis

Our numerical results assume that $m_X = 3$, and the path loss model in (66) with $a = b = 2$. We set $N_I = 6$, representing the first tier of co-channel cells. With

this condition, the incoherently summed INR assumes to have a shadow standard deviation of 3 dB, and the shadow standard deviation of SNR is 6 dB. This section considers that area mean power of summed INR, Ω_Y, is 3 dB, and the threshold SINR is assumed to be $\lambda_{\text{th}} = 10$ dB.

In this section, the AF and DF cooperative-diversity systems with SC are compared to a dual-Rx antenna system that employs SC under the same power constraint. Figures 19, 20, and 21 compare the outage probabilities of the various systems: a system without diversity, dual-Rx antenna system, AF cooperative diversity system, and DF cooperative-diversity system.

Figure 19 depicts the outage probability versus average INR when the SNR of the S-D path is fixed to 25 dB. In the lower INR region, the outage performance of the DF scheme is lower than that of the AF scheme, but over than 9 dB INR, the AF scheme outperforms both the DF system and the dual antenna system. This results show that the AF scheme is robust in interference-limited environments, while the DF scheme shows good performance only for high SNR.

Figure 20 shows the outage probability versus average SNR for the case without CCI (P_Y=0). Thus, the channel is a shadowed-Nakagami channel with $m_X = 3$. In the upper SNR region, the outage performance of the DF scheme is better than that of the AF scheme. In the lower SNR region, the degradation of both cooperative-diversity systems means the single-antenna system with P_{tot} is more effective. However, the transmit power of cooperative system is $\frac{1}{2}P_{tot}$, and the difference gap is comparable. Moreover, both cooperative systems show significant performance improvement in interference-limited system in Fig. 19.

Figure 21 describes the outage probability versus the co-channel reuse factor with $\Omega_Y = 3$ dB. In these figures, the dual-Rx antenna system and cooperative-diversity systems outperform a system without diversity as expected, and significant gap in outage probability is shown between the DF cooperative system without CCI and the

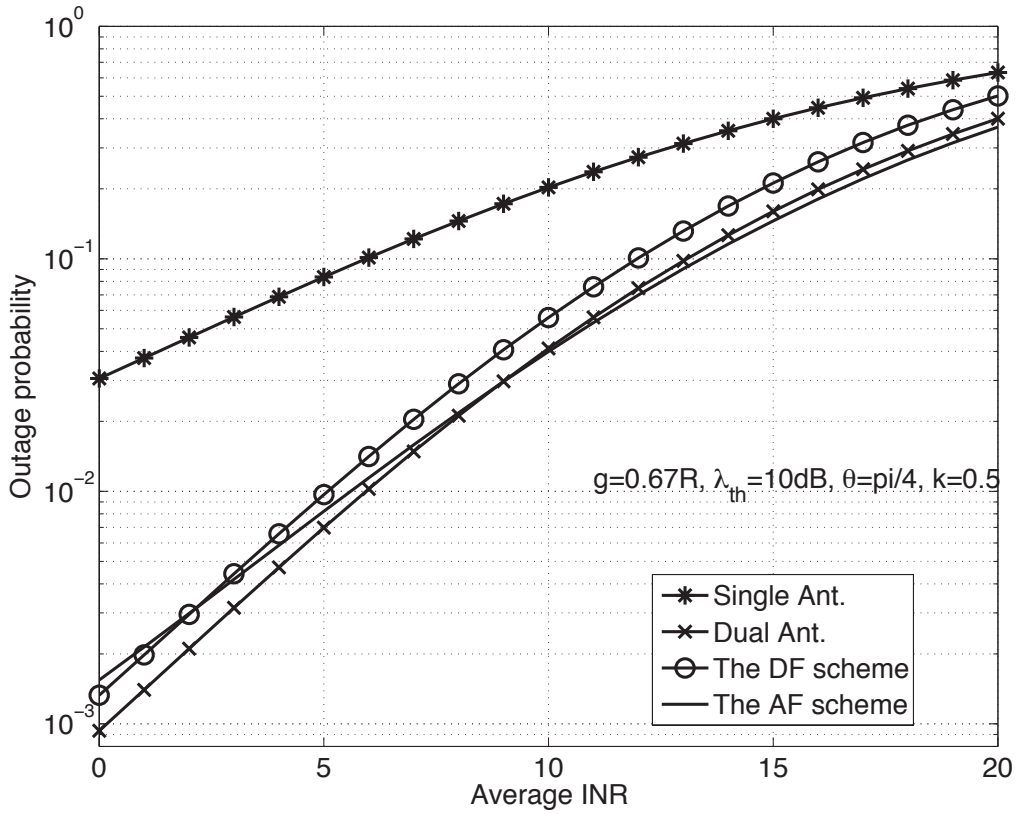

Figure 19: Comparisons of the outage probability versus average INR on a shadowed-Nakagami/shadowed-Rayleigh channel for $\Omega_{S,D} = 25$ dB, where $\zeta = 1$, $R_u = 3$ (3-cell reuse cluster).

other systems. Thus, it is clear that the performance degradation primarily comes from CCI.

This most interesting result is that the outage probability of AF cooperative diversity outperforms that of DF cooperative diversity in this composite channel. In [51], the results showed that the performance of DF relaying is comparable or better to that of AF relaying when there is no CCI and no shadowing in the channel. Since the outage performance of the direct path is the same between both cooperative schemes, the outage performance of cooperative diversity with SC depends on that of the relaying path, but AF cooperative diversity shows superior performance over shadowed-Nakagami fading channel with multiple co-channel interferers. As a result, the DF scheme outperforms the AF scheme only when the channel condition is good

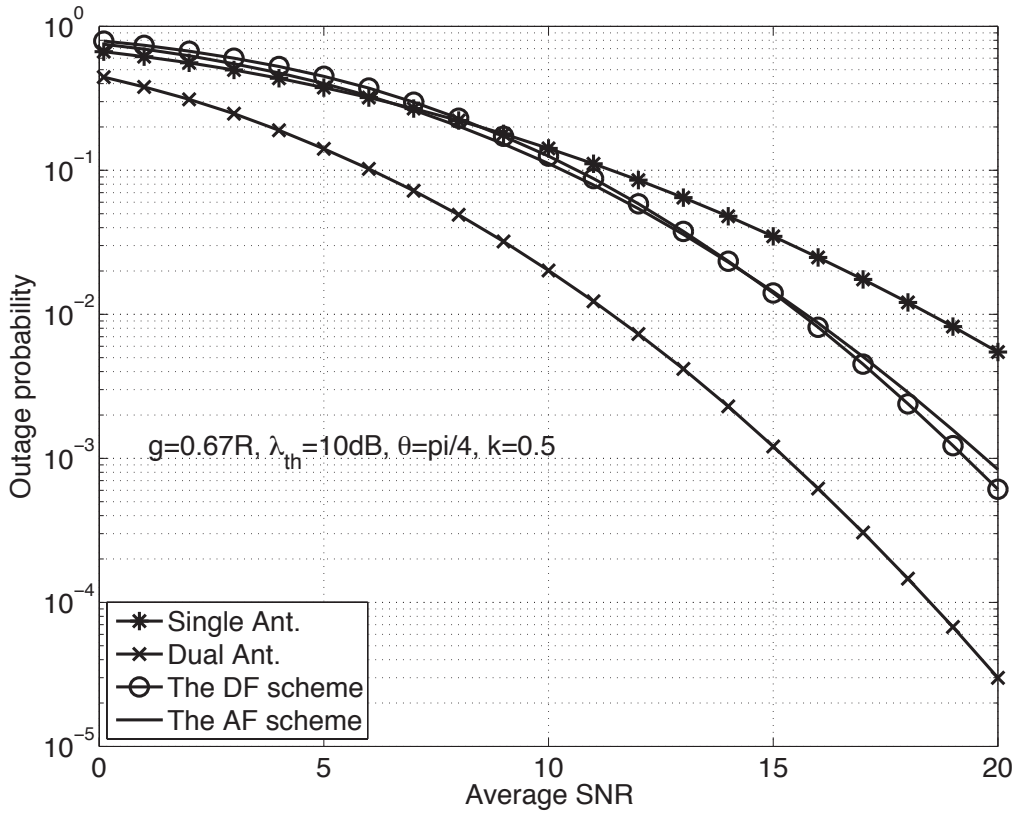

Figure 20: Comparisons of the outage probability versus average SNR on a shadowed-Nakagami channel without CCI, where $\zeta = 1$ and $R_u = 3$.

and SNR is high, but the AF scheme shows better performance than the DF scheme in the high INR. The reason for this interesting behavior is that the DF relay can transmit re-encoded signals without error in the source-relay-destination path when SINR is higher than the threshold, but the AF scheme suffers from noise amplification. Thus, the DF scheme outperforms the AF scheme in the upper SNR region and the lower INR region. In contrast, when the SINR is lower than the threshold the DF relay does not transmit any signal due to detected errors, so it can not contribute to a diversity gain. However, the AF relay transmits amplified signals despite noise amplification; thus, it can contribute to a diversity gain that will overcome the effects of noise amplification. Therefore, the AF scheme outperforms the DF scheme in the upper INR region and the lower SNR region.

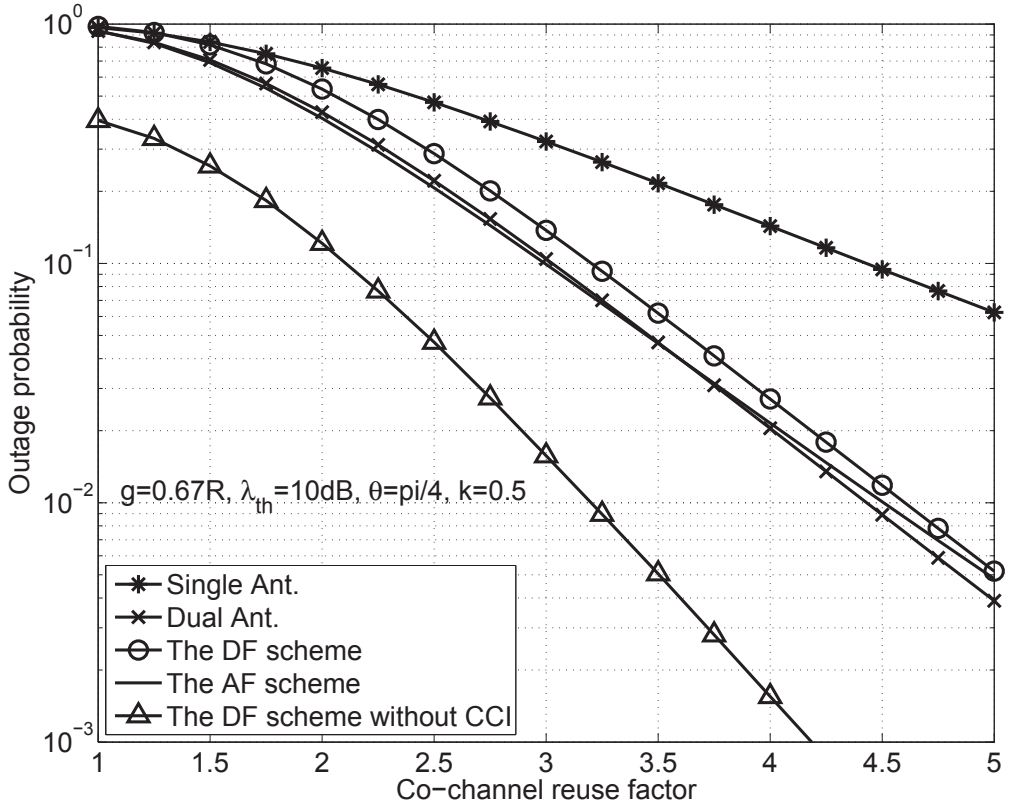

Figure 21: Comparisons of the outage probability versus co-channel reuse factor on a shadowed-Nakagami/shadowed-Rayleigh channel, where $\zeta = 1$ and $\Omega_Y = 3$ dB.

The DF cooperative-diversity system with $\zeta = 1$, which means that $P_S = P_R = \frac{1}{2}P_{\text{tot}}$, shows a performance degradation compared to the dual-Rx antenna system. The reason is that the power of the source P_S in the dual-Rx antenna system is assumed to be the same as total cell power P_{tot} according to the total power constraint. The AF cooperative-diversity system with the same power constraint shows a performance improvement over the lower range of co-channel reuse factor, D/R, in Fig. 21. These results mean that the AF cooperative-diversity system outperforms the other schemes in heavy CCI.

Finally, the relay is fixed with $\theta = \pi/4$ and $k = 0.5$ in Figs. 19, 20, and 21. However, as the geometrical parameters θ and k are varied, the difference between the outage probabilities of the cooperative-diversity systems and the dual-Rx antenna system will vary as well.

Figure 22(a) shows the difference between the outage probabilities of the dual-Rx antenna system and that of the AF cooperative diversity system, and Fig. 22(b) depicts the difference between the outage probabilities of the dual-Rx antenna system and that of the DF cooperative-diversity system, as the relay location is varied in cell. The base station is located in the center of the cell, and the destination mobile terminal is located on the rightmost edge of the cell. Both cooperative-diversity systems in Fig. 22 assume that every node uses the same transmit power, and total power in the cell is the same as P_{tot}. The area of "black" zone does not mean an absolute performance but a relative performance compared to the dual-Rx antenna system. Therefore, the "black" zone represents the region of relay locations where the cooperative-diversity system outperforms the dual-Rx antenna system; otherwise, the dual-Rx antenna system is better. The noticeable results in Fig. 22 are that the AF cooperative-diversity system and the DF cooperative-diversity system do not outperform the dual-Rx antenna system over the entire cell area. The size of the "black" zone of the AF cooperative-diversity system in Fig. 22(a) is larger than that of the DF cooperative diversity system in Fig. 22(b), and it means that the effective coverage, where the outage probability of the AF cooperative-diversity system is lower than the dual-Rx antenna system, is larger than that of the DF cooperative-diversity system.

In realistic environments, the transmit power of the relay is usually much smaller than that of the base station. Figure 23 shows the results for the diversity systems with $\zeta = 0.01$, which considers the realistic environments under the total power constraint. The size of the "black" zone for the relay decreases significantly, and the center of the zone moves to $k = 0.8$ for the AF cooperative-diversity system and $k = 0.9$ for the DF cooperative-diversity system. When $\zeta = 1.0$, the center of the "black" zone moves to $k = 0.4$ for the AF cooperative-diversity system and $k = 0.5$ for the DF cooperative-diversity system, as shown in Fig. 22. These results show that

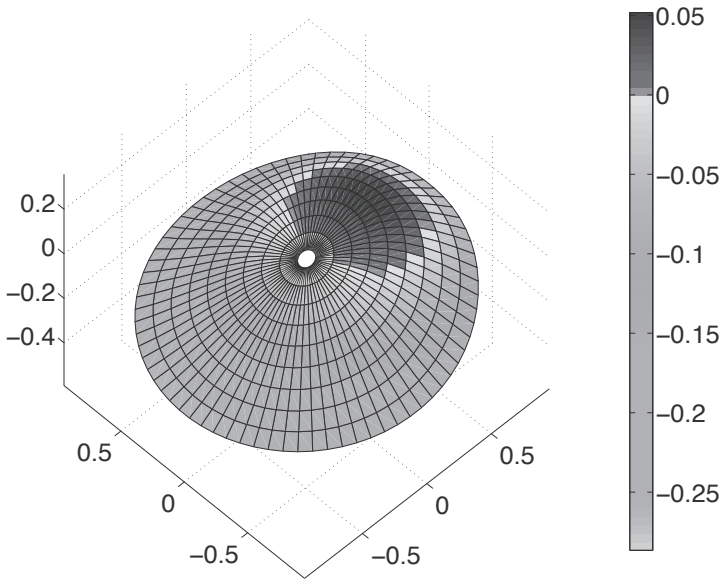

(a) the AF cooperative-diversity system

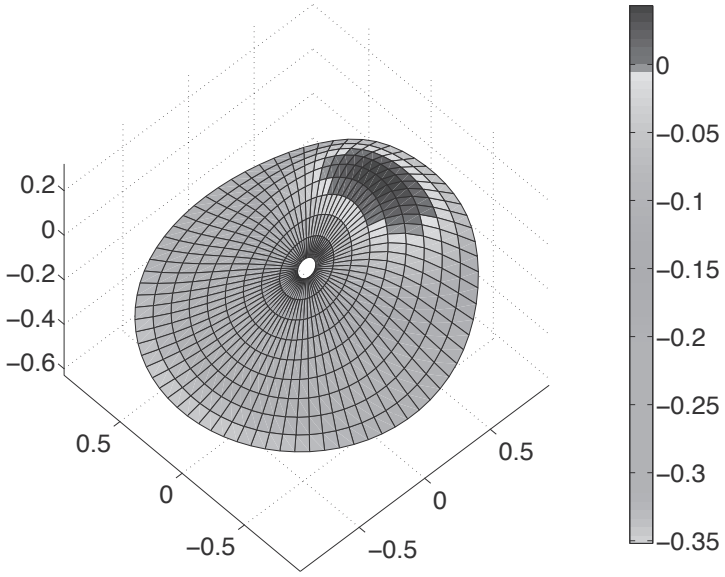

(b) the DF cooperative-diversity system

Figure 22: Difference between the outage probability of the dual-Rx antenna system and the cooperative-diversity system as a function of the relay location, where $m_X = 3$, $R_u = 3$ (3-cell reuse cluster), and $\zeta = 1.0$.

the size of the effective zone depends on the power of the relay, and the center of zone depends on the power of the source.

Finally, Figure 24 shows the case for shadowed-Rayleigh faded desired signal, $m_X = 1$. In Fig. 24(a), the size of "black" zone increases, and the shape is an ellipse compared to Fig. 22(a), which has the same configuration except that $m_X = 3$, while the size of "black" zone in Fig. 24(b) decreases, and the shape is a circle compared to Fig. 22(b). These results are remarkable because the variation of the size shows the AF cooperative-diversity system is more robust than the DF cooperative-diversity system over the channel condition, and the shape shows the DF cooperative-diversity system has more independent outage performance for each path than the AF cooperative-diversity system.

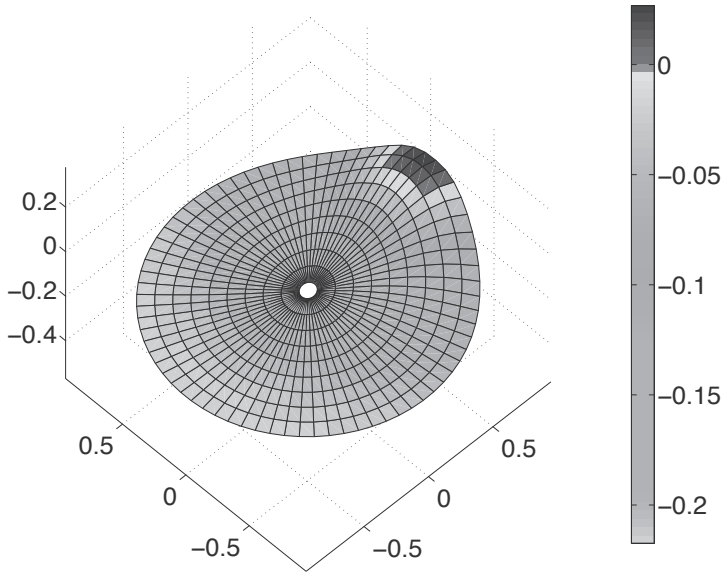

(a) the AF cooperative-diversity system

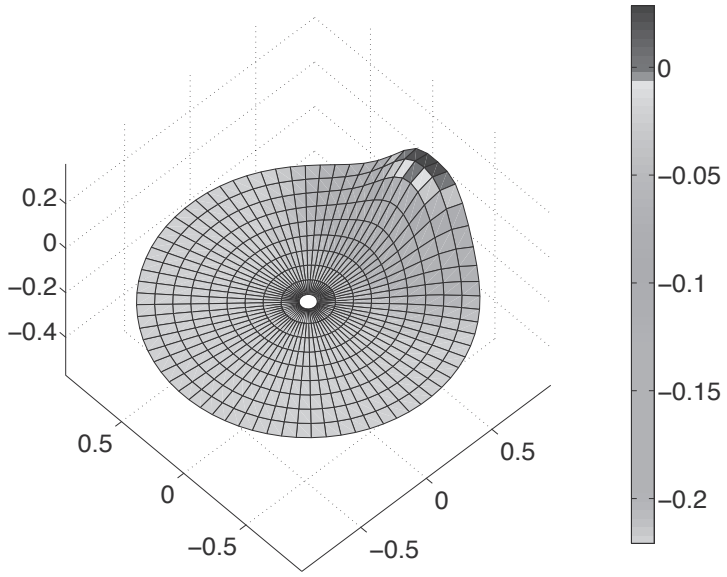

(b) the DF cooperative-diversity system

Figure 23: Difference between the outage probability of the dual-Rx antenna system and the cooperative-diversity system as a function of the relay location, where $m_X = 3$, $R_u = 3$ (3-cell reuse cluster), and $\zeta = 0.01$.

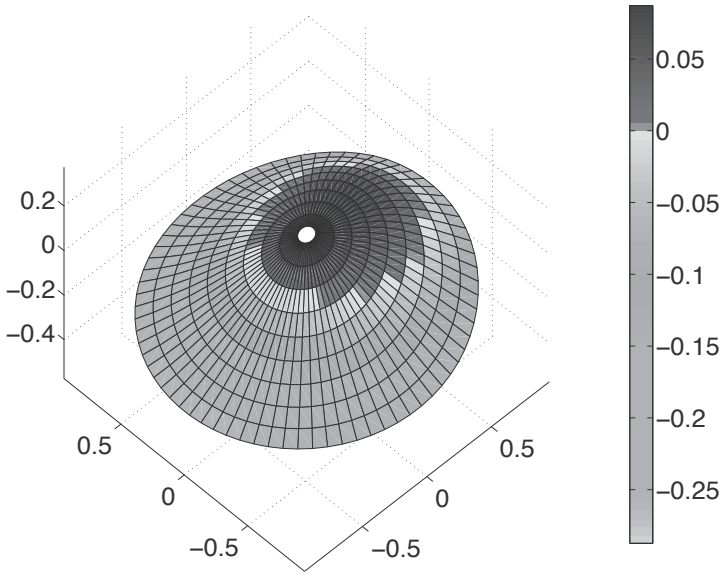

(a) the AF cooperative-diversity system

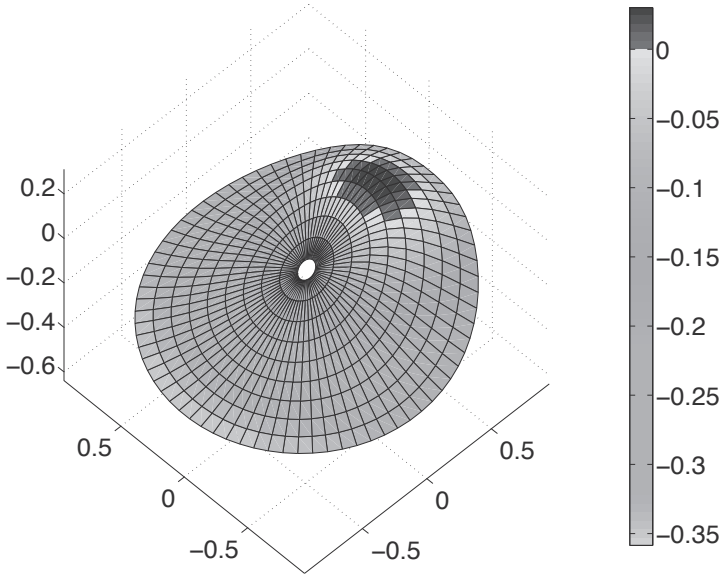

(b) the DF cooperative-diversity system

Figure 24: Difference between the outage probability of the dual-Rx antenna system and the cooperative-diversity system as a function of the relay location, where $m_X = 1$, $R_u = 3$ (3-cell reuse cluster), and $\zeta = 1.0$.

CHAPTER VI

COOPERATIVE DIVERSITY SYSTEMS WITH MAXIMAL RATIO COMBINING IN CELLULAR NETWORKS

6.1 Overview

Because of its low complexity and decentralized nature, cooperative diversity is highly adaptable to the uplink of decentralized networks, so most research has focused on ad-hoc networks or wireless sensor networks [15]. However, cooperative diversity can be more efficiently and simply employed in both the uplink and downlink of cellular networks because a BS knows information about all the channels between the BS and MSs. In particular, a DF selection relay introduced in [1] is regarded as a practical implementation for cellular networks because it can be fit to/utilized in existing digital signal processing blocks without expensive analog components or new hardware structures, and it can prevent error propagation. Although the first commercial relay-assisted cellular network was standardized in IEEE 802.16j activity, it differs from the user cooperative diversity scheme because it employs a fixed infrastructure relay station (RS) [40, 41].

In cellular network environments, frequency reuse is essential for increasing spectrum efficiency, but CCI caused by frequency reuse is the largest performance limiting factor. Therefore, evaluating system performance with respect to CCI has a high importance in the research area of traditional cellular networks. Several statistical models have addressed the effect of CCI on cellular networks. For example, the effect of CCI was investigated on Nakagami/Nakagami, shadowed Rayleigh/shadowed Rayleigh, and shadowed Rician/shadowed Rayleigh channels in [39, 43, 44]. While an

increase in the frequency reuse distance will mitigate CCI, it will also degrade system efficiency. Such tradeoff between frequency reuse distance and spectral efficiency was characterized by Alouini *et al.* in [45]. Without an increase in the frequency reuse distance, the cooperative diversity gain can provide an efficient way to alleviate the effect of CCI as well as multipath fading.

The aim of this chapter is to investigate the performance benefits and tradeoffs of the DF cooperative diversity system in cellular network environments. Thus, we derive closed-form expressions for the outage probability and the spectral efficiency of the DF cooperative diversity system using MRC for non-identical shadowed Nakagami/shadowed Nakagami channels. We then evaluate the outage probability and spectral efficiency with respect to the co-channel reuse factor for omnidirectional and sectorized cells in both the uplink and downlink of cellular networks under worst case CCI condition. In the optimal relay location, the DF cooperative diversity system with a single relay shows better outage performance than the dual-Rx antenna system. However, when the relay location is not optimal, the proposed system might be more vulnerable to CCI than the dual-Rx antennal system. Therefore, this chapter shows the effective zone where the cooperative diversity system outperforms the dual-Rx antenna system. Moreover, since the achieved cooperative diversity gain comes at the cost of decreased spectral efficiency because of the requirement for additional orthogonal channels, we also investigate the spectral efficiency degradation of the proposed systems.

6.2 System and Channel Models

The cooperative-diversity system in this chapter is a traditional three-node-relay system that consists of a source **S**, a destination **D**, and a relay **R**. All terminals have a single antenna and operate on a half-duplex mode. The relay employs the DF scheme, which uses an orthogonal transmission consisting of two orthogonal slots.

6.2.1 Channel Model

In this research, channels are affected by path loss, fading, and shadowing. First, we use the path-loss model which is used in a vehicular test environment [55]. For a 2 GHz carrier frequency, the path-loss model is

$$L = 128.1 + 37.6 \log_{10}(d) \ , \tag{100}$$

where d [Km] is the distance between the Tx and Rx terminals. Second, the shadowing is modeled as log-normally distributed. Third, the multipath fading is characterized by a Nakagami-m distribution assumed to be slowly varying flat-fading. This chapter also assumes that all links are mutually independent and non-identical, since all the terminals are located at a sufficient distance from each another. In addition, we assume interference-limited systems such that addictive white Gaussian noise is negligible relative to CCI. Therefore, the received signals of the source-to-destination, source-to-relay, and relay-to-destination links are

$$\begin{aligned} S_{S,D} &= x_S \cdot g_{S,D}\sqrt{P_S} + \sum_{l=1}^{N_{I,D}} h_{l,D}\, x_l \sqrt{P_l} \ , \\ S_{S,R} &= x_S \cdot g_{S,R}\sqrt{P_S} + \sum_{l=1}^{N_{I,R}} h_{l,R}\, x_l \sqrt{P_l} \ , \\ S_{R,D} &= x_R \cdot g_{R,D}\sqrt{P_R} + \sum_{l=1}^{N_{I,D}} h_{l,D}\, x_l \sqrt{P_l} \ , \end{aligned} \tag{101}$$

where x is the transmitted symbol with unit power and P_S, P_R, and P_l represent the Tx powers of the source, the relay, and the l-th interferer, respectively. All links are affected by incoherently added CCI, where $N_{I,R}$ and $N_{I,D}$ are the maximum number of active co-channel interferers at the relay and the destination, respectively. The ratio of the Tx power of the relay to that of the source is denoted by the cooperative power ratio ζ in (67).

Similarly to Section 4.2, the channel gain g for the desired signal (or h for the

interfering signal) can be written as $g = f\sqrt{c \cdot s \cdot d^{-\alpha}}$, where c is a constant representing the Tx and Rx antenna gains; d is the distance between the transmitter and the receiver; α is the propagation path-loss exponent, which is equal to 3.76 from (100); s is the shadow-fading factor that has a log-normal distribution; and f has a Nakagami distribution, and the squared envelope of this small-scale fading has a Gamma distribution.

6.2.2 Cell Environment Model

We consider a conventional cellular network with a hexagonal grid, in which a serving cell is surrounded by six co-channel-interfering cells in the first-tier, as depicted in Figs. 25 and 26.

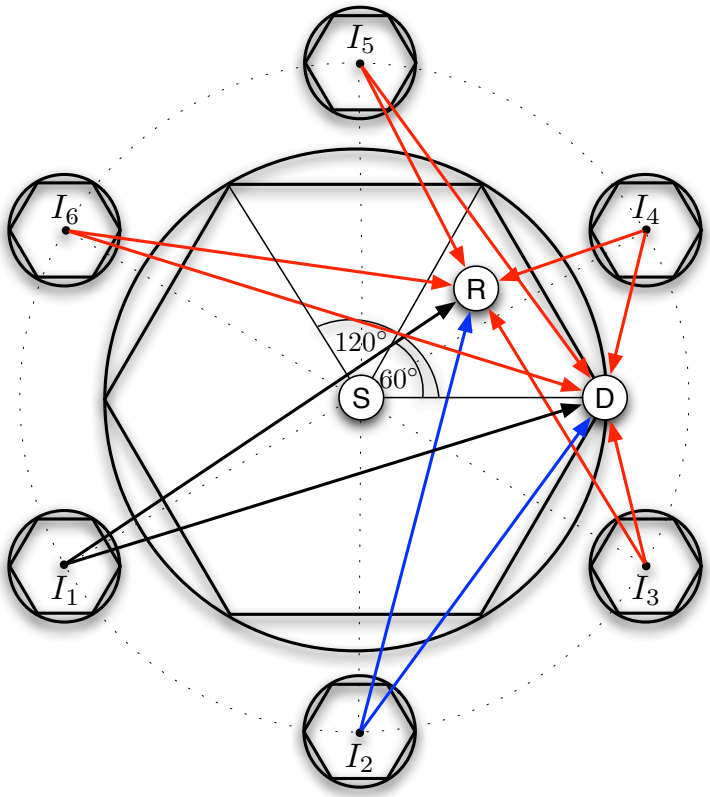

Figure 25: Worst-case CCI scenario in the downlink.

In each cell, the BS can use either omnidirectional and directional antennas, i.e.,

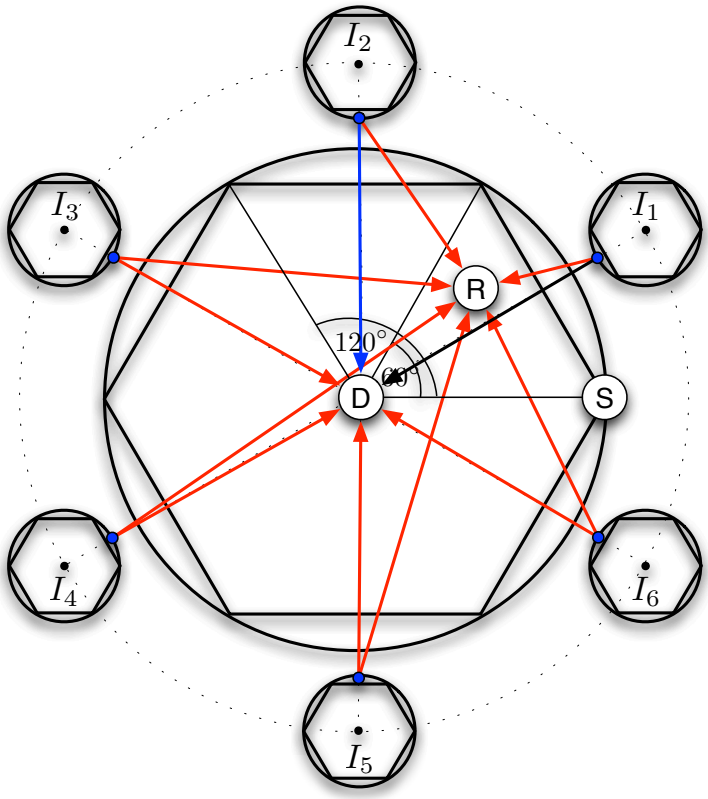

Figure 26: Worst-case CCI scenario in the uplink.

omnidirectional (one sector), 60° sectorized (three sectors), and 120° sectorized cells (six sectors) can be used, but the MSs equip only an omnidirectional antenna. Although the cost of cell sectorization is the degradation of trunking efficiency, this topic is beyond the scope of our research. We also consider the worst-case CCI scenario with a fully-loaded system in both the uplink and the downlink. The BS is located in the center of each cell, and the relay is one of the MSs deployed in the sector. The user's MS is located on the rightmost boundary of the serving cell. Note that the co-channel-interfering cells may employ the same cooperative-diversity system with orthogonal transmission as the serving cell. In this case, since concurrent transmissions are not allowed, a single interferer in each co-channel-interfering cell still exists in the same slot period.

Figure 25 illustrates the worst-case CCI scenario in the downlink. The relay and

the destination at the serving cell are affected by interference from the BSs of the co-channel-interfering cells, and the number of interferers varies according to the coverage of the directional antenna. In the downlink, both $N_{I,R}$ and $N_{I,D}$ are equal to six, two, and one for omnidirectional, 120° sectorized, and 60° sectorized cells, respectively.

Figure 26 illustrates the worst-case CCI scenario in the uplink, which occurs when the destination BS receives the weakest signal from source MS and is subjected to strong interference from the MSs of the co-channel-interfering cells. Unlike in the downlink, in the uplink, $N_{I,R}$ differs from $N_{I,D}$. Since the MSs employ an omnidirectional antenna, the relay is affected by interference from all co-channel-interfering cells; thus, $N_{I,R}$ is six, regardless of cell sectorization. However, because the destination BS uses a directional antenna that narrows the angle of arrival, the $N_{I,D}$ of the uplink is the same as that of the downlink. Note that the numbering of interferers in Fig. 26 differs from that of Fig. 25 so as to match the number and the location of interferers for each case.

6.2.3 Geometry Model

We assume that the radius of every cell is R, and the co-channel reuse distance is D; then the co-channel reuse factor R_u is defined as D/R. When the user's MS is located on the rightmost edge of the serving cell, the relay location can be expressed by polar coordinate $(d_{S,R}, \theta)$, in which $d_{S,R}$ is the distance of the source-to-relay link, and θ is the angle between the source-to-relay link and the source-to-destination link. When the distance of the source-to-destination link $d_{S,D}$ is set to R, the distance of the source-to-relay link $d_{S,R}$ can be expressed as $k \cdot R$, where $0 < k \leq 1$, so the location of the relay is expressed as (k, θ) throughout the chapter. Thus, the distance of the relay-to-destination $d_{R,D}$ is $R\sqrt{k^2 - 2k\cos\theta + 1}$.

Figure 27 describes the geometry between the serving and the co-channel-interfering

cells in the downlink. The distance of the l-th interferer-to-relay $d_{I_l,R}$ is $\sqrt{D^2 - 2kRD\cos(\Theta_l - \theta) + k^2R^2}$, where Θ_l, denoted as $\Theta_l = \pi(2l+5)/6$, is the angle between the source-to-destination link and the l-th interferer-to-destination link. The distance of the l-th interferer-to-destination $d_{I_l,D}$ is $\sqrt{D^2 - 2DR\cos\Theta_l + R^2}$.

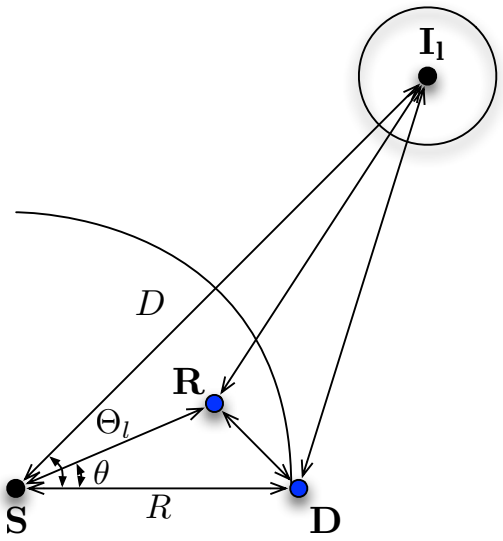

Figure 27: Geometry model of the downlink

Figure 28 illustrates the geometry of the uplink. Interferer I'_l is the nearest MS at the l-th co-channel-interfering cell, and the distance between the MS and the BS of the serving cell is $D - R$. In Fig. 28, the distance of the l-th interferer-to-relay $d_{I'_l,R}$ is $\sqrt{(D-R)^2 - 2kR(D-R)\cos(\Theta'_l - \theta) + k^2R^2}$, where $\Theta'_l = \pi(2l-1)/6$, and the distance of the l-th interferer-to-destination $d_{I'_l,D}$ is $\sqrt{(D-R)^2 - 2R(D-R)\cos\Theta'_l + R^2}$.

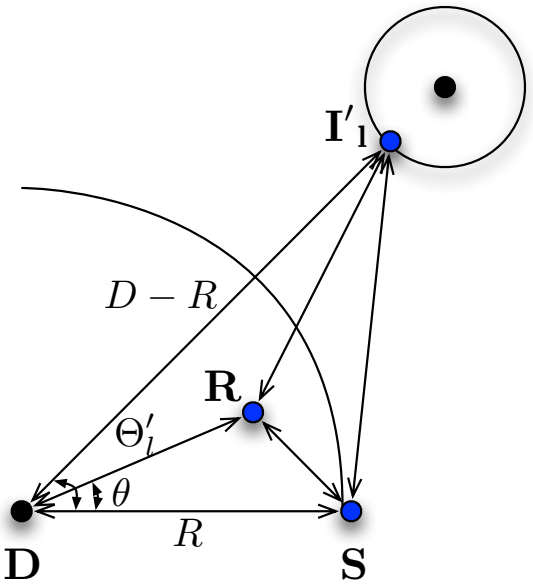

Figure 28: Geometry model of the uplink

6.2.4 CIR Models at a Relay Location

This section provides the CIRs of individual links using both the path-loss model in (100) and the geometry model in the previous section. Throughout the chapter, the area mean powers of the desired and interfering signals are expressed as Ω_X and Ω_Y, respectively.

In the downlink, the CIR of the source-to-destination link is

$$Z^d_{S,D} = \frac{\Omega^d_{X_{S,D}}}{\Omega_{Y_{I,D}}} = \frac{d^{-a}_{S,D}}{\sum_{l=1}^{N_{I,D}} d^{-a}_{I_l,D}} = \frac{1}{\sum_{l=1}^{N_{I,D}} \varphi^{-a}_{I,D}} \ , \tag{102}$$

where $\varphi_{I,D} = \sqrt{R_u^2 - 2R_u \cos\Theta_l + 1}$. In the source-to-destination link, the Tx powers of the source and the interferer are the same, since the source is the BS at the serving cell and the interferer is also the BS at the co-channel-interfering cell.

The CIR of the source-to-relay link can be expressed as

$$Z^d_{S,R}(k,\theta) = \frac{\Omega^d_{X_{S,R}}}{\Omega_{Y_{I,R}}} = \frac{d^{-a}_{S,R}}{\sum_{l=1}^{N_{I,R}} d^{-a}_{I_l,R}} = \frac{k^{-a}}{\sum_{l=1}^{N_{I,R}} \varphi^{-a}_{I,R}} \ , \tag{103}$$

where $\varphi_{I,R} = \sqrt{R_u^2 - 2kR_u \cos(\Theta_l - \theta) + k^2}$. However, the Tx power of the relay is

ζP_S; thus, the CIR of the relay-to-destination link can be written as

$$Z^d_{R,D}(k,\theta) = \frac{\Omega^d_{X_{R,D}}}{\Omega_{Y_{I,D}}} = \frac{d^{-a}_{R,D}}{\zeta \sum_{l=1}^{N_{I,D}} d^{-a}_{I_l,D}} = \frac{\varphi^{-a}_{R,D}}{\zeta \sum_{l=1}^{N_{I,D}} \varphi^{-a}_{I,D}}, \tag{104}$$

where $\varphi_{R,D} = \sqrt{k^2 - 2k\cos\theta + 1}$, and ζ is defined in (67).

In the uplink, the Tx powers of the source, the relay, and the interferer are assumed to be the same since they are all MSs. Therefore, the CIR of the source-to-destination link is

$$Z^u_{S,D} = \frac{\Omega^u_{X_{S,D}}}{\Omega_{Y_{I',D}}} = \frac{d^{-a}_{S,D}}{\sum_{l=1}^{N_{I,D}} d^{-a}_{I'_l,D}} = \frac{1}{\sum_{l=1}^{N_{I,D}} \varphi^{-a}_{I',D}} \ , \tag{105}$$

where $\varphi_{I',D} = \sqrt{(R_u-1)^2 - 2(R_u-1)\cos\Theta'_l + 1}$. The CIR of the source-to-relay link is

$$Z^u_{S,R}(k,\theta) = \frac{\Omega^u_{X_{S,R}}}{\Omega_{Y_{I',R}}} = \frac{d^{-a}_{S,R}}{\sum_{l=1}^{N_{I,R}} d^{-a}_{I'_l,R}} = \frac{k^{-a}}{\sum_{l=1}^{N_{I,R}} \varphi^{-a}_{I',R}} \ , \tag{106}$$

where $\varphi_{I',R} = \sqrt{(R_u-1)^2 - 2k(R_u-1)\cos(\Theta'_l - \theta) + k^2}$, and the CIR of the relay-to-destination is

$$Z^u_{R,D}(k,\theta) = \frac{\Omega^u_{X_{R,D}}}{\Omega_{Y_{I',D}}} = \frac{d^{-a}_{R,D}}{\sum_{l=1}^{N_{I,D}} d^{-a}_{I'_l,D}} = \frac{\varphi^{-a}_{R,D}}{\sum_{l=1}^{N_{I,D}} \varphi^{a}_{I',D}} \ . \tag{107}$$

6.3 Per-Hop Analysis

The selection relaying scheme determines whether or not the relay forwards the source packet by observing the outage probability of the source-to-relay link, which will be shown in Section 6.3.2. Thus, the outage probability and the pdf of the CIR of individual links are required to obtain the end-to-end outage probability. In this section, we present the outage probability and the pdf of the CIR of a single-hop transmission.

6.3.1 Pdfs of X and Y

The channels for both the desired and interfering signals are Nakagami-m faded with log-normal shadowing, so the channels can be modeled by a composite log-normal

Nakagami-m distribution that is closely approximated by applying Hermite-Gaussian quadrature integration [2, eq. 3.68]. Thus, the pdfs of the desired and interfering signal powers, X and Y, are expressed as a composite log-normal Gamma distribution as in Section 4.2.3, as follows:

$$p_X(x) = \sum_{i=1}^{N_p} \frac{H_{x_i}}{\sqrt{\pi}} \left[\left(\frac{m_X}{\Phi_X(x_i)} \right)^{m_X} \frac{x^{m_X-1}}{\Gamma(m_X)} \exp\left(\frac{-m_X x}{\Phi_X(x_i)} \right) \right],$$
$$p_Y(y) = \sum_{j=1}^{N_p} \frac{H_{x_j}}{\sqrt{\pi}} \left[\left(\frac{m_Y}{\Phi_Y(x_j)} \right)^{m_Y} \frac{y^{m_Y-1}}{\Gamma(m_Y)} \exp\left(\frac{-m_Y y}{\Phi_Y(x_j)} \right) \right], \quad (108)$$

respectively, where m_X and m_Y are the Nakagami shape factors, which are assumed to be integer valued; H_{X_i} and H_{X_j} are weight factors; x_i and x_j are the zeros; N_p is the order of the Hermite polynomial; and $\Phi_X(x_i) =: \exp(\sqrt{2}\sigma_X x_i + \ln \Omega_X)$ and $\Phi_Y(x_j) =: \exp(\sqrt{2}\sigma_Y x_j + \ln \Omega_Y)$, where σ_X and σ_Y are the shadow standard deviation of the channels for the desired and interfering signals, respectively.

6.3.2 Pdf and Outage Probability of Z

Since X and Y are mutually independent and CIR Z is defined as X/Y, the pdf of Z can be written as

$$p_Z(z) = \int_0^\infty y\, p_X(z\, y) p_Y(y) dy \ . \quad (109)$$

The outage probability is an important performance measure in the presence of interference to evaluate the probability of unsatisfactory signal reception over the intended coverage area.

A single-hop transmission can assume three configurations: i) a single interferer without signal combining; ii) multiple interferers without signal combining; and iii) multiple interferers with MRC. With regard to the first configuration, we consider a case in which a single interferer ($N_I = 1$) lies between two terminals, but signal combining is not employed. In this case, the pdf of CIR Z can be obtained by

substituting (108) into (109) as follows:

$$p_Z(z) = \sum_{i=1}^{N_p} \sum_{j=1}^{N_p} \frac{1}{\pi} H_{x_i} H_{x_j} H(z; m_X, m_Y, \alpha_X(x_i), \alpha_Y(x_j)) \,, \tag{110}$$

where the H-function is defined as

$$\begin{aligned} &H(z; m_X, m_Y, \alpha_X(x_i), \alpha_Y(x_j)) \\ &= \frac{\Gamma(m_X + m_Y)}{\Gamma(m_X)\Gamma(m_Y)} z^{m_X - 1} (z + \Phi_Z(x_i, x_j))^{-(m_X + m_Y)} \Phi_Z(x_i, x_j)^{m_Y} \quad , \end{aligned} \tag{111}$$

and where $\alpha_X(x_i) =: \Phi_X(x_i)/m_X$, $\alpha_Y(x_j) =: \Phi_Y(x_j)/m_Y$, $\Phi_Z(x_i, x_j) = \frac{m_Y}{m_X} \exp\{\sqrt{2}(\sigma_X x_i - \sigma_Y x_j) + \ln z\}$, and $z = \Omega_X/\Omega_Y$. The outage probability can be obtained by solving (58) in Chapter 4 with (110) as

$$P_o(\lambda) = 1 - \sum_{i=1}^{N_p} \sum_{j=1}^{N_p} \frac{1}{\pi} H_{x_i} H_{x_j} F(\lambda; m_X, m_Y, \alpha_X(x_i), \alpha_Y(x_j)) \,, \tag{112}$$

where the F-function is defined as

$$\begin{aligned} &F(\lambda; m_X, m_Y, \alpha_X(x_i), \alpha_Y(x_j)) \\ &= \Phi_Z(x_i, x_j)^{m_Y} \sum_{n=0}^{m_X - 1} \frac{\lambda^n}{n!} (\lambda + \Phi_Z(x_i, x_j))^{-(m_Y + n)} \frac{\Gamma(m_Y + n)}{\Gamma(m_Y)} \,. \end{aligned} \tag{113}$$

Second, when multiple interferers ($N_I > 1$) affect a single-hop link between two terminals without diversity, Y is the sum of the interfering signal powers, and the pdf of Y is the sum of mutually-independent log-normal Gamma distributions. The expression for the sum of multiple Gamma distributions was derived by using a partial fraction technique and inverse Laplace transform in [24]; thus, by applying (108) to the same method in [24], we can derive the pdf of Y as

$$p_Y(y) = \sum_{a=1}^{N_I} \sum_{b=1}^{m_{Y_a}} \sum_{j_a=1}^{N_p} \frac{1}{\sqrt{\pi}} H_{x_{j_a}} \frac{(-1)^b}{\Gamma(b)} \beta_{a,b}^{Y}(x_{j_a}) y^{b-1} \exp\left(\frac{-y}{\alpha_{Y_a}(x_{j_a})}\right) \quad , \tag{114}$$

where coefficient $\beta_{a,b}^{Y}(x_{j_a})$ is defined in (48) of Chapter 4. Applying the pdfs of X in (108) and Y in (114) to (109), the pdf of CIR Z for a single-hop link with multiple

interferers can be written by using the H-function in (111) as

$$p_Z(z) = \sum_{a=1}^{N_I} \sum_{b=1}^{m_{Y_a}} \sum_{i=1}^{N_p} \sum_{j_a=1}^{N_p} \frac{1}{\pi} H_{x_i} H_{x_{j_a}} \beta_{a,b}^{Y}(x_{j_a})(-\alpha_{Y_a}(x_{j_a}))^b \times H(z; m_X, b, \alpha_X(x_i), \alpha_{Y_a}(x_{j_a})). \quad (115)$$

Substituting (115) into (58) in Chapter 4 yields the outage probability

$$P_o(\lambda) = 1 - \sum_{a=1}^{N_I} \sum_{b=1}^{m_{Y_a}} \sum_{i=1}^{N_p} \sum_{j_a=1}^{N_p} \frac{1}{\pi} H_{x_i} H_{x_{j_a}} \beta_{a,b}^{Y}(x_{j_a})(-\alpha_{Y_a}(x_{j_a}))^b \times F(\lambda; m_X, b, \alpha_X(x_i), \alpha_{Y_a}(x_{j_a})). \quad (116)$$

Note that this case represents a single-Rx antenna system, discussed in Section V.

Next, we can consider the case of multiple interferers, where the receiver uses an MRC technique. In this case, the pdfs of X and Y are the sum of mutually independent log-normal Gamma distributions. If the number of diversity branches is M, the pdf of X has the same form as (111),

$$p_X(x) = \sum_{a=1}^{M} \sum_{b=1}^{m_{X_a}} \sum_{i_a=1}^{N_p} \frac{1}{\sqrt{\pi}} H_{x_{i_a}} \frac{(-1)^b}{\Gamma(b)} \beta_{a,b}^{X}(x_{i_a}) x^{b-1} \exp\left(\frac{-x}{\alpha_{X_a}(x_{i_a})}\right) , \quad (117)$$

where $\beta_{a,b}^{X}(x_{i_a})$ is the same as (54) of Chapter 4. Substituting (114) and (117) into (109) yields the pdf of Z,

$$p_Z(z) = \sum_{a=1}^{M} \sum_{b=1}^{m_{X_a}} \sum_{c=1}^{N_I} \sum_{d=1}^{m_{Y_c}} \sum_{i_a=1}^{N_p} \sum_{j_c=1}^{N_p} \frac{1}{\pi} H_{x_{i_a}} H_{x_{j_c}} \beta_{a,b}^{X}(x_{i_a}) \beta_{c,d}^{Y}(x_{j_c})(-\alpha_{X_a}(x_{i_a}))^b (-\alpha_{Y_c}(x_{j_c}))^d \times H(z; b, d, \alpha_{X_a}(x_{i_a}), \alpha_{Y_c}(x_{j_c})) \ . \quad (118)$$

The outage probability for M-branch MRC with multiple interferers can be derived by solving (58) with (118) as follows:

$$P_o(\lambda) = 1 - \sum_{a=1}^{M} \sum_{b=1}^{m_{X_a}} \sum_{c=1}^{N_I} \sum_{d=1}^{m_{Y_c}} \sum_{i_a=1}^{N_p} \sum_{j_c=1}^{N_p} \frac{1}{\pi} H_{x_{i_a}} H_{x_{j_c}} \beta_{a,b}^{X}(x_{i_a}) \beta_{c,d}^{Y}(x_{j_c})(-\alpha_{X_a}(x_{i_a}))^b \times (-\alpha_{Y_c}(x_{j_c}))^d F(\lambda; b, d, \alpha_{X_a}(x_{i_a}), \alpha_{Y_c}(x_{j_c})) \ . \quad (119)$$

Note that this case represents the multi-Rx antenna system with MRC discussed in Section V.

6.4 Cooperative Dual-hop Analysis

In this section, we derive the outage probability, the spectral efficiency, and the end-to-end pdf of the CIR of the DF cooperative diversity system in cellular environments. Since we consider a three-node-relay system, the number of diversity branches M is two, and we let X_1 and X_2 denote the desired signal power of the source-to-destination link and relay-to-destination link, respectively.

6.4.1 End-to-End Pdf and Outage Probability

Applying the composite log-normal Gamma distribution for X in (108) to the same method of Chapter 3, we can obtain the end-to-end pdf of the desired signal power at a given relay location in the proposed system as follows:

$$p_X(x|k,\theta) = P_o \sum_{i_1}^{N_p} \frac{H_{x_{i_1}}}{\sqrt{\pi}} \left(\frac{m_{X_1}}{\Phi_{X_1}(x_{i_1})} \right)^{m_{X_1}} \frac{x^{m_{X_1}-1}}{\Gamma(m_{X_1})} \exp\left(\frac{-m_{X_1} x}{\Phi_{X_1}(x_{i_1})} \right) + (1-P_o) \sum_{a=1}^{2} \sum_{b=1}^{m_{X_a}} \sum_{i_a}^{N_p} \frac{H_{x_{i_a}}}{\sqrt{\pi}} \frac{(-1)^b x^{b-1}}{\Gamma(b)} \beta_{a,b}^{X} \exp\left(\frac{-m_{X_a} x}{\Phi_{X_a}(x_{i_a})} \right), \quad (120)$$

where P_o is the outage probability of the source-to-relay link, which is derived in (116), and the number of interferers of the link is $N_{I,R}$. The end-to-end pdf of CIR Z_{out} can be obtained by substituting the end-to-end pdf of X in (120) and the pdf of Y in (114) into (109) as follows:

$$p_Z^{\text{ete}}(z|k,\theta) = P_o \sum_{c=1}^{N_{I,D}} \sum_{d=1}^{m_{Y_c}} \sum_{i_1=1}^{N_p} \sum_{j_c=1}^{N_p} \frac{1}{\pi} H_{x_{i_1}} H_{x_{j_c}} (-\alpha_{Y_c}(x_{j_c}))^d \beta_{c,d}^{Y}(x_{j_c}) \times H(z; m_{X_1}, d, \alpha_{X_1}(x_{i_1}), \alpha_{Y_c}(x_{j_c})) + (1-P_o) \sum_{a=1}^{2} \sum_{b=1}^{m_{X_a}} \sum_{i_a=1}^{N_p} \frac{1}{\sqrt{\pi}} H_{x_{i_a}} \{-\alpha_{X_a}(x_{i_a})\}^b \times \beta_{a,b}^{X}(x_{i_a}) \sum_{c=1}^{N_{I,D}} \sum_{d=1}^{m_{Y_c}} \sum_{j_c=1}^{N_p} \frac{1}{\sqrt{\pi}} H_{x_{j_c}} \beta_{c,d}^{Y}(x_{j_c}) \{-\alpha_{Y_c}(x_{j_c})\}^d H(z; b, d, \alpha_{X_a}(x_{i_a}), \alpha_{Y_c}(x_{j_c})). \quad (121)$$

The end-to-end outage probability at a given relay location is derived by solving (58) with (121) as follows:

$$P_o^{\text{ete}}(\lambda|k,\theta) = 1 - \Bigg[P_o \sum_{c=1}^{N_{I,D}} \sum_{d=1}^{m_{Y_c}} \sum_{i_1=1}^{N_p} \sum_{j_c=1}^{N_p} \frac{1}{\pi} H_{x_{i_1}} H_{x_{j_c}} (-\alpha_{Y_c}(x_{j_c}))^d \beta_{c,d}^{Y}(x_{j_c}) \\ \times F(\lambda; m_{X_1}, d, \alpha_{X_1}(x_{i_1}), \alpha_{Y_c}(x_{j_c})) + (1-P_o) \sum_{a=1}^{2} \sum_{b=1}^{m_{X_a}} \sum_{i_a=1}^{N_p} \frac{1}{\sqrt{\pi}} H_{x_{i_a}} \{-\alpha_{X_a}(x_{i_a})\}^b \\ \times \beta_{a,b}^{X}(x_{i_a}) \sum_{c=1}^{N_{I,D}} \sum_{d=1}^{m_{Y_c}} \sum_{j_c=1}^{N_p} \frac{1}{\sqrt{\pi}} H_{x_{j_c}} \beta_{c,d}^{Y}(x_{j_c}) \{-\alpha_{Y_c}(x_{j_c})\}^d F(\lambda; b, d, \alpha_{X_a}(x_{i_a}), \alpha_{Y_c}(x_{j_c})) \Bigg]. \tag{122}$$

6.4.2 Spectral Efficiency Analysis

In the DF cooperative diversity system, orthogonal transmission requires an additional channel per branch. Therefore, the spectral efficiency of the proposed system is defined as

$$\bar{C}/w = \frac{1}{M+1} \int_0^\infty \log_2(1+z) p_{Z_{out}}(z) \mathrm{d}z \ , \tag{123}$$

where $\bar{C}$ [b/s] is the average date rate per user, w [Hz] is the allocated bandwidth per user, and M is the number of slots. Substituting (121) into (123) yields the end-to-end spectral efficiency. In the integral in (123), variable z is related to only the H-function in (121), so the integral can be solved with the ρ-th order generalized Stieltjes transform (GST), as in [45], as follows:

$$\int_0^\infty \log_2(1+z) z^{m_X-1} (z+\Phi_Z)^{-(m_X+m_Y)} \mathrm{d}z \\ = \mathcal{G}_{m_X+m_Y}\{\log_2(1+z) z^{m_X-1}; \Phi_Z\} \\ = \left| \sum_{j=0}^{m_X-1} (-1)^j \binom{m_X-1}{j} \frac{\log_2(e) \Phi_Z^{1-m_Y}}{(m_X+m_Y-j-1)^2} \psi(1,1; m_X+m_Y-j; 1-\Phi_Z) \right| \ , \tag{124}$$

where $\mathcal{G}_\rho\{f(x); y\}$ is the GST of order ρ of function $f(x)$, and $\psi(\cdot,\cdot;\cdot;\cdot)$ is the Gauss hypergeometric function. Therefore, the end-to-end spectral efficiency at a given relay

location is written with the C-function as

$$\bar{C}^{\text{ete}}(k,\theta)/w = P_o \sum_{c=1}^{N_{I,D}} \sum_{d=1}^{m_{Y_c}} \sum_{i_1=1}^{N_p} \sum_{j_c=1}^{N_p} \frac{1}{\pi} H_{x_{i_1}} H_{x_{j_c}} (-\alpha_{Y_c}(x_{j_c}))^d \beta_{c,d}^{Y}(x_{j_c}) C(\Phi_Z(x_{i_1}, x_{j_c}); m_{X_1}, d)$$
$$+ (1-P_o) \sum_{a=1}^{2} \sum_{b=1}^{m_{X_a}} \sum_{i_a=1}^{N_p} \frac{1}{\sqrt{\pi}} H_{x_{i_a}} \beta_{a,b}^{X}(x_{i_a}) \{-\alpha_{X_a}(x_{i_a})\}^b$$
$$\times \sum_{c=1}^{N_{I,D}} \sum_{d=1}^{m_{Y_c}} \sum_{j_c=1}^{N_p} \frac{1}{\sqrt{\pi}} H_{x_{j_c}} \beta_{c,d}^{Y}(x_{j_c}) \{-\alpha_{Y_c}(x_{j_c})\}^d C(\Phi_Z(x_{i_a}, x_{j_c}); b, d) \ , \tag{125}$$

where

$$C(\Phi_Z; m_X, m_Y) = \frac{\Gamma(m_X+m_Y)}{\Gamma(m_X)\Gamma(m_Y)} \Phi_Z^{m_Y} \Bigg| \sum_{j=0}^{m_X-1} (-1)^j \binom{m_X-1}{j} \frac{\log_2(e)\Phi_Z^{1-m_Y}}{(m_X+m_Y-j-1)^2}$$
$$\times \psi(1,1; m_X+m_Y-j; 1-\Phi_Z) \Bigg| \ . \tag{126}$$

6.5 Performance Analysis

In this section, fully-loaded cooperative cellular relaying systems are investigated on non-identical shadowed-Nakagami/shadowed-Nakagami channels. The outage probability and spectral efficiency of the proposed system are evaluated with respect to the co-channel reuse factor for omnidirectional, 120° sectorized, and 60° sectorized cells in both the uplink and the downlink. The results in the section assume a typical macro-cellular system, in which the Tx powers of the MS and the BS are 24 dBm and 43 dBm, respectively, and the shadow standard deviations for the desired and interfering signals are all 8 dB according to [55]. The CIR threshold λ is 12 dB, and the Nakagami shape factors for the desired and interfering signals are two and one, respectively. The analytic results for the outage probability in (122) are verified by Monte Carlo simulations. In the simulations, first, area mean powers for the desired and interfering signals (Ω_X and Ω_Y) are calculated by the path-loss model in (100). Second, local mean powers are randomly generated with a log-normal distribution with the area mean powers and shadow standard deviations (σ_X and σ_Y). Third,

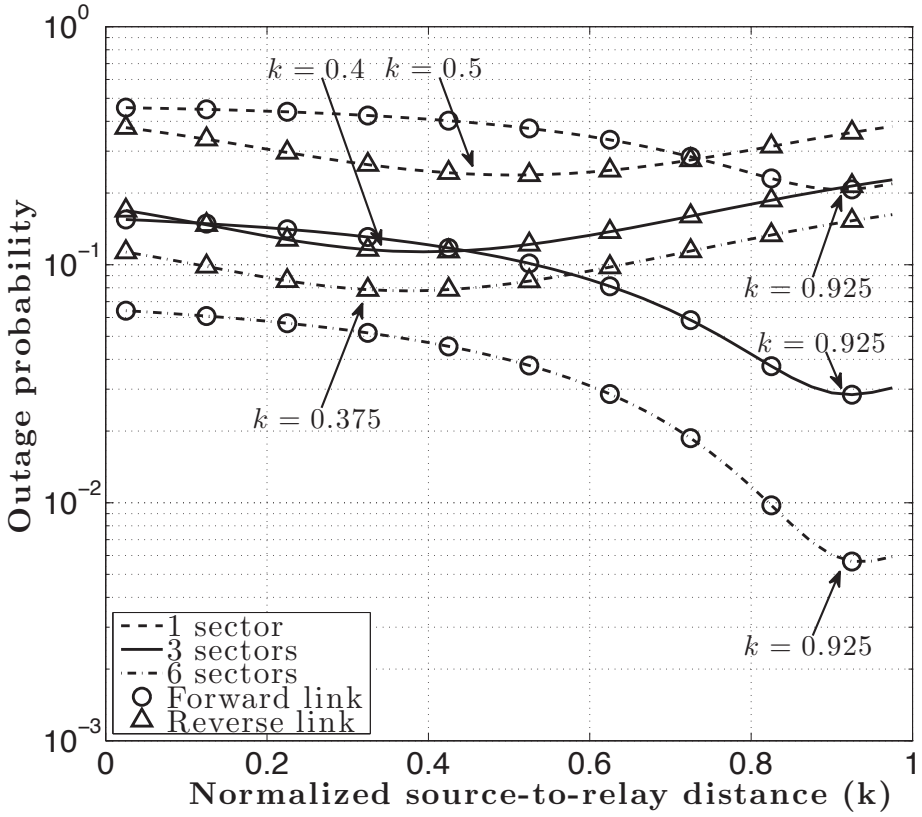

Figure 29: End-to-end outage probability with respect to the normalized source-to-relay distance ($R_u = 5$)

instantaneous received powers are randomly generated with a gamma distribution with the local mean powers and Nakagami shape factors (m_X and m_Y). To obtain a sufficient precision level, the process is performed in 10^8 trials. Note that the markers in Figs. 30 and 31 describe the simulation results, and the solid lines show the analytical results. Since the spectral efficiency in (125) is derived from (122), the simulation does not necessarily verify the analytic results after Fig. 31. From Fig. 34, the co-channel reuse factor R_u is assumed to be 5.

Figure 29 presents the optimal-relay location in terms of the outage probability. For the best outage performance, the relay should be located on the line connecting the source and the destination, i.e., $\theta = 0°$, but the normalized distance of the source-to-relay link, k, varies according to the cooperative power ratio, ζ, and the channel

conditions. The different location of the optimal relay between the uplink and the downlink can explain the effect of ζ. In the omnidirectional cell, the optimal-relay location is $k = 0.925$ in the downlink, but $k = 0.5$ in the uplink. The reason for the difference is that $\zeta = 0.01$ ($P_R = 0.01P_S$), in the downlink, but in the uplink, $\zeta = 1$ ($P_R = P_S$). An interesting result is that in the uplink, k is 0.5 for the omnidirectional cell, but it decreases to 0.375 for the 60° sectorized cell, while k is fixed at 0.925 in the downlink. Recall that in the uplink, the $N_{I,R}$ is six, regardless of sectorization, but $N_{I,D}$ are six, two, and one for for omnidirectional, 120° sectorized, and 60° sectorized cells, respectively; that is, the number of interferers at the relay is larger than that at the destination when the 60° sectorized cell is employed in the uplink. Thus, it can be clearly observed that the optimal-relay location moves toward the source-to-relay link, which has a relatively weak CIR compared to the relay-to-destination link. However, $N_{I,R}$ and $N_{I,D}$ are the same in the downlink. Thus, the relay location does not move because the CIRs of the source-to-relay and relay-to-destination links do not change respectively.

Figures 30 and 31 present a comparison between the outage probabilities of the DF cooperative-diversity system and those of the dual-Rx antenna system with respect to the co-channel reuse factor in the downlink and the uplink. The relay locations of the cooperative-diversity system are the same as the optimal-relay location obtained in Fig. 29. These figures show that the analytic results agree with the simulation results. In Fig. 30, the outage performance of the cooperative-diversity system in the downlink outperforms that of the dual-Rx antenna system, which employs MRC, for the entire co-channel reuse factor range, and cell sectorization reduces the number of interferers, improving the outage probability. The performance gap of the two systems is the largest for the 60° sectorized cell, but the smallest for the omnidirectional cell. Although Fig. 31 shows performance improvements in the cooperative-diversity system in the uplink, an important result is that the performance gap is the largest

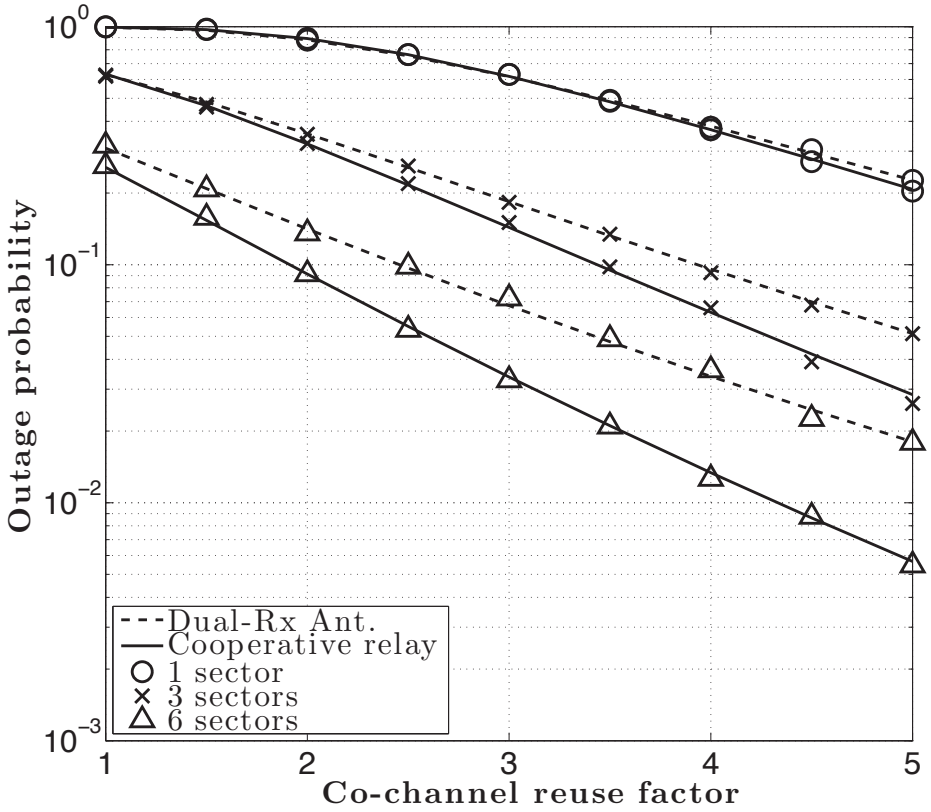

Figure 30: Downlink end-to-end outage probability versus co-channel reuse factor

when the BS uses an omnidirectional antenna, while the gap is the smallest when the cell is 60° sectorized, unlike the result in Fig. 30. These results can be explained by both the cooperative power ratio and the number of interferers. Figure 30 shows that since P_R is relatively small compared to P_S and k is close to the destination, the outage performance of the two systems is similar for the omnidirectional cell, but Fig. 31 indicates that, as shown in Fig. 29, the performance gap becomes more in the downlink than in the uplink because of the same Tx power ($P_R = P_S$), the reduced path-loss ($k = 0.5$), and reducing $N_{I,R}$ as well as $N_{I,D}$ by using the cell sectorization. Thus, Figures 30 and 31 show opposite behaviors in the performance gap.

Figures 32 and 33 compare the spectral efficiency of the DF cooperative-diversity system and that of the single-Rx antenna system with respect to the co-channel reuse

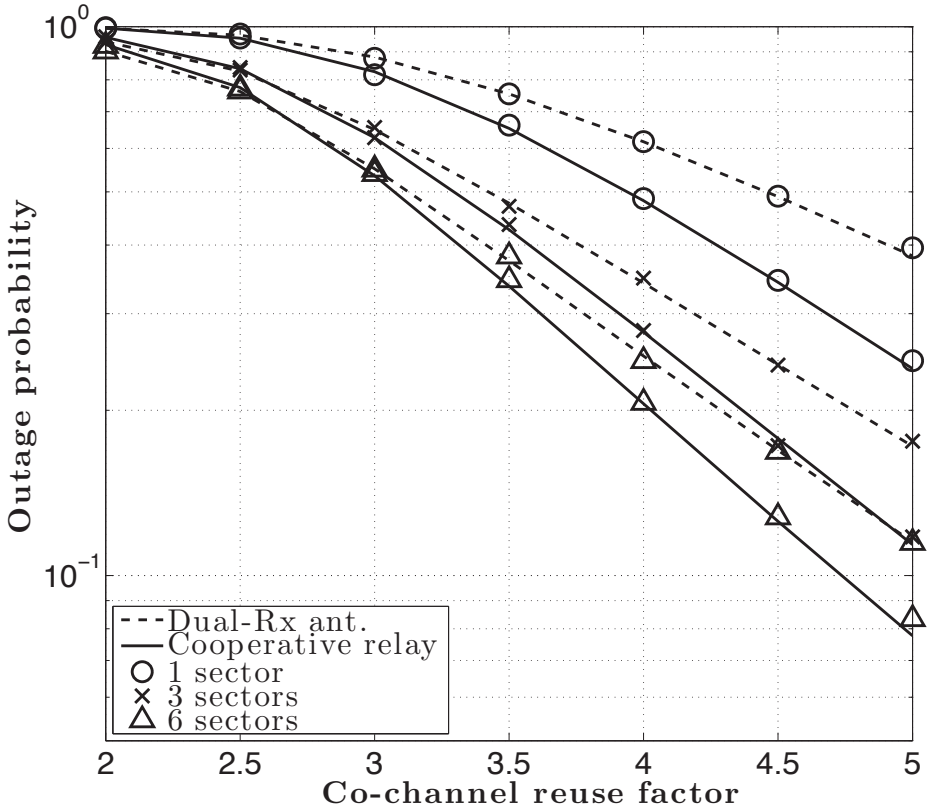

Figure 31: Uplink end-to-end outage probability versus co-channel reuse factor

factor in the downlink and the uplink. As mentioned earlier, the cooperative-diversity gain comes at the cost of decreased spectral efficiency. Thus, compared to the spectral efficiency of the dual-Rx system, that of the cooperative-diversity system deteriorates in both the uplink and the downlink. However, when cell sectorization is employed, the performance of the latter improves such that it is comparable to that of the single-Rx system in Fig. 32.

Figure 33 illustrates a more extensive performance degradation when cell sectorization is employed than in Fig. 32, and the performance does not improve as the co-channel reuse factor increases; however, the spectral efficiency of the proposed system using the omnidirectional cell becomes comparable to that of the single-Rx system.

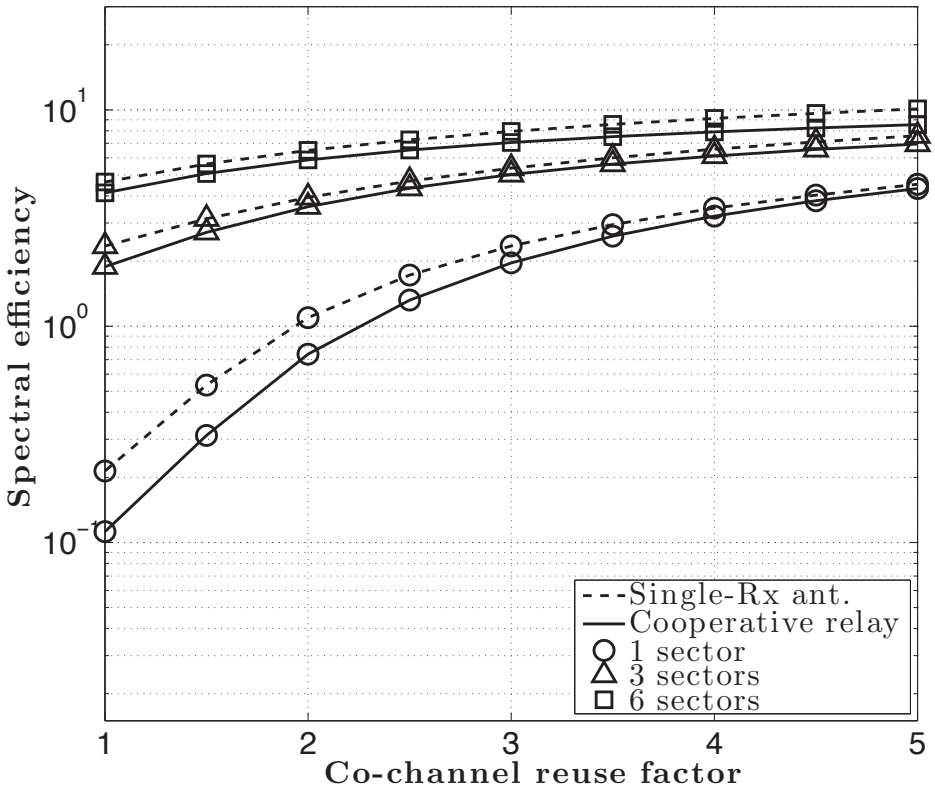

Figure 32: Downlink spectral efficiency versus co-channel reuse factor

The differences between the outage probabilities of the DF cooperative-diversity system and the dual-Rx antenna system as the relay location varies are depicted in Fig. 34 for the omnidirectional, Fig. 35 for 120° sectorized, and Fig. 36 for 60° sectorized cells in the downlink, respectively. The "black" zone does not provide absolute performance of the proposed system but relative performance compared to the dual-Rx antenna system. Therefore, the "black" zone represents the region of relay location where the cooperative-diversity system outperforms the dual-Rx antenna system; otherwise, the dual-Rx antenna system performs better.

In the uplink, the differences between the outage probabilities of the DF cooperative-diversity system and the dual-Rx antenna system as the relay location varies are depicted in Fig. 37 for the omnidirectional, Fig. 38 for 120° sectorized, and Fig. 39 for

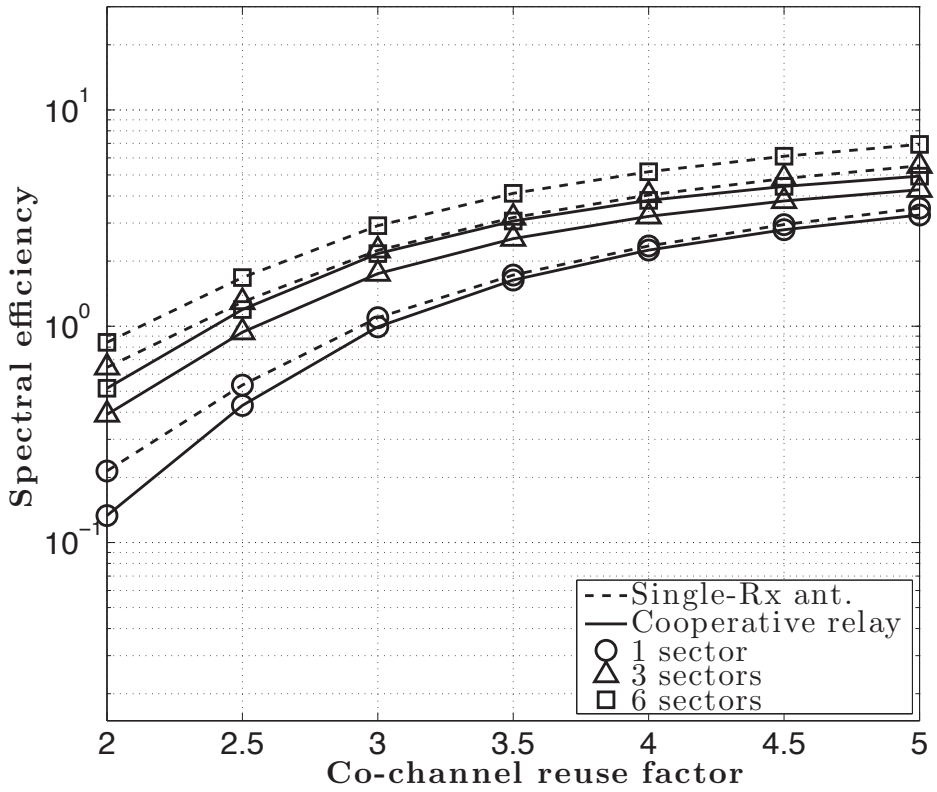

Figure 33: Uplink spectral efficiency versus co-channel reuse factor

60° sectorized cells, respectively. From Fig. 34 to Fig. 36, as the number of sectors in the cell increases, the size of the "black" zone of the downlink also increases, and the center of the "black" zone is close to the user's MS. Noticeable results are that the size of the uplink "black" zone in Figs. 37, 38, and 39 are significantly larger than that of downlink in Figs. 34, 35, and 36, so the relay selection of the uplink can be performed more efficiently than that of the downlink. However, as the number of the sectors in the cell increases, the size of the uplink "black" zone also increases but that of the downlink "black" zone decreases, and the center of the downlink "black" zone moves toward destination BS. Another important result is that when cell sectorization is employed, the uplink "black" zone does not overlap with the downlink "black" zone. From the viewpoint of system management, a common relay for both

the uplink and the downlink is more efficient than different relays for each link. The common relay should be located the overlapped area of both the "black" zones to show better performance than the dual-Rx antenna system for all links. However, the effective zone of downlink in Figs. 34, 35, and 36 is not overlapped with that of uplink in Figs. 37, 38, and 39. Thus, this show that different relays should be considered for cell sectorization under the worst-case CCI scenario in the uplink and the downlink. Establishing a common relay region necessitates an increase in the cooperative power ratio of the downlink, or a reduction in the number of interferers at the relay, from the results shown in Fig. 29.

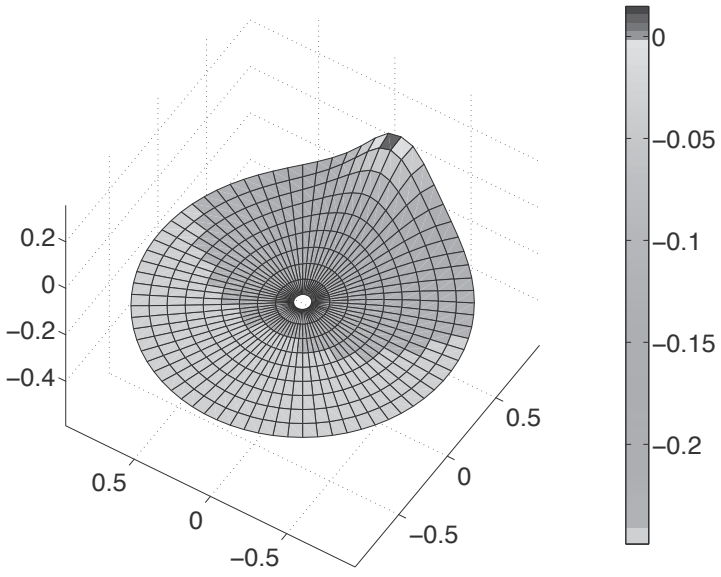

Figure 34: Difference between the outage probabilities of the DF cooperative system and the dual-Rx antenna system as a function of the relay location in the downlink of omnidirectional cell.

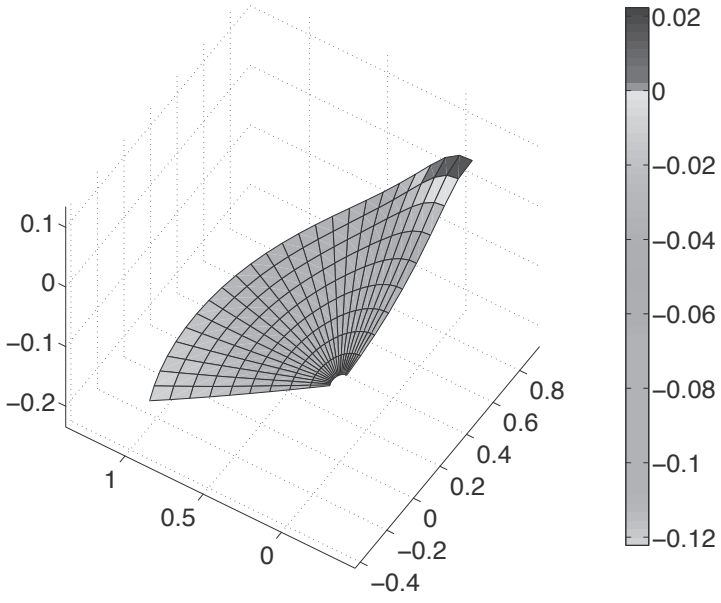

Figure 35: Difference between the outage probabilities of the DF cooperative system and the dual-Rx antenna system as a function of the relay location in the downlink of 120° sectorized cell.

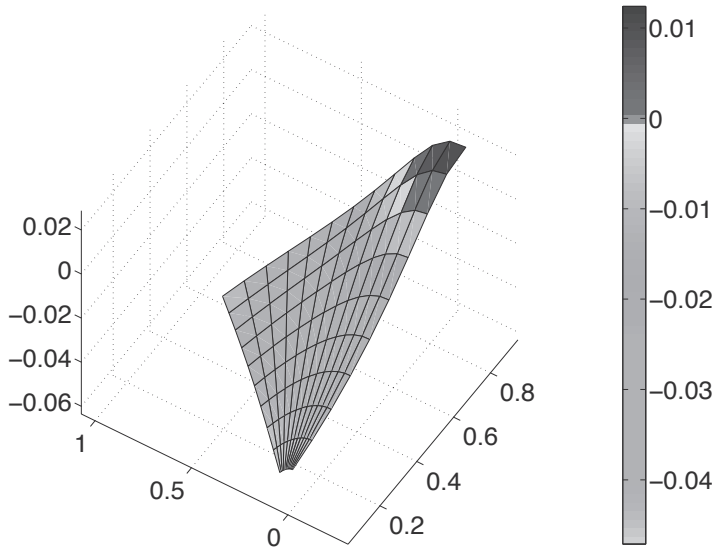

Figure 36: Difference between the outage probabilities of the DF cooperative system and the dual-Rx antenna system as a function of the relay location in the downlink of 60° sectorized cell.

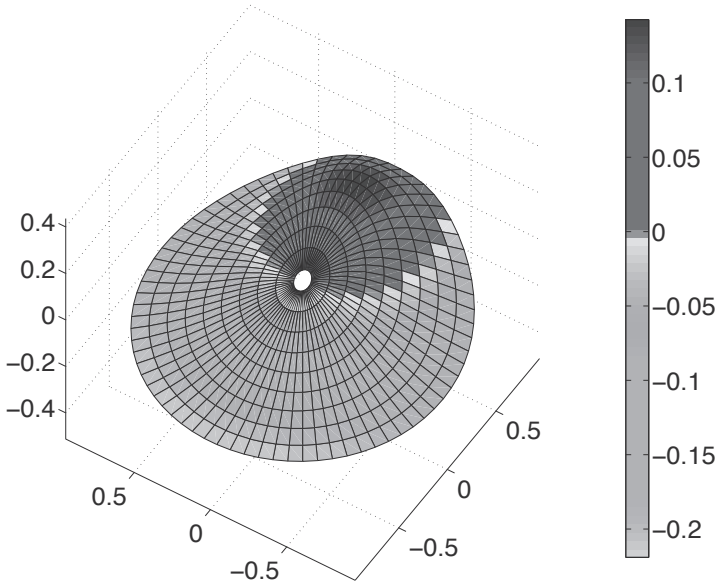

Figure 37: Difference between the outage probabilities of the DF cooperative system and the dual-Rx antenna system as a function of the relay location in the uplink of omnidirectional cell.

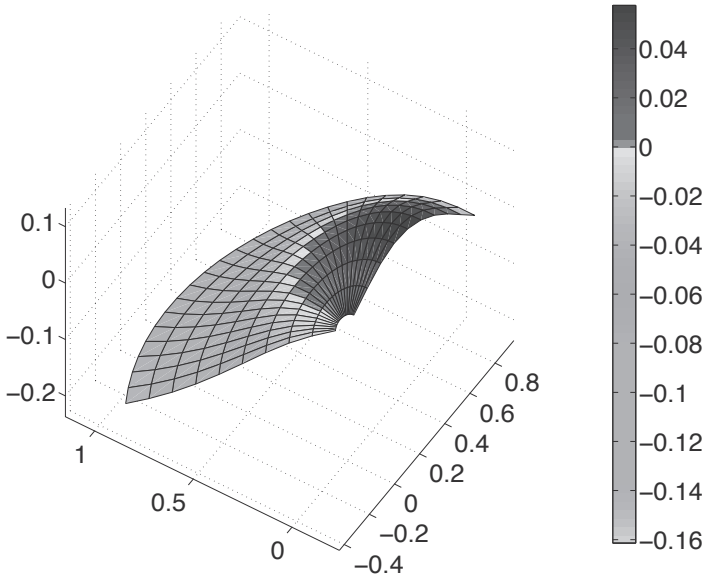

Figure 38: Difference between the outage probabilities of the DF cooperative system and the dual-Rx antenna system as a function of the relay location in the uplink of 120° sectorized cell.

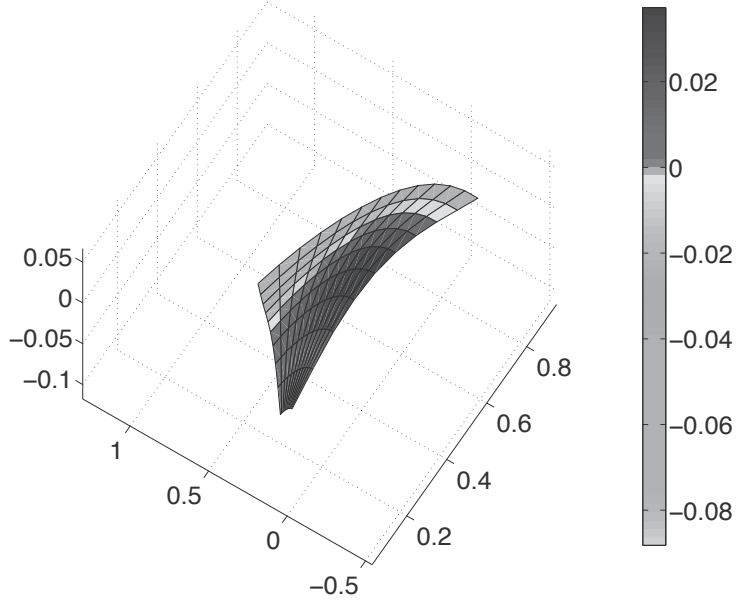

Figure 39: Difference between the outage probabilities of the DF cooperative system and the dual-Rx antenna system as a function of the relay location in the uplink of 60° sectorized cell.

CHAPTER VII

COOPERATIVE DIVERSITY SYSTEMS WITH PACKET TRANSMISSION IN CELLULAR NETWORKS

7.1 Overview

Extensive studies have analyzed the performance of selection DF relaying systems, but most have focused on either the outage probability or the ASEP performance and, moreover, they assumed symbol-by-symbol decoding [1]. For practical purposes, symbol-by-symbol decoding is not feasible when considering signaling overhead, since the message should be transmitted through multiple packets in packet-based wireless communication systems [42]. In addition, SNR estimation was originally used to make relaying decisions in selection DF relay networks, which is referred as the outage-based relaying. However, a CRC code was employed in [57], since it can reduce the system complexity and fully exploit the benefit of DF relaying for per-packet error detection in practical cooperative transmission, which is referred as the CRC-based relaying. Therefore, an important metric for evaluating the performance of DF relaying is the APEP rather than the ASEP.

We investigate the APEP performance of selection DF cooperative diversity in both the uplink and the downlink of cellular networks. We first derive closed-form expressions for the pdf of the CIR, outage probability, and the end-to-end ASEP of the selection DF cooperative diversity system using MRC on non-identical Nakagami/Nakagami channels. We then evaluate APEP with respect to the co-channel reuse factor for omnidirectional cells in the cellular uplink and the downlink under worst case CCI conditions. For the selection DF relaying schemes, we compare the

APEP performances for various schemes: i) outage-based symbol relaying, ii) outage-based packet relaying, and iii) CRC-based packet relaying. In addition, the effect of FEC on the selection DF relaying schemes will be discussed. This chapter shows that outage-based packet relaying shows better performance than the other relaying schemes for uncoded systems, but the effect of FEC can significantly improve the performance of CRC-based packet relaying system since the error correction as well as error detection can be performed at the relay.

7.2 System and Channel Models

The cooperative diversity system in this chapter is similar to Section 6.2, which consists of a source **S**, a destination **D**, and a relay **R**. Compared to Section 6.2, the proposed systems can employ a block or convolutional code, or a combination of both for channel coding over a packet. Even though a convolutional code does not use blocks (packets), since cooperative transmission in the system is performed with a packet, a convolutional code with tail-biting and termination can be assumed in the system [59]. To determine whether decoded packet is erroneous or not in the relay, the CRC-based packet relaying scheme uses a CRC code concatenated with FEC to check for erroneous packets. The relay in outage-based packet relaying regards the packet as erroneous if the average CIR for the packet duration falls below a specified threshold. Likewise, the relay in outage-based symbol relaying regards the packet as erroneous if the CIR for any symbol falls below a specified threshold. The proposed systems employ perfect symbol interleaving, which results in statistically independent symbol errors. The delay or latency caused by such interleaving is beyond the scope of this thesis. For orthogonal transmission, either time-division multiple access or frequency-division multiple access can be employed. Therefore, the received signals of the source-to-destination, source-to-relay, and relay-to-destination links are the same to (101), but the channel in this chapter is Nakagami-m faded for

both desired and interfering signals, which the same to those of Section 3.2. However, we use the propagation path-loss exponent α is equal to 3.76 from (100) and power allocation is defined in (67) according to cellular environments. We consider a conventional cellular network with a hexagonal grid where the serving cell is surrounded by six co-channel interfering cells in the first-tier, as depicted in Figs. 25 and 26 of Section 6.2.2. We consider the worst case CCI scenario with a fully-loaded system in both the uplink and the downlink, but sectorization is not employed. According to the geometry model in Section 6.2.3, the CIR of the source-to-destination link is $Z^u_{S,D} = 1/\sum_{l=1}^{N_{I,D}} \varphi^{-a}_{I',D}$, where $\varphi_{I',D} = \sqrt{(R_u-1)^2 - 2(R_u-1)\cos\Theta'_l + 1}$. The CIR of the source-to-relay link is $Z^u_{S,R}(k,\theta) = k^{-a}/\sum_{l=1}^{N_{I,R}} \varphi^{-a}_{I',R}$, where $\varphi_{I',R} = \sqrt{(R_u-1)^2 - 2k(R_u-1)\cos(\Theta'_l-\theta) + k^2}$, and the CIR of the relay-to-destination link is $Z^u_{R,D}(k,\theta) = \varphi^{-a}_{R,D}/\sum_{l=1}^{N_{I,D}} \varphi^{a}_{I',D}$.

In the downlink, the CIR of the source-to-destination link is $Z^d_{S,D} = 1/\sum_{l=1}^{N_{I,D}} \varphi^{-a}_{I,D}$, where $\varphi_{I,D} = \sqrt{R_u^2 - 2R_u\cos\Theta_l + 1}$. The CIR of the source-to-relay link can be expressed as $Z^d_{S,R}(k,\theta) = k^{-a}/\sum_{l=1}^{N_{I,R}} \varphi^{-a}_{I,R}$, where $\varphi_{I,R} = \sqrt{R_u^2 - 2kR_u\cos(\Theta_l-\theta) + k^2}$. However, the Tx power of the relay is ζP_S; thus, the CIR of the relay-to-destination link can be written as $Z^d_{R,D}(k,\theta) = \varphi^{-a}_{R,D}/\zeta\sum_{l=1}^{N_{I,D}} \varphi^{-a}_{I,D}$, where $\varphi_{R,D} = \sqrt{k^2 - 2k\cos\theta + 1}$, and ζ is defined in (67).

7.3 Pdf and Outage Analysis

In this section, we derive the outage probability and pdf of the CIR of each link. We consider a three-node-relay system, so the number of diversity branches is two, and we let X_1 and X_2 denote the desired signal power of the source-to-destination link and relay-to-destination link, respectively. Since the selection DF scheme determines whether or not the relay forwards the source packet by observing the CRC status, the end-to-end pdf of CIR Z can be expressed by using conditional probability as

$$p^{ete}_Z(z) = \Phi_{SR}\, p_{Z_{X_1}}(z) + (1-\Phi_{SR})\, p_{Z_{X_1X_2}}(z)\,, \tag{127}$$

where Φ_{SR} is the probability of the event which the relay detects erroneous packets, $p_{Z_{X_1}}(z)$ is the pdf of the CIR for the source-to-destination link, and $p_{Z_{X_1X_2}}(z)$ is the pdf of the CIR for the signal combining with the source-to-destination and the relay-to-destination branches. First, we present the outage probability and the pdf of the CIR of a single-branch transmission.

7.3.1 Pdf and Outage Probability of Single-branch Transmission

The proposed systems consist of a single-branch transmission with multiple interferers and a multiple-branches transmission with multiple interferers. The source-to-destination and the source-to-relay links are applicable to the single-branch transmission with multiple interferers, and the signal combining with the source-to-destination and the relay-to-destination links corresponds to a multiple-branches transmission with multiple interferers.

The channels for both the desired and interfering signals are Nakagami-m faded, thus, the pdfs of the desired and interfering signal powers, X and Y, have the following Gamma distributions

$$\begin{aligned} p_X(x) &= \left(\frac{m_X}{\omega_X}\right)^{m_X} \frac{x^{m_X-1}}{\Gamma(m_X)} \exp\left(\frac{-m_X x}{\omega_X}\right), \\ p_Y(y) &= \left(\frac{m_Y}{\omega_Y}\right)^{m_Y} \frac{y^{m_Y-1}}{\Gamma(m_Y)} \exp\left(\frac{-m_Y y}{\omega_Y}\right), \end{aligned} \tag{128}$$

respectively, where $\Gamma(\cdot)$ is the gamma function, m_X and m_Y are the Nakagami shape factors, which are assumed to be integer valued as mentioned in Section 3.3.1, and ω_X and ω_Y are the local means of X and Y, respectively. Let $\alpha_Y =: \omega_Y/m_Y$ and $\alpha_X =: \omega_X/m_X$. When multiple interferers ($N_I > 1$) affect a single-branch link between two terminals without diversity, Y is the sum of the interfering signal powers, and the pdf of Y is the sum of mutually independent Gamma distributions. The pdf for the sum of multiple Gamma distributions was derived by using a partial fraction technique

and inverse Laplace transform in [24] as

$$p_Y(y) = \sum_{a=1}^{N_I} \sum_{b=1}^{m_{Y_a}} \frac{(-1)^b}{\Gamma(b)} \beta_{a,b}^Y y^{b-1} \exp\left(\frac{-y}{\alpha_{Y_a}}\right) \ , \tag{129}$$

where the coefficient $\beta_{a,b}^Y$ is denoted in (27) of Chapter 3.

The pdf of Z can be obtained by (109) in Section 6.3.2. Applying the pdfs of X in (128) and Y in (129) to (109), the pdf of the CIR Z for a single branch with multiple interferers can be written by using the H-function defined in (111) as

$$p_Z(z) = \sum_{a=1}^{N_I} \sum_{b=1}^{m_{Y_a}} \beta_{a,b}^Y (x_{j_a}) (-\alpha_{Y_a})^b H(z; m_X, b, \alpha_X, \alpha_{Y_a}) \ . \tag{130}$$

Since the outage probability is defined in (58), substituting (130) into (58) yields the outage probability, which can be applied to the source-to-relay link.

$$P_o(\lambda) = 1 - \sum_{a=1}^{N_I} \sum_{b=1}^{m_{Y_a}} \beta_{a,b}^Y (-\alpha_{Y_a})^b F(\lambda; m_X, b, \alpha_X, \alpha_{Y_a}) \ , \tag{131}$$

where the F-function is defined in (113).

7.3.2 Pdf and Outage Probability of Multi-branch Transmission

In the destination, the receiver combines the branch signals by using MRC. Thus, the pdfs of X and Y are the sum of mutually independent Gamma distributions, and if the number of diversity branches is $\mathcal{M}$, the pdf of X has the same form as (129),

$$p_X(x) = \sum_{a=1}^{\mathcal{M}} \sum_{b=1}^{m_{X_a}} \frac{(-1)^b}{\Gamma(b)} \beta_{a,b}^X x^{b-1} \exp\left(\frac{-x}{\alpha_{X_a}}\right) \ , \tag{132}$$

where the coefficient $\beta_{a,b}^X$ is denoted in (14) of Chapter 3. Applying the pdfs of X in (132) and Y in (129) to (109), the pdf of CIR Z for multiple branches with multiple interferers can be written as

$$p_Z(z) = \sum_{a=1}^{\mathcal{M}} \sum_{b=1}^{m_{X_a}} \beta_{a,b}^X (-\alpha_{X_a})^b \sum_{c=1}^{N_I} \sum_{d=1}^{m_{Y_c}} \beta_{c,d}^Y (-\alpha_{Y_c})^d H(z; b, d, \alpha_{X_a}, \alpha_{Y_c}) \ , \tag{133}$$

and the outage probability of (133) can be likewise obtained from (131) as

$$P_o(\lambda) = 1 - \sum_{a=1}^{\mathcal{M}} \sum_{b=1}^{m_{X_a}} \beta_{a,b}^X (-\alpha_{X_a})^b \sum_{c=1}^{N_I} \sum_{d=1}^{m_{Y_c}} \beta_{c,d}^Y (-\alpha_{Y_c})^d F(\lambda; b, d, \alpha_{X_a}, \alpha_{Y_c}) \ . \tag{134}$$

7.3.3 End-to-End Pdf and Outage Probability

We derive the end-to-end pdf of the CIR Z and outage probability of outage-based symbol relaying. In the outage-based symbol relaying, Φ_{SR} in (127) is the outage probability of the source-to-relay link, which is derived in (131), and the number of interferers of the link is $N_{I,R}$. In (127), $p_{Z_{X_1}}(z)$ is equal to (130), and $p_{Z_{X_1X_2}}(z)$ is equal to (133) with $\mathcal{M} = 2$ and $N_I = N_{I,D}$. Therefore, the end-to-end pdf at a given relay location can be obtained as follows:

$$p_Z^{\text{ete}}(z|k,\theta) = \Phi_{SR} \sum_{c=1}^{N_{I,D}} \sum_{d=1}^{m_{Y_c}} (-\alpha_{Y_c})^d \beta_{c,d}^Y H(z; m_{X_1}, d, \alpha_{X_1}, \alpha_{Y_c})$$
$$+ (1-\Phi_{SR}) \sum_{a=1}^{2} \sum_{b=1}^{m_{X_a}} \beta_{a,b}^X \{-\alpha_{X_a}\}^b \sum_{c=1}^{N_{I,D}} \sum_{d=1}^{m_{Y_c}} \beta_{c,d}^Y (-\alpha_{Y_c})^d H(z; b, d, \alpha_{X_a}, \alpha_{Y_c}) \ . \quad (135)$$

The end-to-end outage probability at a given relay location is derived by solving (127) with (58), and it consists of the outage probabilities in (131) and (134) as follows:

$$P_o^{\text{ete}}(\lambda|k,\theta) = 1 - \Bigg[\Phi_{SR} \sum_{c=1}^{N_{I,D}} \sum_{d=1}^{m_{Y_c}} (-\alpha_{Y_c})^d \beta_{c,d}^Y F(\lambda; m_{X_1}, d, \alpha_{X_1}, \alpha_{Y_c}) + (1-\Phi_{SR})$$
$$\times \sum_{a=1}^{2} \sum_{b=1}^{m_{X_a}} \beta_{a,b}^X \{-\alpha_{X_a}\}^b \sum_{c=1}^{N_{I,D}} \sum_{d=1}^{m_{Y_c}} \beta_{c,d}^Y \{-\alpha_{Y_c}\}^d F(\lambda; b, d, \alpha_{X_a}, \alpha_{Y_c}) \Bigg] \ . \quad (136)$$

7.4 APEP Analysis

This section presents closed-form expressions for the ASEP and APEP of the proposed systems. The ASEP derived in this section can be applied to M-PSK and M-QAM systems. One of the advantages of the DF scheme is that every link can employ different modulation schemes, but all terminals in our system use the same modulation scheme to reduce system complexity. Closed-form expressions for APEP are not available except for non-coherent frequency shift keying and, moreover, there is no relation between the average ASEP and APEP for slow-fading environments [60]. This is because averaging the conditional PEP over fading environments results

in integer powers of the Gaussian-Q function, which makes the analysis challenging. However, systems employing suitable interleaving could result in a memoryless channel, where two adjacent symbols are considered to be faded independently [61, 62, 63, 64]. Assuming a bounded distance decoder with ideal interleaving, the APEP of the single-hop transmission with $\mathcal{M}$-ary modulation for a block of T coded symbols capable of correcting K coded-symbol errors can be expressed as

$$P_p = 1 - \sum_{i=0}^{K} \binom{T}{i} P_s{}^i (1 - P_s)^{T-i}, \tag{137}$$

where $T = \mathcal{L}/\log_2 \mathcal{M}$, and $\mathcal{L}$ is the total packet bit length, and P_s is the ASEP of the single-hop transmission system.

We derived the end-to-end ASEP for cooperative relaying systems in Chapter 4. Therefore, with (63) in Section 4.5 and (127), ASEP can be divided into two parts. First, for the event that the relay fails to decode, the ASEP can be obtained by substituting the outage probability in (131) into (63) in Section 4.5 as

$$P_{s,X_1} = \frac{\alpha}{2} - \sum_{c=1}^{N_{I,D}} \sum_{d=1}^{m_{Y_c}} (-\alpha_{Y_c})^d \beta_{c,d}^{Y} S(\alpha, \beta, m_{X_1}, d, \alpha_{X_1}, \alpha_{Y_c}), \tag{138}$$

where S-function is defined as

$$\begin{aligned} S(\alpha, \beta, m_X, m_Y, \alpha_X, \alpha_Y) = \frac{\alpha}{2\sqrt{\pi}} (\alpha_Z \beta)^{m_Y} \sum_{n=0}^{m_X - 1} \frac{\Gamma(m_Y + n)\Gamma(n + 1/2)}{\Gamma(m_Y)\Gamma(n+1)} \\ \times \Psi[m_Y + n, m_Y + 1/2, \alpha_Z \beta], \end{aligned} \tag{139}$$

and $\Psi[\cdot, \cdot, \cdot]$ is the confluent hypergeometric function of the second kind.

Second, for the event that the relay successfully recovers the packet, the ASEP can be obtained by substituting (134) into (63) as

$$\begin{aligned} P_{s,X_1X_2} = \frac{\alpha}{2} - \sum_{a=1}^{2} \sum_{b=1}^{m_{X_a}} \beta_{a,b}^{X} \{-\alpha_{X_a}\}^b \sum_{c=1}^{N_{I,D}} \sum_{d=1}^{m_{Y_c}} \beta_{c,d}^{Y} \{-\alpha_{Y_c}\}^d \\ \times S(\alpha, \beta, b, d, \alpha_{X_a}, \alpha_{Y_c}). \end{aligned} \tag{140}$$

7.4.1 APEP of Outage-based Symbol Relaying

The ASEP of the outage-based symbol relaying has a similar form to (127) as

$$P_s^{ete} = \Phi_{SR}\, P_{s,X_1} + (1 - \Phi_{SR})\, P_{s,X_1X_2}\,, \tag{141}$$

where Φ_{SR} is the same as (131). Since symbol-by-symbol detection is employed, the end-to-end APEP can be obtained by substituting (141) into (137) as

$$P_p^{ete} = 1 - \sum_{i=0}^{K} (P_s^{ete})^i (1 - P_s^{ete})^{T-i}\,. \tag{142}$$

7.4.2 APEP of Outage-based Packet Relaying

In contrast to symbol relaying, packet relaying forwards the packet, and the destination combines the signals for a packet unit. Therefore, the end-to-end APEP can be written by using conditional probability and APEPs for single-branch transmission and multi-branch transmission, as follows:

$$P_p^{ete} = \Phi_{SR}\, P_{p,X_1} + (1 - \Phi_{SR})\, P_{p,X_1X_2}\,, \tag{143}$$

where

$$P_{p,X_1} = 1 - \sum_{i=0}^{K} {P_{s,X_1}}^i (1 - P_{s,X_1})^{T-i}\,,$$

and

$$P_{p,X_1X_2} = 1 - \sum_{i=0}^{K} {P_{s,X_1X_2}}^i (1 - P_{s,X_1X_2})^{T-i}\,.$$

7.4.3 APEP of CRC-based Packet Relaying

In the CRC-based packet relaying, Φ_{SR} in (143) is the APEP of the source-to-relay link which can be derived from (138), where the number of interferers of the link is $N_{I,R}$, as follows:

$$\Phi_{SR} = 1 - \sum_{i=0}^{K} {P_{s,X_{SR}}}^i (1 - P_{s,X_{SR}})^{T-i}\,. \tag{144}$$

7.5 Performance Analysis

In this section, fully-loaded cooperative cellular relaying systems are considered on non-identical Nakagami/Nakagami channels. The outage probability and APEP of the proposed systems are evaluated with respect to the co-channel reuse factor and the relay location in both the uplink and the downlink of the cellular networks. The results in the chapter assume a typical macro-cellular system where the Tx powers of the MS and the BS are 24 dBm and 43 dBm, respectively according to [55]. The CIR threshold λ is assumed as 12 dB for all nodes. The Nakagami shape factors for the desired and interfering signals are two and one, respectively. The analytic results for the outage probability in (136) are verified by Monte Carlo simulations. To obtain a sufficient precision level, the simulation process is performed in 10^8 trials. Note that the markers in Fig. 40 describe the simulation results, and the solid lines show the analytical results. Since the ASEP in Section 7.4 is derived from (136), the simulation does not necessarily verify the analytic results after Fig. 40. Each system after Fig. 42 employs 4-QAM with 256 bits packet length, and the relays are located in the optimal location derived in Fig. 41.

Figure 40 presents the optimal relay location in terms of the outage probability for both the uplink and the downlink. For the best outage performance, the relay should be located on the line connecting the source and the destination, i.e., $\theta = 0^\circ$, but the normalized distance of the source-to-relay link, k, varies according to the channel conditions. The different location of the optimal relay between the uplink and the downlink can explain the effect of P_S/P_R. In the figure, the optimal relay location is $k = 0.775$ in the downlink, but $k = 0.475$ in the uplink. The reason for the difference is that $P_R = 0.01P_S$ in the downlink, but $P_R = P_S$ in the uplink. In the figure, it also shows that the analytic results agree with the simulation results.

Figure 41 provides the end-to-end ASEP of the outage-based packet relaying for the uplink and the downlink when the packet length increases from 256 bits to 1024

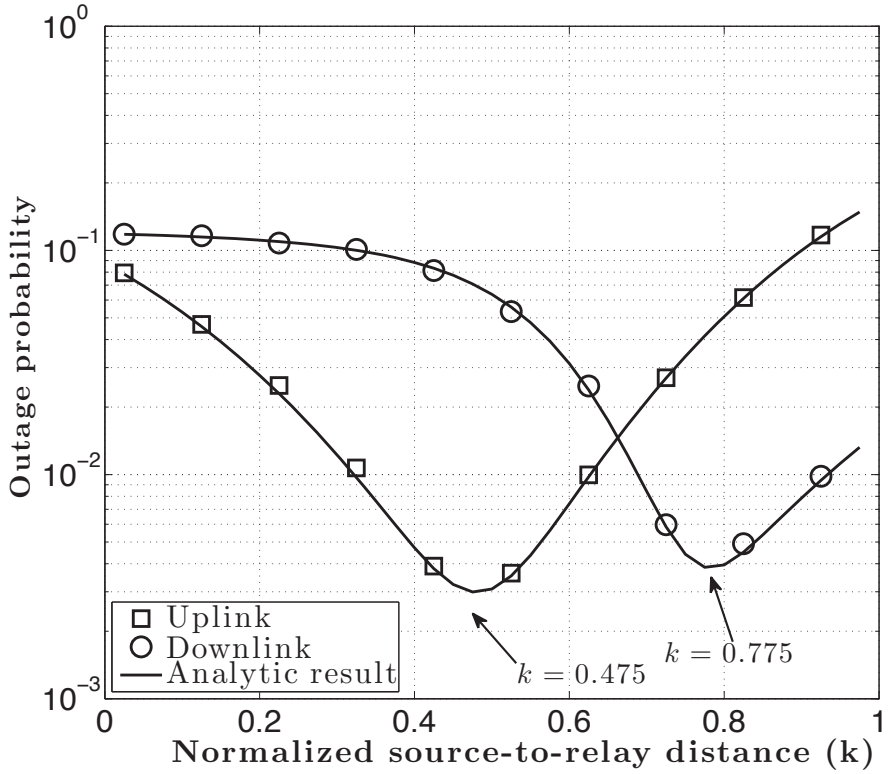

Figure 40: End-to-end outage probability with respect to the normalized source-to-relay distance ($R_u = 5$)

bits for both 4-QAM and 16-QAM, but FEC is not employed ($K = 0$). As expected, the end-to-end APEP performance is degraded as the packet length and modulation order increase, in a similar fashion to a single-hop transmission. Compared to Fig. 40, this figure shows that the optimal relay location in terms of APEP depends on the packet length and modulation order. As the packet length increases, the optimal relay location moves to the destination, and the effect of increasing the modulation order is larger than that of increasing the packet length. When the packet length and modulation order are increased, the APEP performances of respective links are degraded. However, when the relay is close to the destination, the performance gap is small; otherwise the performance gap increases. The reason is that as the relay is located close to the destination, the channel condition of the relay-to-destination

is improved, and the improved channel condition dominates the performance degradation due to increasing packet length and modulation order. As the relay is close to the source, the improved channel condition of the source-to-relay cannot limit the impact of packet length and modulation order. These results show that the end-to-end APEP performance is more susceptible to the APEP of the relay-to-destination link than that of the source-to-relay link.

Figure 42 shows the effect of FEC over the end-to-end APEP of outage-based packet relaying. In the figure, the error-correction capability is increased from zero coded symbol ($K = 0$) to two coded symbols ($K = 2$). Compared to Fig. 41, the end-to-end APEP performance can be significantly improved by the effect of FEC. As the error-correction capability is decreased, the optimal relay location moves toward the destination. The reason is that the destination requires a higher CIR than the relay since the relay-to-destination link is more vulnerable to the interference than the source-to-relay link.

Figure 43 presents comparisons of the end-to-end APEP of various selection DF schemes with respect to normalized source-to-relay distance in both the uplink and the downlink when the effect of FEC is considered. In both the uplink and the downlink, when there is no error correction ($K = 0$), outage-based packet relaying outperforms the other systems in the entire distance. In contrast to Figs. 41 and 42, the end-to-end APEP performances of the respective systems are similar when the relay location is close to the source, but as the relay moves to the destination, the performance gap increases. This is because the channel condition of the source-to-relay link determines the performance of the error detection at the relay. When the channel condition of the source-to-relay link is good, both CIR estimation and CRC checking show similar performance, but otherwise, CRC checking of the uncoded system will reduce the possible cooperative gain. In addition, outage-based packet relaying outperforms outage-based symbol relaying because fixed outage threshold for

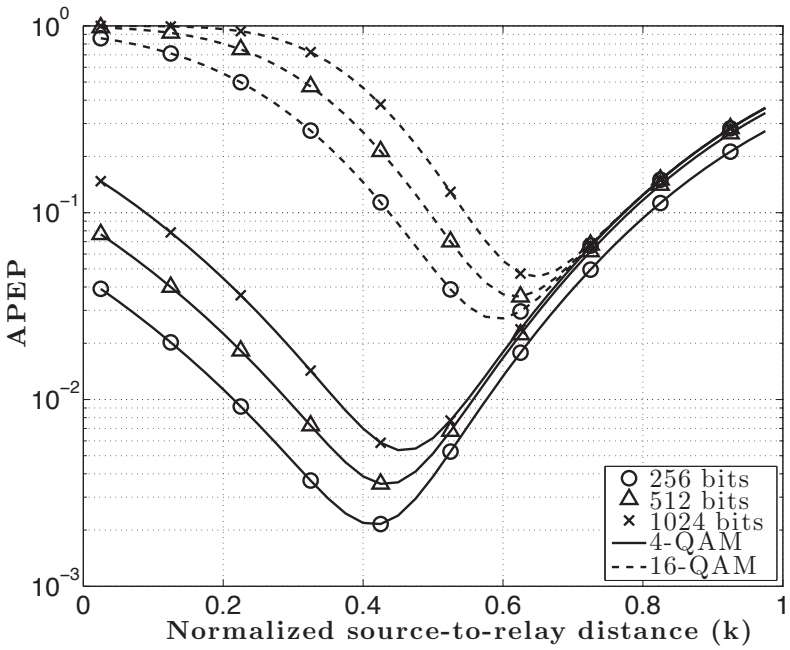

(a) Uplink.

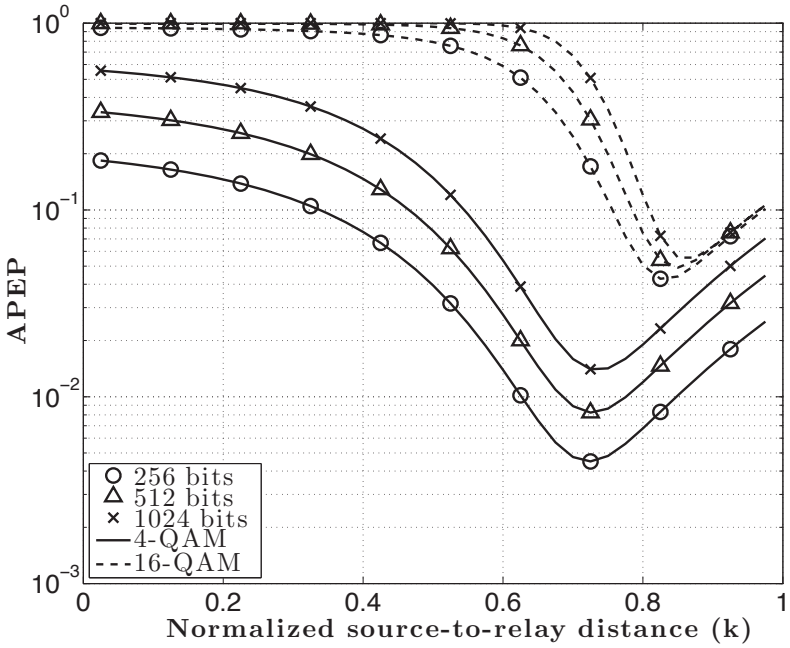

(b) Downlink.

Figure 41: End-to-end APEP of outage-based packet relaying with respect to the normalized source-to-relay distance for various packet lengths and modulation orders.

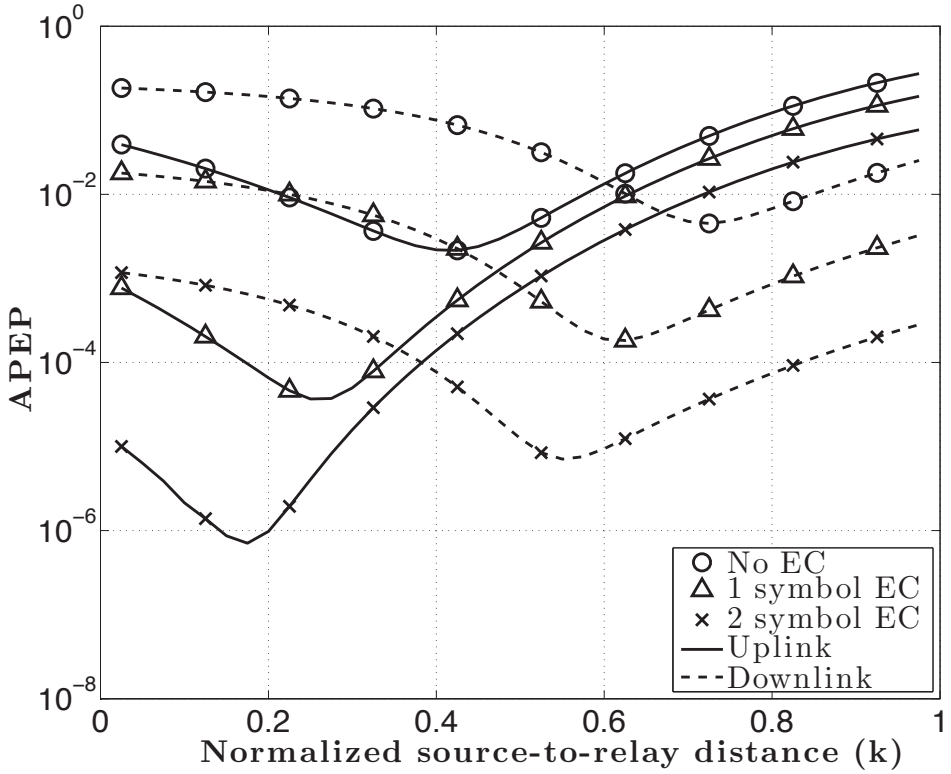

Figure 42: End-to-end APEP of outage-based packet relaying with respect to the normalized source-to-relay distance under the effect of FEC.

every symbol allows more error propagation which degrades the end-to-end APEP. However, an interesting result is that CRC-based packet relaying outperforms the other systems under the effect of FEC. When error correction is considered, the performances of all systems are improved, but the performance of CRC-based packet relaying is significantly improved compared to the other systems. The reason is that the relay using CIR estimation cannot obtain coding gain compared to CRC checking. Even though the performance of the destination receiver can be improved by the coding gain, the relay using CIR estimation determines the cooperation according to the channel condition of the source-to-relay before decoding the source packet, while the relay using CRC checking determines it after decoding the source packet. In the realistic system, it is difficult to select a suitable CIR threshold for every symbol

or packet since it depends on the actual value of the channel fading coefficients, and since most systems usually use FEC, CRC-based packet relaying system is practically effective.

Figure 44 shows that as co-channel reuse factor is increased (i.e. the distance between the co-channel interfering cells and the serving cell is increased), the end-to-end APEP of each system is improved. Without error correction, the performance order is the same as in Fig. 43 for the entire co-channel reuse factor range in both the uplink and the downlink. However, the performance gap between the systems is decreased as co-channel reuse factor is increased. When the effect of FEC is considered, outage-based packet relaying outperforms the other systems in the low co-channel reuse factor region, while CRC-based packet relaying shows better performance in the high co-channel reuse factor region as mentioned in Fig. 43. Compared to the case without FEC, the performance gap between the system is increased as co-channel reuse factor is increased. The results show that even though FEC is employed, outage-based packet relaying can show better performance than CRC-based packet relaying when FEC cannot recover the erroneous packet due to strong CCI.

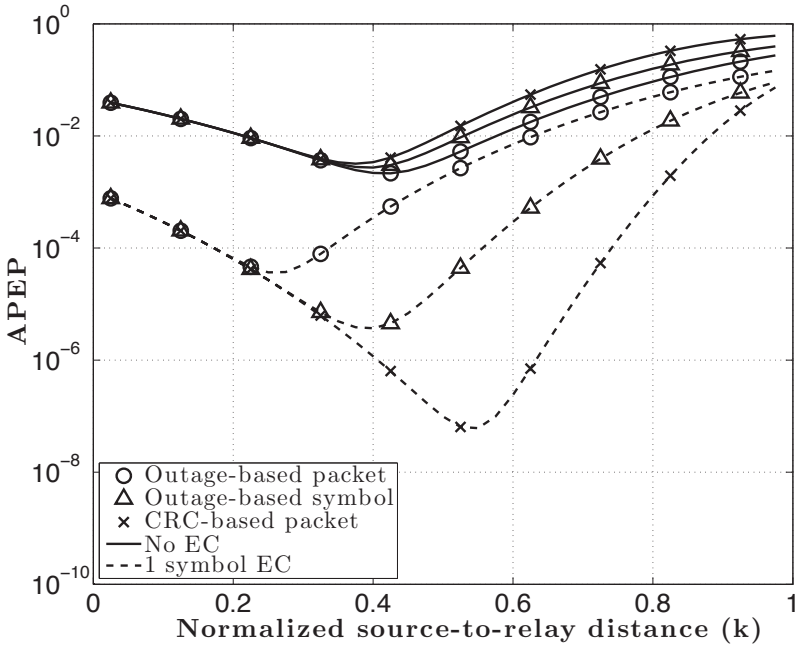

(a) Uplink.

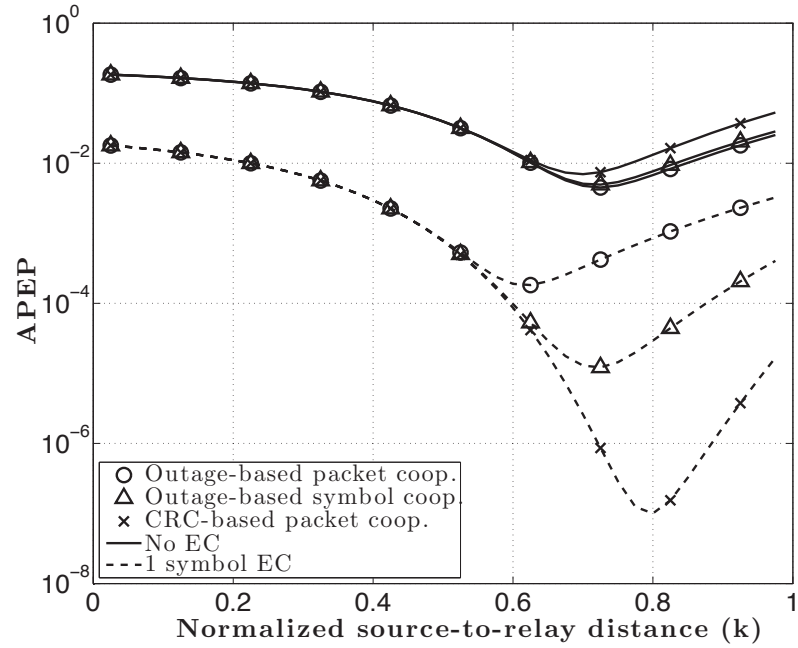

(b) Downlink.

Figure 43: Comparison of end-to-end APEP of various selection DF cooperative transmissions with respect to the normalized source-to-relay distance

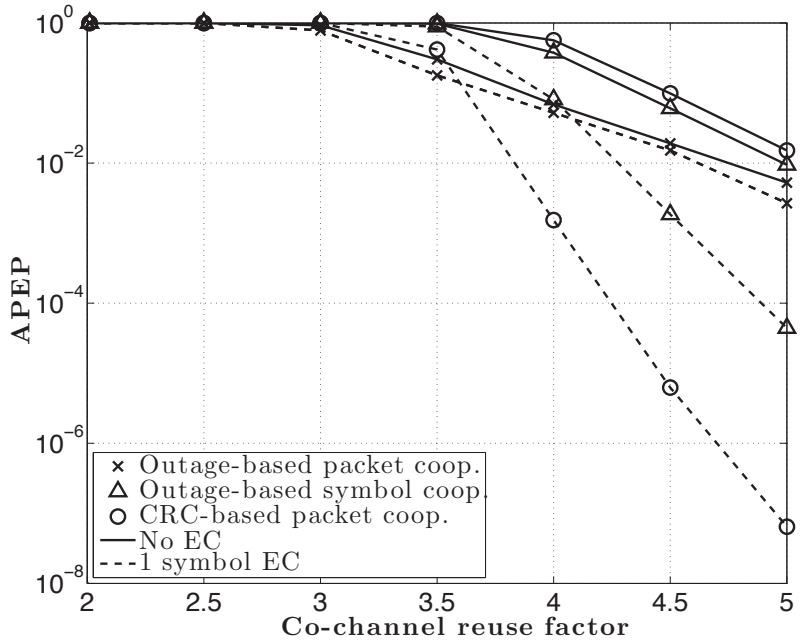

(a) Uplink.

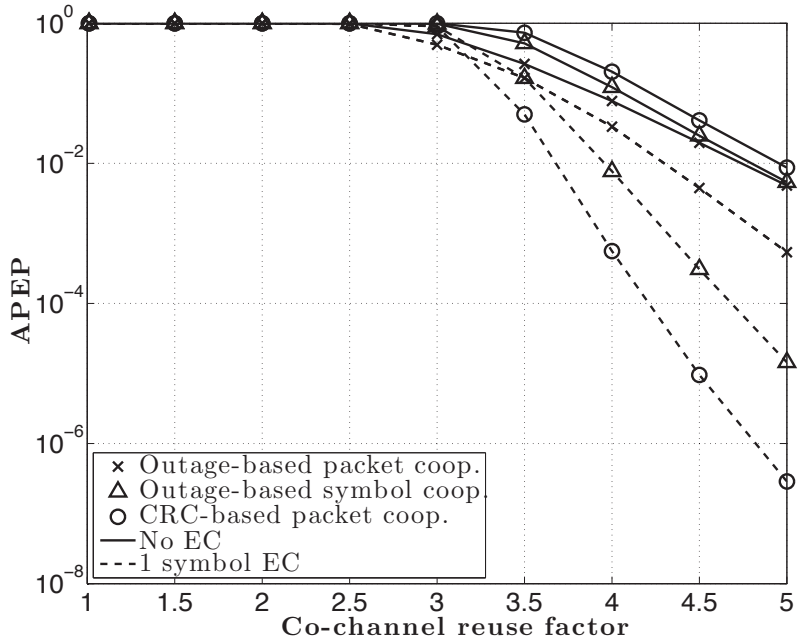

(b) Downlink.

Figure 44: End-to-end APEP versus co-channel reuse factor for various selection DF schemes

CHAPTER VIII

THROUGHPUT ANALYSIS FOR COOPERATIVE DIVERSITY SYSTEMS WITH PACKET TRANSMISSION

8.1 Overview

The spatial diversity of cooperative relaying with orthogonal relay transmission costs in terms of decreased spectral efficiency and, thus, the average throughput diminishes to zero as the number of relays approaches infinity [9]. To alleviate this limitation, the best relay selection scheme, which includes opportunistic relaying, and the DSTC scheme were studied in [5, 19, 20, 65, 66, 67, 68]. However, the best relay selection scheme requires global/local CSI for all channels, so that it imposes excessive amount of feedback data as the number of relays is increased [68]. In addition, the DSTC design is quite difficult in practice because of the distributed and ad-hoc nature of cooperative networks, and the need and availability of global CSI as well [20]. On the other hand, since synchronization across multiple relay channels is not critical in orthogonal transmission due to the orthogonality between the slots, cooperative relaying with orthogonal transmission does not require additional interference canceling techniques to avoid inter-relay interference. Therefore, cooperative relaying with orthogonal transmission is still attractive for networks composed of numerous, small, low-powered relays such as wireless sensor networks.

Throughput is affected by symbol rate, modulation alphabet size, packet length, the maximum number of retransmissions, and power level. Among the design parameters, to maximize throughput, power level and symbol rate in [69], retransmission by using ARQ in [57], and the modulation alphabet size in [70] were considered in

cooperative relaying networks. This chapter further improves throughput by using dynamic slot allocation operating on CRC-based relaying. Dynamic slot allocation was proposed for efficient resource scheduling in the cellular systems [71, 72], but there are still many unresolved problems of resource scheduling in cooperative relaying systems with packet transmission.

For the selection DF packet cooperative relaying systems, we analyze and compare the outage and throughput performances for various schemes: i) fixed-slot selection DF (FSDF), ii) repeated-slot selection DF (RSDF), and iii) variable-slot selection DF (VSDF). We derive closed-form expressions for the end-to-end outage probability, APEP, and throughput of the proposed schemes are derived with a closed form for non-identical Nakagami/Nakagami channels.

8.2 System and Channel Models

Laneman *et al.* proposed the fixed and selection DF schemes in [1]. While the fixed DF scheme always forwards a source packet to the destination, the selection DF scheme measures the received SNR for the packet, and if the measured SNR falls below a threshold, the source repeats its packet to the destination. In [1], this is referred to as the RSDF scheme. Compared to the selection DF scheme, the DF scheme in [3, 31, 32, 47] detects the erroneous packet by using CRC or SNR estimation, but the source does not repeat its packet when the relay detects erroneous packet. We call this the FSDF scheme in the chapter. Since cooperative relays using orthogonal transmission transmit their packets in different assigned slots, the system architectures for both RSDF and FSDF require $M+1$ orthogonal slots including the direct source-to-destination transmission of the first part as described in Fig. 45. In Fig. 45(a), the FSDF scheme does not use the $(m+1)$th slot when the m-th relay fails to decode the source packet. However, the RSDF scheme in Fig. 45(b) assigns the $(m+1)$th slot to the source in order to repeat its packet. Note that the RSDF scheme

requires request-to-send (RTS) / clear-to-send (CTS) signals between the source and the other nodes, or CSI for all nodes at the source.

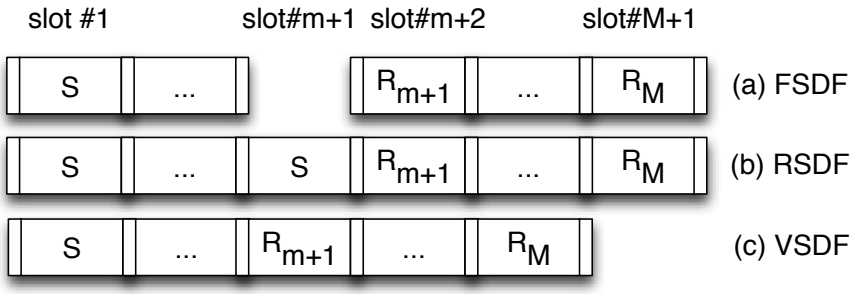

Figure 45: Slot assignment when the m-th relay fails to decode the source packet among M relays

In regard to diversity combining, the RSDF scheme can achieve full diversity order [1], but as the number of relays is increased, throughput performance is decreased due to the fixed number of slots as $M + 1$. To reduce the number of unused slots, we propose a VSDF scheme which employs a dynamic slot assignment by utilizing a single-bit indicating signal in the control channels between the relays and the destination in a distributed manner. After decoding the source packet at the relays, the indicating signals are transmitted to the destination. The destination then sends RTS signal to only the relays which transmitted the decoding success signal. Thus, the skipped $(m + 1)$th slot in Fig. 45(a) can be used by another relay as shown in Fig. 45(c). Contrasted to the RSDF scheme, VSDF does not require the communication between the source and the other nodes. Moreover, since diversity combining in the destination already requires coherent reception, using a single-bit indicating signal between the relays and the destination is not a burden to the system complexity. The VSDF scheme differs from incremental and ARQ relaying protocols in that the retransmission of the source packet is not required, moreover, it can be combined with incremental and ARQ relaying protocols. In addition, since the VSDF scheme can combine all successfully decoded slots, it also differs from cooperative diversity

with selection combining.

The orthogonal cooperative transmission assumed in our system is less efficient in terms of spectral resources than the DSTC and the opportunistic relay selection systems. However, since DSTC systems allow for all relays to transmit on the same time or the same frequency slot, inter-relay interference is introduced and, thus, the destination receiver must cancel this interference, which increases system complexity due to coherent reception between the multiple relays and the destination [9, 20]. Even though orthogonal cooperative transmission employs signal combining techniques that require coherent reception as well, it can avoid inter-relay interference due to the orthogonality between the slots. In addition, opportunistic relay selection requires CSI of all links, which implies a significant amount of control overhead. Thus, as the number of relays is increased, it might not be feasible in practice. As a result, the proposed system using orthogonal transmission is still attractive for distributed networks consisting of low-cost, small-sized, and low-powered terminals.

On the other hand, according to the error detection method, there are CRC-based and outage-based selection schemes, and a CRC-based selection scheme is employed in this chapter. Since the SNR estimation approach used in the outage-based selection scheme depends on the actual value of the channel fading coefficient, the system complexity is increased according to how often the receivers estimate the channel fading coefficient. Thus, CRC checking is usually used for packet-error detection [42, 57].

This chapter considers the multi-branch dual-hop cooperative relaying network as shown in Fig. 5, and the channel model, the signal representation, and power allocation are the same as those of Section 3.2.

8.3 Outage Probability Analysis

In this section, based on the per-hop analysis in Chapters 3 and 7, we derive closed-form expressions for the end-to-end outage probability of for the FSDF, RSDF, and VSDF schemes employing the packet cooperative transmission with CRC-based relaying. Since the proposed DF schemes determine whether or not the relay forwards the source packet by observing the CRC status and the respective links are independent, the end-to-end outage probability can be expressed by using conditional probability [31].

First, compared to FSDF and VSDF, the RSDF scheme repeats the source packet when the relay detects erroneous packet. Therefore, the total number of cooperative branches of RSDF is always $(M+1)$. For the case that the number of relays is M, the end-to-end outage probability of RSDF can be expressed by using the multinomial formula in [32, 37] and the conditional probability as follows:

$$P_{o,RSDF}^{ete}(\lambda;z) = \left(\prod_{m=1}^{M}\Phi_m\right)\left\{P_o^c\left(\lambda;\sum_{a=1}^{M+1}z_0^h\right) + \sum_{m=1}^{M}\sum_{\lambda_1=1}^{M-m+1} + \cdots \sum_{\lambda_m=\lambda_{m-1}+1}^{M}\left(\prod_{n=1}^{m}\frac{1-\Phi_{\lambda_n}}{\Phi_{\lambda_n}}\right)P_o^c\left(\lambda;\sum_{a=0}^{m}z_{\lambda_a}^h + \sum_{a=1}^{M-m}z_0^h\right)\right\}, \quad (145)$$

where Φ_m is the probability of the event that the m-th relay detects erroneous packets which is derived in (153), and P_o^c is the outage probability for M-branch transmission with L-interferers, which is given in (134) of Chapter 7 as

$$P_o^c(\lambda;z) = 1 - \sum_{a=0}^{M}\sum_{b=1}^{m_{X_a}}\beta_{a,b}^X(-\alpha_{X_a})^b\sum_{c=1}^{L}\sum_{d=1}^{m_{Y_c}}\beta_{c,d}^Y(-\alpha_{Y_c})^d\hat{F}(\lambda;b,d,\alpha_{X_a},\alpha_{Y_c}), \quad (146)$$

where $\hat{F}$-function is denoted for the case of SINR Z in Appendix B, the coefficient $\beta_{a,b}^X$ is denoted in (14), and $\beta_{a,b}^Y$ is denoted in (27) of Chapter 3. Note that the total number of cooperative branches of RSDF is $(M+1)$ in the first term and the second term of (145) due to the retransmissions.

Second, the end-to-end outage probabilities of FSDF and VSDF are the same since the difference between two systems is only the number of assigned slots, and

the SINR of the source-to-relay link and the combined SINR at the destination are the same. Thus, the end-to-end outage probability of both FSDF and VSDF is also described as follows:

$$P_{o,VSDF}^{ete}(\lambda;z)=\left(\prod_{m=1}^{M}\Phi_m\right)\left\{P_o^s(\lambda;z_0^h)+\sum_{m=1}^{M}\sum_{\lambda_1=1}^{M-m+1}\cdots \right.$$
$$\left.\times\sum_{\lambda_m=\lambda_{m-1}+1}^{M}\left(\prod_{n=1}^{m}\frac{1-\Phi_{\lambda_n}}{\Phi_{\lambda_n}}\right)P_o^c\left(\lambda;\sum_{a=0}^{m}z_{\lambda_a}^h\right)\right\}\ , \tag{147}$$

where the outage probability of a single branch transmission with L-interferers is given in (131) of Chapter 7 by

$$P_o^s(\lambda;z)=1-\sum_{a=1}^{L}\sum_{b=1}^{m_{Y_a}}\beta_{a,b}^{Y}(-\alpha_{Y_a})^b\hat{F}(\lambda;m_X,b,\alpha_X,\alpha_{Y_a}). \tag{148}$$

Note that the first terms of (145) and (147) represent the event that all the relays cannot forward the source packet and only the source send its packet to the destination at the broadcasting step.

8.4 APEP and Throughput Analysis

In this section, we derive closed-form expressions for the end-to-end APEP and throughput for the FSDF, RSDF, and VSDF schemes employing the packet cooperative transmission with CRC-based relaying. One of the advantages of the DF scheme is that every link can employ different modulation schemes, but all terminals in our system use the same modulation scheme to reduce system complexity.

There is no relation between the average ASEP and APEP for slow-fading environments [60]. This is because averaging the conditional PEP over fading environments results in integer powers of the Gaussian-Q function, which makes the analysis challenging. However, systems employing suitable interleaving could result in a memoryless channel, where two adjacent symbols are considered to be faded independently

[61, 62, 63, 64]. Under the assumption of ideal interleaving, the APEP of the single-hop transmission with $\mathcal{M}$-ary modulation can be expressed as

$$\bar{P}_p(z) = 1 - (1 - \bar{P}_s(z))^{\mathcal{L}/b}, \tag{149}$$

where $b = \log_2 \mathcal{M}$ bit/symbols and $\mathcal{L}$ is the total packet bit length, and $\bar{P}_s$ is the ASEP of the single-hop transmission system.

Similarly to (147), under the assumption of packet-by-packet combining, we can obtain the end-to-end APEP of both FSDF and VSDF as follows:

$$\bar{P}^{ete}_{p,VSDF} = \left(\prod_{m=1}^{M} \Phi_m\right) \left\{ \bar{P}^s_p(z_0^h) + \sum_{m=1}^{M} \sum_{\lambda_1=1}^{M-m+1} \cdots \right.$$
$$\left. \times \sum_{\lambda_m=\lambda_{m-1}+1}^{M} \left(\prod_{n=1}^{m} \frac{1-\Phi_{\lambda_n}}{\Phi_{\lambda_n}}\right) \bar{P}^c_p \left(\sum_{a=0}^{m} z^h_{\lambda_a}\right) \right\}, \tag{150}$$

where the first term is the APEP using a single branch transmission with multiple interferer, but the second term is the APEP using multi-branch transmission with multiple interferers which will be derived in (152).

Also, the end-to-end APEP of RSDF with M-relays can be expressed as

$$\bar{P}^{ete}_{p,RSDF} = \left(\prod_{m=1}^{M} \Phi_m\right) \left\{ \bar{P}^c_p \left(\sum_{a=1}^{M+1} z_0^h\right) + \sum_{m=1}^{M} \sum_{\lambda_1=1}^{M-m+1} \cdots \right.$$
$$\left. \times \sum_{\lambda_m=\lambda_{m-1}+1}^{M} \left(\prod_{n=1}^{m} \frac{1-\Phi_{\lambda_n}}{\Phi_{\lambda_n}}\right) \bar{P}^c_p \left(\sum_{a=0}^{m} z^h_{\lambda_a} + \sum_{a=1}^{M-m} z_0^h\right) \right\}, \tag{151}$$

where the first and the second terms are the APEP using multi-branch transmission with multiple interferers.

From (149), the APEP using the single branch and the multi-branch transmissions with multiple interferers can be expressed as

$$\bar{P}^s_p(z) = 1 - (1 - \bar{P}^s_s(z))^{\mathcal{L}/b},$$
$$\bar{P}^c_p(z) = 1 - (1 - \bar{P}^c_s(z))^{\mathcal{L}/b}, \tag{152}$$

where, the ASEP of a single branch transmission with L-interferers is given in (138) of Chapter 7 with $\hat{S}$-function in Appendix B and, under the perfect CRC, Φ_m

is the same as the APEP of m-th relay as follows:

$$\bar{P}_s^s(Z_m^g) = \Phi_m = \alpha/2 - \sum_{a=1}^{L}\sum_{b=1}^{m_{Y_a}} \beta_{a,b}^{Y}(-\alpha_{Y_a})^b \hat{S}(\alpha, \beta, m_{X_m^g}, b, \alpha_{X_m^g}, \alpha_{Y_a}) \ , \tag{153}$$

where $\hat{S}$-function is denoted in Appendix B, and, α and β are modulation-specific constants that depend on the modulation order $\mathcal{M}$. In the case of $\mathcal{M}$-PAM, $\alpha = 2(\mathcal{M}-1)/\mathcal{M}$ and $\beta = 3/(\mathcal{M}^2-1)$ [49, eq. 5.2-44]. In the case of $\mathcal{M}$-PSK, $\alpha = 2$ and $\beta = \sin^2(\pi/\mathcal{M})$ [49, eq. 5.2-61]. The ASEP of $\mathcal{M}$-QAM system with $\mathcal{M} = 4^k, k = 1, 2, \ldots,$ can be written by using that of $\sqrt{\mathcal{M}}$-PAM as

$$\bar{P}_s(\mathcal{M}) = 1 - (1 - \bar{P}_s(\sqrt{\mathcal{M}}))^2 \ , \tag{154}$$

where $\bar{P}_s(\sqrt{\mathcal{M}})$ is the ASEP of $\sqrt{\mathcal{M}}$-PAM system. The APEP using the single branch and the multi-branch transmissions with multiple interferers can be regarded as that of the source-to-relay, relay-to-destination, and source-to-destination links. Likewise, the ASEP of M-branch transmission with L-interferers is given in (140) of Chapter 7 with $\hat{S}$-function as

$$\bar{P}_s^c(Z^h) = \alpha/2 - \sum_{a=0}^{M}\sum_{b=1}^{m_{X_a^h}} \beta_{a,b}^{X}(-\alpha_{X_{\lambda_a}^h})^b \sum_{c=1}^{L}\sum_{d=1}^{m_{Y_c}} \beta_{c,d}^{Y}(-\alpha_{Y_c})^d \hat{S}(\alpha, \beta, b, d, \alpha_{X_{\lambda_a}^h}, \alpha_{Y_c}) \ . \tag{155}$$

In the uncoded packet cooperative system with CRC-based relaying, assume that C-bit CRC is attached to the packet and the number of assigned slots is $\bar{N}$, the end-to-end throughput is then given by [57]

$$T^{ete} = \frac{\mathcal{L} - C}{\mathcal{L}} b(1 - \bar{P}_p^{ete})/\bar{N} \ , \tag{156}$$

where $\bar{P}_p^{ete}$ is the end-to-end APEP.

In the FSDF and RSDF schemes, the number of assigned slots is fixed as $M + 1$ as shown in Fig. 45. However, the number of slots for the VSDF scheme is varied according to the CRC status at the relays. By using the multinomial formula of

(154), the average number of assigned slots in the VSDF scheme can be generalized for M-relays as follows:

$$\bar{N}_{VSDF} = 1 + \left(\prod_{m=1}^{M} \Phi_m \right) \sum_{m=1}^{M} m \sum_{\lambda_1=1}^{M-m+1} \cdots \sum_{\lambda_m=\lambda_{m-1}+1}^{M} \left(\prod_{n=1}^{m} \frac{1-\Phi_{\lambda_n}}{\Phi_{\lambda_n}} \right) \quad . \tag{157}$$

8.5 Performance Analysis

In this section, the outage performance and the average throughput are evaluated in various scenarios for FSDF, RSDF, and VSDF over Nakagami/Nakagami channels. The results of the chapter assume that the Nakagami shape factor of the desired signals $m_X = 2$, and that of the interfering signals $m_Y = 1$ since a line-of-sight may exist between the nodes but the interferers are usually located in the distance with non line-of-sight conditions. The threshold SINR is $\lambda_{th} = 12$ dB, and the path-loss exponent is $\alpha = 3$. The number of co-channel interferers at each relay and destination is three, where the Tx powers of the individual interferers are {2,3,5}. Thus, the total Tx power of the interferers is fixed as ten, and the total Tx INR is 10 dB with $\sigma^2 = 1$ for all curves. To exclude the effect of the placement of relays, the relays are uniformly distributed close to a middle point between the source and the destination such that the normalized distance $d_{S,R_m}/d_{S,D}$ is in the interval (0.4, 0.6). The normalized distance between the destination and the interferers is fixed as $d_{I,D} = d_{I_l,D}/d_{S,D} = 1$, but we consider two cases for the normalized distance between the relays and the interferers, $d_{I,R} = d_{I_l,R_m}/d_{S,D}$, which are assumed to be uniformly distributed on the around 0.5 and 1 such that interferers are placed near the relays. In particular, we consider the QPSK and 16-QAM systems in this section, but the type of modulation is not limited. In the packet, $C = 16$ bits is employed and the packet length $\mathcal{L}$ is 1024 bits.

In Figs. 46 and 47, the outage performance of the VSDF, FSDF, and RSDF schemes are compared when the number of relays is increased from one to three for QPSK and 16-QAM, respectively.

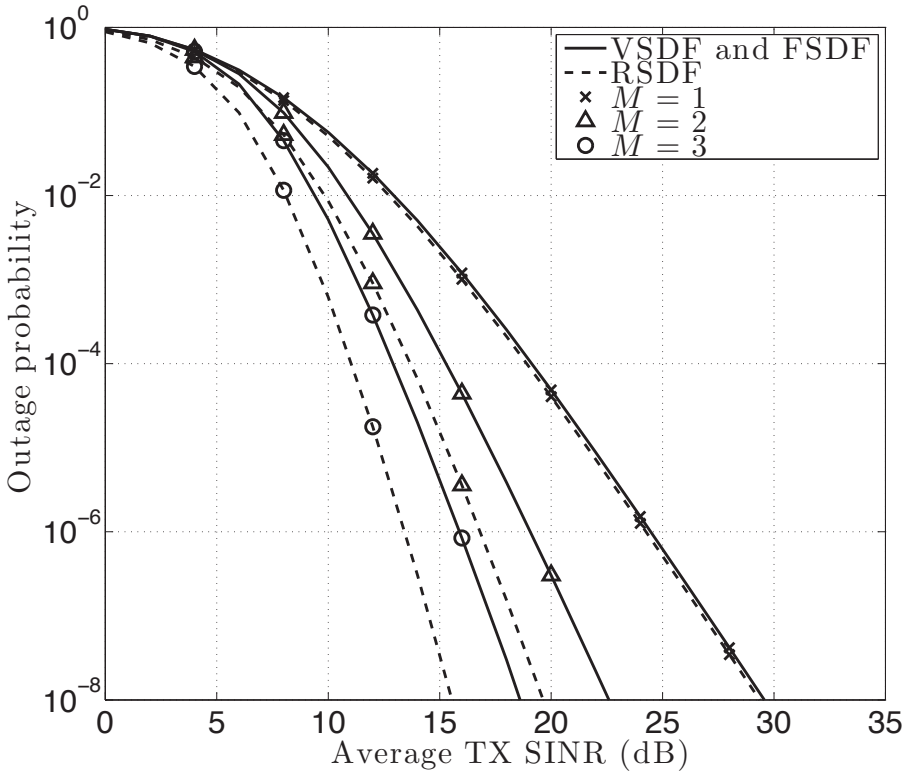

Figure 46: Outage performances of the VSDF, FSDF, and RSDF schemes with various number of relays in the QPSK system.

Figure 46 shows that as the number of relays is increased, the cooperative diversity order increases for all DF schemes. As mentioned earlier, the outage performances of both FSDF and VSDF are the same since the unused slot does not affect the performance of cooperative diversity combining. However, as expected, RSDF shows better cooperative diversity gain than the other systems. This is because RSDF can exploit all $(M + 1)$ slots even though the relay fails to decode the source packet. When $M = 1$, the outage performances among the proposed systems are almost similar, however the performance gap is increased as the number of relay is increased.

Figure 47 describes the outage probabilities of the VSDF, FSDF, and RSDF schemes when 16-QAM is employed. Compared to Fig. 46, the outage performances

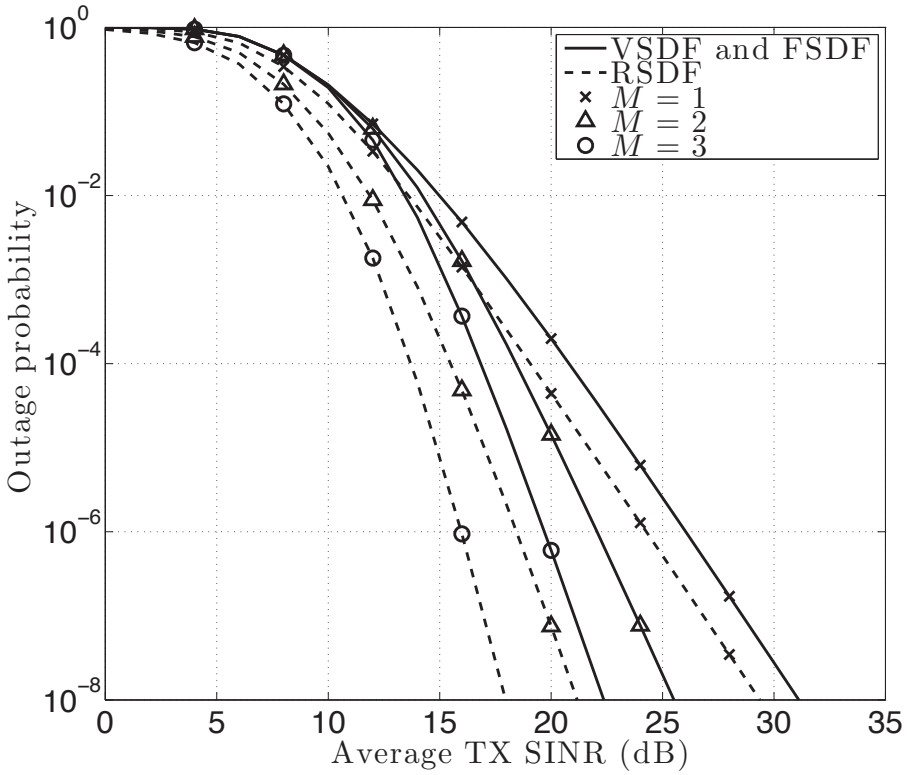

Figure 47: Outage performances of the VSDF, FSDF, and RSDF schemes with various number of relays in the 16-QAM system.

for all the systems are degraded since the proposed systems employ CRC-based relaying and the cooperative diversity gain depends on the APEP at the relays. In particular, the performance gap between RSDF and the other systmes is larger than that of Fig. 46. The reason is that the APEP degradation due to the modulation order at the relay can be compensated by the increased cooperative diversity gain of the RSDF scheme.

Figures 48, 49, and 50 show the throughputs of the VSDF, FSDF, and RSDF schemes for various number of relays when the normalized distance between the relay and the interferer changed from 0.5 to 1. In Fig. 48, when a single relay is used, the throughputs of VSDF, FSDF, and RSDF with $d_{I,R} = 1$ are similar to each other. This is because the cooperative diversity gain by using a single relay is relatively

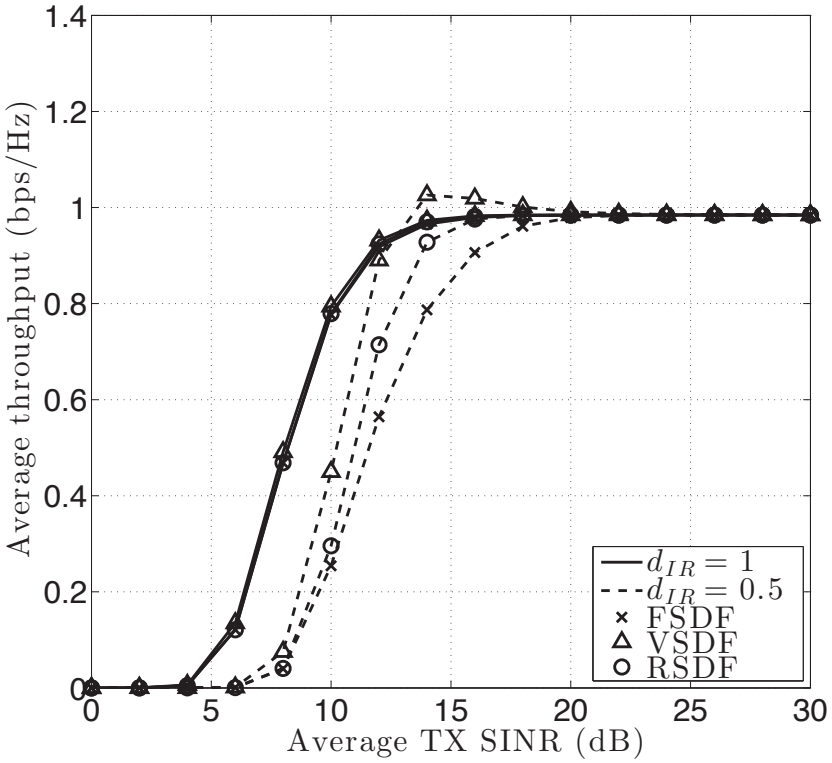

Figure 48: Throughputs of the VSDF, FSDF, and RSDF schemes with $M = 1$ in the QPSK system when $d_{I,R} = 0.5$ and $d_{I,R} = 1$.

small compared to the reduced throughput due to additional slots. In addition, the probability of the event that the relay fails to decode the source packet is a small portion of the total number of used slots.

However, when the number of relays is increased to two and three as shown in Figs. 49 and 50, VSDF shows the best throughput performance, and RSDF outperforms FSDF in the low and moderate SINR region. The reason is that in the low and moderate SINR region the reduced number of assigned slots for VSDF dominates the cooperative diversity gain of RSDF, but the cooperative diversity gain of RSDF improves throughput performance more than that of FSDF for the same number of relays. In the high SINR region, since most of the relays can decode the source packet and cooperate to forward it, the total number of assigned slots is fixed as $M + 1$. In

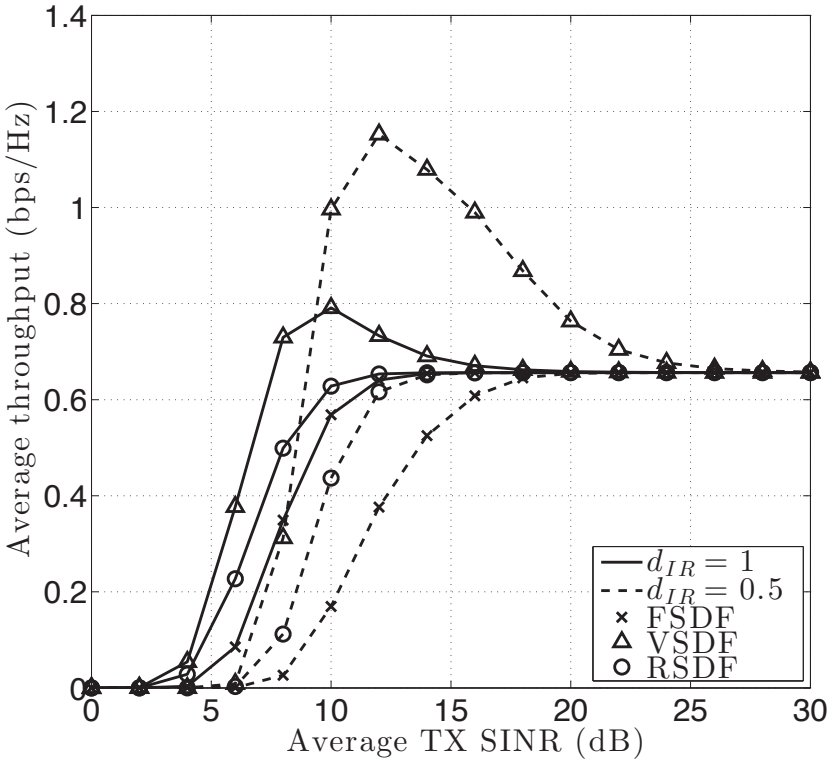

Figure 49: Throughputs of the VSDF, FSDF, and RSDF schemes with $M = 2$ in the QPSK system when $d_{I,R} = 0.5$ and $d_{I,R} = 1$.

addition, the cooperative diversity gain is the same to all the proposed systems. Thus, the throughputs of respective systems are converged to the same value in the high SINR region.

In Figs. 48, 49, and 50, when the normalized distance between the relay and the interferer is decreased from 1 to 0.5, all curves move to the right side since the throughputs of the proposed systems are degraded by increasing Rx interference power. An interesting result is that the maximum throughput of VSDF for the case of $d_{I,R} = 0.5$ is larger than the case of $d_{I,R} = 1$. The reason is that VSDF has smaller number of assigned slots for the case of $d_{I,R} = 0.5$ than that of $d_{I,R} = 1$. In addition, compared to all the systems in Fig. 48, VSDF in Figs. 49 and 50 shows better maximum throughput even though the number of relays is larger than that of Fig.

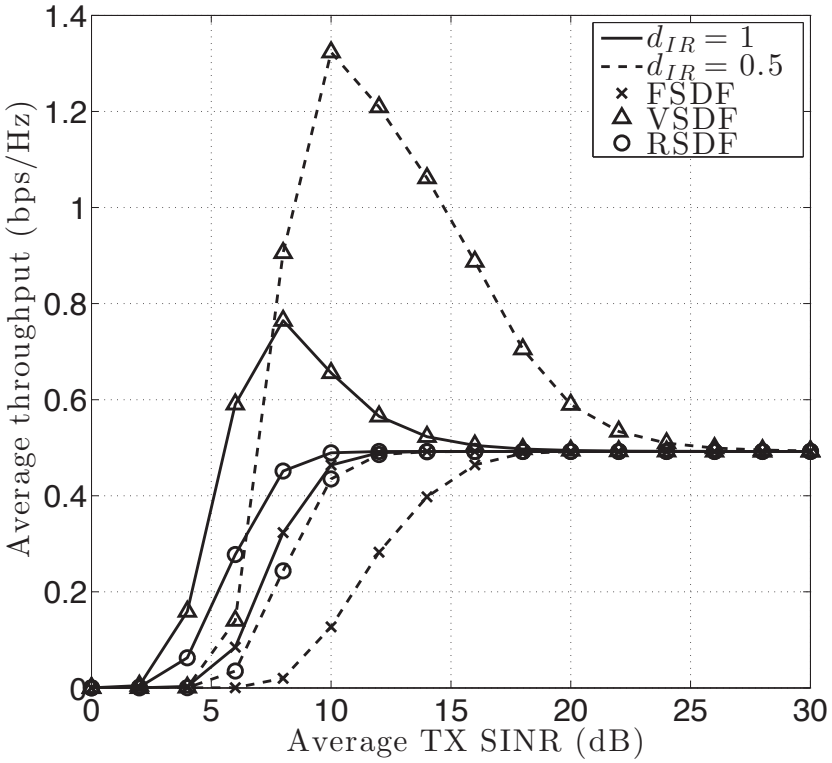

Figure 50: Throughputs of the VSDF, FSDF, and RSDF schemes with $M = 3$ in the QPSK system when $d_{I,R} = 0.5$ and $d_{I,R} = 1$.

48. The proposed VSDF system can achieve cooperative diversity gain by increasing the number of relays in spite of the reduced number of assigned relays. Therefore, the maximum throughput point shows that the proposed VSDF scheme can take advantage of both cooperative diversity gain and efficient slot resource scheduling at the same time, since the maximum throughput occurs when the system has the minimum outage performance for the minimum number of assigned slots as shown in (156). Moreover, the proposed VSDF scheme is practical since the maximum throughput point of VSDF occurs in the low and moderate SINR region, where the actual operating SINR region lays for low-powered, dense relay networks.

CHAPTER IX

CONTRIBUTIONS AND FUTURE RESEARCH

This final chapter summarizes the contributions of the dissertation and shows the various areas for future research.

9.1 Contributions

This dissertation primarily focused on analyzing the performance of DF cooperative relaying systems in the presence of multiple interferers and improving the throughput for the proposed systems. We proposed and summarized various DF schemes in the view of network topology (multi-branch dual-hop relaying and multi-branch multi-hop relaying), transmission structure (outage-based symbol relaying, outage-based packet relaying, and CRC-based packet relaying), slot allocation (fixed-slot selection DF, repeated-slot selection DF, and variable-slot selection DF), and network environments (ad-hoc and cellular networks).

In Chapter 3, the outage probability of MBDH DF cooperative relaying systems over non-identical Nakagami/Nakagami fading channels was studied. The exact closed-form expression of outage probability was derived, and this theoretical analysis was verified by Monte Carlo simulations. Also, the effects of noise and interference on the outage probability were analyzed in terms of diversity and channel condition. The results show that increasing the number of relays improves the outage probability against CCI, and the outage performance is more severely degraded by the noise than CCI in the low and moderate SINR region. Moreover, the robustness of the destination against interference is more important than robustness of the relay against interference from an interference management perspective.

In Chapter 4, the selection DF MBMH cooperative relaying system was considered

on non-identical shadowed Nakagami/shadowed Nakagami channels. Closed-form expressions of the pdf of the SINR, the outage probability, and the ASEP were derived, and the results were also confirmed by Monte Carlo simulations. The effects of the numbers of branches and hops were analyzed in terms of outage probability and ASEP, and compared to the cases with and without shadowing for various relay topologies. The impact of the placement of co-channel interferers was also analyzed. The results show that increasing the number of branches yields better outage and error performance improvements against shadowing than increasing the number of hops in the selection DF MBMH cooperative relaying system.

Chapter 5 analyzed the SINR outage probability of both the AD and the DF cooperative diversity systems with SC for a log-normal shadowed Nakagami-m faded desired signal channel and log-normal shadowed Rayleigh faded interfering signals. This chapter shows plots for the effective "black" zone for the relay location, where the cooperative diversity systems will outperform the dual Rx antenna system. The results show that the cooperative diversity gain of the AF system outperforms that of the DF system in spite of noise amplification for interference-limited environments. Both the cooperative diversity systems can outperform the dual Rx antenna system, but only when the relay is located in a relatively small portion of the total cell area with respect the the destination mobile terminal.

Chapter 6 analyzed the outage probability and a spectral efficiency analysis for the DF cooperative diversity system with MRC over non-identical shadowed Nakagami/shadowed Nakagami channels in cellular networks. The optimal relay location in terms of the outage probability was evaluated for omnidirectional and sectorized cells in both the uplink and the downlink. Based on the results of the analysis, this study shows that the cooperative diversity system outperforms the dual-Rx antenna system in terms of outage probability and exhibits spectral efficiency comparable to

that of the single-Rx antenna system. However, performance improves in only a particular region of the cell with respect to the relay location, not in the entire cell. The results show that the area of the effective region is significantly larger in the uplink than in the downlink, and as the number of sectors in the cell increases, the size of effective region in the uplink also increases, but the size of the effective region in the downlink decreases. The results also show that as the number of sectors increases, the center of the region moves toward destination BS; however, it does not change in the downlink. In addition, since the effective regions of the uplink and the downlink do not overlap, different relays should be utilized for cell sectorization in the uplink and the downlink.

Chapter 7 considered the outage probability and APEP analysis for the selection DF cooperative diversity systems with MRC over non-identical Nakagami/Nakagami channels in cellular networks. For the selection DF relaying schemes, we analyzed the APEP for various schemes: i) outage-based symbol relaying, ii) outage-based packet relaying, and iii) CRC-based packet relaying. Without error-correction coding, outage-based packet relaying showed better APEP performance than the other schemes, while CRC-based packet relaying outperformed outage-based packet relaying when error-correction coding is employed. However, when the effect of CCI dominates the error-correction capability, the outage-based packet relaying still outperformed than the other schemes. The results show that the end-to-end APEP performance is more susceptible to the APEP of the relay-to-destination link than that of the source-to-relay link.

Chapter 8 investigated the network throughput for selection DF packet cooperative relaying systems over non-identical Nakagami/Nakagami channels. By using the dynamic slot assignment operating on CRC-based relaying, we proposed a new selection DF scheme, which is referred as the VSDF scheme. We derived closed forms of the end-to-end outage probability, APEP and throughput for FSDF, RSDF, and VSDF

by taking into account packet transmission. Compared to RSDF, VSDF has lower cooperative diversity gain, but it has the same outage performance as FSDF. However, VSDF shows better throughput performance than both RSDF and FSDF in the low and moderate SINR region, and the maximum throughput point of VSDF shows that it can take advantage of both cooperative diversity gain and efficient slot resource scheduling at the same time. Moreover, VSDF outperforms the other systems even when the Rx interference power is increased. Therefore, the proposed VSDF scheme is practical since it can reduce the system complexity, and the maximum throughput point occurs in the low and moderate SINR region.

9.2 Future Research

Since the research on the effect of interference in cooperative diversity has been limited so far, the design of the cooperative relaying systems considering CCI is an open field. Thus, we expect that existing modeling and analytical consideration can be further explored by using our research.

- **AF cooperative relaying:** In this dissertation, we analyzed the performance of DF cooperative relaying systems. However, even though most researchers focused on the end-to-end performance of AF scheme [7, 11, 34, 35, 36] earlier than DF scheme, the closed-form expressions for outage probability of AF cooperative relaying system considering both CCI and AWGN is an open problem.

- **Practical coding implementation:** Although we showed the effect of FEC on the proposed system in Chapter 7, practical implementing of coding scheme by considering CCI is an ongoing issue. In particular, we showed that the effect of FEC in the relay can significantly improve the end-to-end performance of the proposed system in Chapter 7. Thus, if the relay adaptively obtain coding arguments by estimating CCI, the end-to-end performance of the proposed system would be better than that of the system with fixed coding arguments, and

this can be regarded as interference-aware coded cooperation.

- **Optimization:** In Chapter 3, we showed that the optimal relay position for outage probability is varied according to CCI. However, a closed-form solution for the optimal relay position with regard to CCI is an open problem. In addition, it would be interesting to determine the optimal SINR point for the maximum throughput by power control in Chapter 8. Since the CSI of the relay-to-destination link is available and the maximum throughput point occurs in the low and moderate SINR region, an optimizing Tx power with regard to CCI can be useful further study.

- **Spectral efficiency:** As mentioned earlier, orthogonal transmission requires $M+1$ slots when the number of relays is M. When we use less number of slots than the number of relays, inter-relay interference occurs at the duplicately assigned slots. However, if we assign the active relay which has the largest Tx power to the slot which has the smallest CCI, inter-relay interference would be minimized. Moreover, since the limited slot resources can be fully exploited, spectral efficiency also significantly increases.

APPENDIX A

PROOF OF LEMMA

Lemma 1 *Let the integral term of (32), Φ, be defined as follows:*

$$\Phi = \int_0^\infty x^{M-1} e^{-ax} \int_{x+1}^\infty y^{N-1} e^{-by}\, dy\, dx \ .$$

The second integral term can be reduced to an incomplete gamma function, and it can be simplified with the help of [54]. By using the binomial expansion, Φ becomes

$$\Phi = \Gamma(N) e^{-b} \sum_{n=0}^{N-1} \frac{b^{n-N}}{n!} \sum_{k=0}^{n} \binom{n}{k} (a+b)^{-(M+k)} \Gamma(M+k).$$

Lemma 2 *From the definition of the confluent hypergeometric function of the second kind in [54, 9.211.4], solving the integral term by using the binomial expansion yields*

$$\Psi[a, 1+a+b, c] = \frac{1}{\Gamma(a)} \int_0^\infty x^{a-1} (1+x)^b \exp(-c\,x)\, dx = \sum_{k=0}^{b} \binom{b}{k} c^{-(a+k)} \frac{\Gamma(a+k)}{\Gamma(a)} \ ,$$

where a, b, and c are nonnegative integers.

APPENDIX B

THE DEFINITION OF FUNCTION

B.1 Derivation of the $\hat{H}$-function

In Section 4.3.1, the equation obtained by substituting (44) into (47) has a common term, so we denote this term as the $\hat{H}$-function as follows:

$$\begin{aligned}
&\hat{H}(z; m_X, m_Y, \alpha_X, \alpha_Y) \\
&\triangleq \frac{z^{m_X-1}}{(\alpha_X)^{m_X}(\alpha_Y)^{m_Y}} \frac{e^{(-z/\alpha_X)}}{\Gamma(m_X)\Gamma(m_Y)} \int_0^\infty y^{m_Y-1}(1+y)^{m_X} \exp\left\{-y\left(\frac{z}{\alpha_X}+\frac{1}{\alpha_Y}\right)\right\} \mathrm{d}y \\
&= \frac{z^{m_X-1}e^{(-z/\alpha_X)}}{(\alpha_X)^{m_X}(\alpha_Y)^{m_Y}} \sum_{k=0}^{m_X} \binom{m_X}{k} \left(\frac{z}{\alpha_X}+\frac{1}{\alpha_Y}\right)^{-(m_Y+k)} \frac{\Gamma(m_Y+k)}{\Gamma(m_X)\Gamma(m_Y)} \ .
\end{aligned}$$

B.2 Derivation of the $\hat{F}$-function

In Section 4.4.1, the outage probability of interest can be derived by substituting (57) into (58). This equation can be simplified by using the identities of [54, 3.381.1] and [54, 8.352.7] and by solving the integral term with *Lemma 2*. The common term of the outage probabilities is denoted as

$$\begin{aligned}
&\hat{F}(\lambda; m_X, m_Y, \alpha_X, \alpha_Y) \\
&\triangleq 1 - \frac{1}{(\alpha_Y)^{m_Y}(\alpha_X)^{m_X}\Gamma(m_X)\Gamma(m_Y)} \int_0^\infty y^{(m_Y-1)}(1+y)^{m_Y} e^{(-y/\alpha_Y)} \\
&\quad \times \int_0^\lambda z^{(m_X-1)} e^{-z(1+y)/\alpha_X} \,\mathrm{d}z \,\mathrm{d}y \\
&= \sum_{n=0}^{m_X-1} \sum_{k=0}^{n} \binom{n}{k} \frac{(\lambda/\alpha_X)^n e^{(-\lambda/\alpha_X)}}{\Gamma(n+1)(\alpha_Y)^{m_Y}} \left(\frac{1}{\alpha_Y}+\frac{\lambda}{\alpha_X}\right)^{-(m_Y+k)} \frac{\Gamma(m_Y+k)}{\Gamma(m_Y)} \ .
\end{aligned}$$

B.3 Derivation of the $\hat{S}$-function

In the outage probabilities derived in Section 4.4, only the $\hat{F}$-function has variable λ for the integral in (63). Thus, the $\hat{S}$-function can be denoted by substituting the $\hat{F}$-function in Appendix B into (63) and using the identity of [54, 9.211.4] to solve the integral term as

$$\begin{aligned}
&\hat{S}(\alpha,\beta,m_X,m_Y,\alpha_X,\alpha_Y) \triangleq \frac{\alpha\sqrt{\beta}}{2\sqrt{\pi}}\int_0^\infty \frac{e^{-\beta\lambda}}{\sqrt{\lambda}}F(\lambda;m_X,m_Y,\alpha_X,\alpha_Y)\,\mathrm{d}\lambda \\
&= \frac{\alpha\sqrt{\beta}}{2\sqrt{\pi}}\sum_{n=0}^{m_X-1}\frac{1}{(\alpha_Y)^{m_Y}\Gamma(n+1)}\sum_{k=0}^{n}\binom{n}{k}\frac{\Gamma(m_Y+k)}{\Gamma(m_Y)}(\alpha_X)^{m_Y+k-n} \\
&\quad\times\int_0^\infty \exp\left\{-\lambda\left(\beta+\frac{1}{\alpha_X}\right)\right\}\lambda^{(n-1/2)}\left(\lambda+\frac{\alpha_X}{\alpha_Y}\right)^{-(m_Y+k)}\mathrm{d}\lambda \\
&= \frac{\alpha\sqrt{\beta}}{2\sqrt{\pi}}\sum_{n=0}^{m_X-1}\sum_{k=0}^{n}\binom{n}{k}\frac{\Gamma(n+1/2)\Gamma(m_Y+k)}{\Gamma(n+1)\Gamma(m_Y)}\frac{\alpha_X^{(1/2)}}{\alpha_Y^{(n-k+1/2)}} \\
&\quad\times\Psi[n+1/2,n-m_Y-k+3/2,(1+\alpha_X\beta)/\alpha_Y]\ ,
\end{aligned}$$

where $\Psi[\cdot,\cdot,\cdot]$ is the confluent hypergeometric function of the second kind [54].

REFERENCES

[1] Laneman, J., Tse, D., and Wornell, G., "Cooperative diversity in wireless networks: Efficient protocols and outage behavior," *IEEE Trans. Inform. Theory*, vol. 50, pp. 3062–3080, Dec. 2004.

[2] Stüber, G. L., *Principles of mobile communication*. Boston: Kluwer Academic, 2nd ed ed., 2001.

[3] Yang, Q., Kwak, K. S., and Fu, F., "Closed-form expression for outage probability of DF relaying with unequal Nakagami interferers in Nakagami fading," in *Proc. IEEE Int. Symp. Personal, Indoor and Mobile Radio Commun. (PIMRC'09)*, pp. 335–339, Sept. 2009.

[4] Romero-Jerez, J., Pena-Martin, J., Aguilera, G., and Goldsmith, A., "Performance of MIMO MRC systems with co-channel interference," in *Proc. IEEE Int. Conf. Commun.*, vol. 3, pp. 1343–1349, June 2006.

[5] Kim, J.-B. and Kim, D., "Exact and closed-form outage probability of opportunistic decode-and-forward relaying with unequal-power interferers," *IEEE Trans. Wireless Commun.*, vol. 9, pp. 3601 –3606, Dec. 2010.

[6] Hasna, M. and Alouini, M.-S., "Outage probability of multihop transmission over Nakagami fading channels," *IEEE Commun. Lett.*, vol. 7, pp. 216–218, May 2003.

[7] Ribeiro, A., Cai, X., and Giannakis, G., "Symbol error probabilities for general cooperative links," *IEEE Trans. Wireless Commun.*, vol. 4, pp. 1264–1273, May 2005.

[8] Muller, A. and Speidel, J., "Exact symbol error probability of M-PSK for multihop transmission with regenerative relays," *IEEE Commun. Lett.*, vol. 11, pp. 952–954, Dec. 2007.

[9] Zhao, B. and Valenti, M., "Practical relay networks: a generalization of hybrid-ARQ," *IEEE J. Select. Areas Commun.*, vol. 23, pp. 7–18, Jan. 2005.

[10] Boyer, J., Falconer, D., and Yanikomeroglu, H., "Multihop diversity in wireless relaying channels," *IEEE Trans. Commun.*, vol. 52, pp. 1820–1830, Oct. 2004.

[11] Farhadi, G. and Beaulieu, N., "Fixed relaying versus selective relaying in multi-hop diversity transmission systems," *IEEE Trans. Commun.*, vol. 58, pp. 956–965, Mar. 2010.

[12] Sendonaris, A., Erkip, E., and Aazhang, B., "Increasing uplink capacity via user cooperation diversity," in *Proc. IEEE Int. Symp. Inform. Theory (ISIT'98)*, p. 156, Aug. 1998.

[13] Sendonaris, A., Erkip, E., and Aazhang, B., "User cooperation diversity, part i: System description," *IEEE Trans. Commun.*, vol. 51, pp. 1927–1938, Nov. 2003.

[14] Sendonaris, A., Erkip, E., and Aazhang, B., "User cooperation diversity, part ii: Implementation aspects and performance analysis," *IEEE Trans. Commun.*, vol. 51, pp. 1939–1948, Nov. 2003.

[15] Stankovic, V., Host-Madsen., A., and Zixiang, X., "Cooperative diversity for wireless ad hoc networks," *IEEE Sig. Proc. Mag.*, vol. 23, pp. 37–49, Sept. 2006.

[16] Simon, M. K. and Alouini, M.-S., *Digital communication over fading channels*. Hoboken, N.J.: Wiley-Interscience, 2nd ed ed., 2005.

[17] van der Meulen, E. C., "Three-terminal communication channels," *Advances in Applied Probability*, no. 3, pp. 120–154, 1971.

[18] Cover, T. and Gamal, A. E., "Capacity theorems for the relay channel," *IEEE Trans. Inf. Theory*, vol. 25, pp. 572–584, Sept. 1979.

[19] Laneman, J. N. and Wornell, G. W., "Distributed space-time-coded protocols for exploiting cooperative diversity in wireless networks," *IEEE Trans. Inform. Theory*, vol. 49, pp. 2415–2425, Oct. 2003.

[20] Bletsas, A., Shin, H., and Win, M., "Cooperative communications with outage-optimal opportunistic relaying," *IEEE Trans Wireless Commun.*, vol. 6, pp. 3450–3460, Sept. 2007.

[21] Anghel, P., Kaveh, M., and Luo, Z.-Q., "An efficient algorithm for optimum power allocation in a decode-and-forward cooperative system with orthogonal transmissions," in *Proc. IEEE Int. Conf. Acoust., Speech and Signal Process. (ICASSP'06)*, vol. 4, p. IV, May 2006.

[22] Srinivas, K., Giridhar, K., and Koilpillai, R., "Orthogonal decode and forward relaying with improved spectral efficiency," *IEEE Commun. Lett.*, vol. 13, pp. 109–111, Feb. 2009.

[23] Aalo, V. and Zhang, J., "Performance analysis of maximal ratio combining in the presence of multiple equal-power co-channel interferers in a Nakagami fading channel," *IEEE Trans. Veh. Tech.*, vol. 50, pp. 497–503, Mar. 2001.

[24] Cui, X., Zhang, Q., and Feng, Z., "Outage performance for maximal ratio combiner in the presence of unequal-power co-channel interferers," *IEEE Commun. Lett.*, vol. 8, pp. 289–291, May 2004.

[25] Romero-Jerez, J., Martin, J., and Goldsmith, A., "Outage probability of MRC with arbitrary power co-channel interferers in Nakagami fading," *IEEE Trans. Commun.*, vol. 55, pp. 1283–1286, July 2007.

[26] Zhang, X. and Beaulieu, N., "Outage probability of MRC with unequal-power co-channel interferers in correlated Rayleigh fading," *IEEE Commun. Lett.*, vol. 10, pp. 7 – 9, Jan. 2006.

[27] Ikki, S. and Ahmed, M., "Performance analysis of multi-branch decode-and-forward cooperative diversity networks over Nakagami-m fading channels," in *Proc IEEE Int. Conf. Commun. (ICC'09)*, pp. 1–6, June 2009.

[28] Suraweera, H. A., Garg, H. K., and Nallanathan, A., "Performance analysis of two hop amplify-and-forward systems with interference at the relay," *IEEE Commun. Lett.*, vol. 14, pp. 692–694, Aug. 2010.

[29] Zhong, C., Jin, S., and Wong, K.-K., "Dual-hop systems with noisy relay and interference-limited destination," *IEEE Trans. Commun.*, vol. 58, pp. 764–768, Mar. 2010.

[30] Lee, D. and Lee, J. H., "Outage probability for dual-hop relaying systems with multiple interferers over Rayleigh fading channels," *IEEE Trans. Veh. Tech.*, vol. 60, pp. 333–338, Jan. 2011.

[31] Hu, J. and Beaulieu, N., "Closed-form expressions for the outage and error probabilities of decode-and-forward relaying in dissimilar Rayleigh fading channels," in *Proc. IEEE Int. Conf. Commun. (ICC'07)*, pp. 5553–5557, June 2007.

[32] Sagias, N., Lazarakis, F., Tombras, G., and Datsikas, C., "Outage analysis of decode-and-forward relaying over Nakagami- fading channels," *IEEE Sig. Process. Lett.*, vol. 15, pp. 41–44, 2008.

[33] Safari, M. and Uysal, M., "Cooperative diversity over log-normal fading channels: performance analysis and optimization," *IEEE Trans. Wireless Commun.,* vol. 7, no. 5, pp. 1963–1972, May 2008.

[34] Di Renzo, M., Graziosi, F., and Santucci, F., "On the performance of CSI-assisted cooperative communications over generalized fading channels," in *Proc. IEEE Int Conf. Commun. (ICC'08)*, pp. 1001 –1007, may 2008.

[35] Renzo, M., Graziosi, F., and Santucci, F., "A comprehensive framework for performance analysis of cooperative multi-hop wireless systems over log-normal fading channels," *IEEE Trans. Commun.*, vol. 58, pp. 531–544, Feb. 2010.

[36] Nikjah, R. and Beaulieu, N., "Exact capacity analysis of rate adaptive power nonadaptive multi-branch multi-hop decode-and-forward relaying networks," in *Proc. IEEE Global Telecommun. Conf. (GLOBECOM'09)*, pp. 1–8, Dec. 2009.

[37] H. Yu, I.-H. Lee, and Stüber, G. L., "Outage probability of decode-and-forward cooperative relaying systems with co-channel interference," *accepted to IEEE Trans. Wireless Commun.*

[38] Farhadi, G. and Beaulieu, N., "On the performance of amplify-and-forward cooperative systems with fixed gain relays," *IEEE Trans. Wireless Commun.*, vol. 7, pp. 1851–1856, May 2008.

[39] Yao, Y. D. and Sheikh, A. U. H., "Investigations into co-channel interference in microcellular mobile radio systems," *IEEE Trans. Veh. Tech.*, vol. 41, pp. 114–122, May 1992.

[40] Peters, S. W. and Heath, R. W. Jr., "The future of WiMAX: Multihop relaying with IEEE 802.16j," *IEEE Commun. Mag.,* vol. 47, pp. 104–111, Jan, 2009.

[41] Sheen, W. -H. , Lin, S. -J., and Huang, C. -C., "Downlink optimization and performance of relay-assisted cellular networks in multicell environments," *IEEE Trans. Veh. Tech.,* vol. 59, no. 5, pp. 2529–2542, June 2010.

[42] Xi, Y., Liu, S. Huang, S., Burr, A. and Grace, D., "Performance analysis and optimum power allocation for packet decode-and-forward cooperative relaying system," in *Proc IEEE Veh. Tech. Conf. (VTC'10)* pp. 1–5, Sept. 2010.

[43] Prasad, R. and Kegel, A., "Improved assessment of interference limits in cellular radio performance," *IEEE Trans. Veh. Tech.*, vol. 40, pp. 412–419, May 1991.

[44] Wang, L.-C. and Lea, C.-T., "Incoherent estimation on co-channel interference probability for microcellular systems," *IEEE Trans. Veh. Tech.*, vol. 45, pp. 164–173, Feb. 1996.

[45] Alouini, M. and Goldsmith, A., "Area spectral efficiency of cellular mobile radio systems," *IEEE Trans. Veh. Tech.*, vol. 48, pp. 1047–1066, July 1999.

[46] Yu, H. and Stüber, G. L., "Outage probability for cooperative diversity with selective combining in cellular networks," *J. Wireless Commun. Mob. Comput.*, vol. 10, pp. 1563–1575, Dec. 2010.

[47] Sadek, A., Su, W., and Liu, K., "Performance analysis for multi-node decode-and-forward relaying in cooperative wireless networks," in *Proc. IEEE Int. Conf. Acoustics, Speech, and Signal Processing (ICASSP'05)*, vol. 3, pp. 521–524, Mar. 2005.

[48] Abu-Dayya, A. and Beaulieu, N., "Outage probabilities of cellular mobile radio systems with multiple Nakagami interferers," *IEEE Trans. Veh. Tech.*, vol. 40, pp. 757–768, Nov. 1991.

[49] Proakis, J. G. and Salehi, M., *Digital communications*. Boston: McGraw-Hill, 5th ed ed., 2008.

[50] McKay, M., Grant, A., and Collings, I., "Performance analysis of MIMO-MRC in double-correlated Rayleigh environments," *IEEE Trans. Commun.*, vol. 55, pp. 497–507, Mar. 2007.

[51] Hasna, M. and Alouini, M.-S., "A performance study of dual-hop transmissions with fixed gain relays," *IEEE Trans. Wireless Commun.*, vol. 3, pp. 1963–1968, Nov. 2004.

[52] Bletsas, A., Shin, H., and Win, M., "Outage-optimal cooperative communications with regenerative relays," in *Proc. Annual Conf. Inform. Sciences and Systems (CISS'06)*, pp. 632–637, Mar. 2006.

[53] Tjhung, T. T., Tan, S. H., and Chai, C. C., "BER and outage probability performance of $\pi/4$ DQPSK for Rice-lognormal channels," *Electron. Lett.*, vol. 32, p. 422, Feb. 1996.

[54] Gradshteĭn, I. S., Ryzhik, I. M., and Jeffrey, A., *Table of integrals, series, and products*. Amsterdam: Academic Press, 7th ed ed., 2007.

[55] 3GPP ts 25.814, v7.1.0, 2006.

[56] Luo, Y. and Cai, L., "Throughput maximization for user cooperative wireless system with adaptive modulation," in *Proc. IEEE Int. Conf. Commun. (ICC'10)*, pp. 1–5, May 2010.

[57] Dai, L. and Letief, K. B., "Throughput maximization of Ad-hoc wireless networks using adaptive cooperative diversity and truncated ARQ," *IEEE Trans. Commun.*, vol.56, no. 11, pp. 1907–1918, Nov. 2008.

[58] Bastami, A. H. and Olfat, A., "Selection relaying schemes for cooperative wireless networks with adaptive modulation," *IEEE Trans. Veh. Tech.*, vol. 60, no.4, pp. 1539–1558, May 2011.

[59] Lassing, J., Ottosson, T., and Strom, E., "Packet error rates of terminated and tailbiting convolutional codes." *Advanced signal processing for communication systems,* Kluwer international series in engineering and computer science, vol.703, Boston, Sep. 2002.

[60] Isukapalli, Y. and Rao, B. D., "Packet error probability of a transmit beamforming system with imperfect feedback," *IEEE Trans. Sig. Process.,* vol. 58, no. 4, pp. 2298–2314, Apr. 2010.

[61] Yao, Y.-D., Le-Lgoc, T., and Sheikh, U. H., "Block error probabilities in a Nakagami fading channel," in *Proc IEEE Veh. Tech. Conf. (VTC'93)* pp. 130–133, May 1993.

[62] Somehk, O., Simeone, O., Poor, V., and Shamai(Shitz), S., "Cellular systems with non-regenerative relaying and cooperative base station," *IEEE Trans. Wireless Commun.,* vol. 9, no. 8, pp. 2654–2663, Aug. 2010.

[63] Bischl, H., and Lutz, E., "Packet error rate in the non-interleaved Rayleigh channel," *IEEE Trans. Commun.,* vol. 43, no. 2/3/4, pp. 1375–1382, Feb./Mar./Apr. 1995.

[64] Hagenauer, J. and Lutz, E., "Forward error correction coding for fading compensation in mobile satellite channels," *IEEE Trans. Selected Area Commun.,* vol. SAC-5, pp. 215–225, Feb. 1987.

[65] Ju, M., Kim, I. -M., and Kim, D. I., "Joint relay selection and relay ordering for DF-based cooperative relay networks," *IEEE Trans. Commun.*, vol. 60, no. 4, pp. 908–915, Apr. 2012.

[66] Michalopoulos, D. S. and Karagiannisdis, G. K. "Performance Analysis of Single Relay Selection in Rayleigh Fading," *IEEE Trans. Wireless Commun.*, vol. 7, no. 10, pp. 3718–3724, Oct. 2008.

[67] Beres, E. and Adve, R. "Selection Cooperation in multi-source cooperative networks," *IEEE Trans. Wireless Commun.*, vol. 7, no. 1, pp. 118–127, Jan. 2008.

[68] Ren, S., Letaief, K. B., and de Marca, J. R. B., "Outage reduction in cooperative networks with limited feedback," *IEEE Trans. Commun.*, vol. 58, no. 3, pp. 748–752, Mar. 2010.

[69] Ahmed, N. and Aazhang, B. "Throughput gain using rate and power control in cooperative relay networks," *IEEE Trans. Commun.*, vol. 55, no. 4, pp. 656–660, Apr. 2007.

[70] Srinivas, K. V., Giridhar, K., and Koilpillai, R. D., "Orthogonal decode and forward relaying with improved spectral efficiency," *IEEE Commun. Lett.*, vol. 13, no. 2, pp. 109–111, Feb. 2009.

[71] Verdone, R. and Zanella, A., "On the effect of user mobility in mobile radio systems with distributed DCA," *IEEE Trans. Veh Tech.,* vol. 56, no. 2, pp. 874–887, Mar. 2007.

[72] Li, W., Wei, J. -B., and Wang, S., "An evolutionary-dynamic TDMA slot assignment protocol for Ad-hoc networks," in *Proc. IEEE Wireless Commun. Networking Conf.,* pp. 138–142, Mar. 2007.

VITA

Hyungseok Yu received his B.S. and M.S. degrees in electrical engineering from Yonsei University, Seoul, Korea, in 1997 and 1999, respectively. Since 1999, he has been working for Samsung Electronics, Korea, where he was involved on the development of GSM S/W platform. Since August 2007, he has studied toward his Ph.D. degrees in electrical and computer engineering from the Georgia Institute of Technology, Atlanta. His research interests include performance analysis and resource management of cooperative relaying networks.

Performance of Cooperative Relaying Systems with Co-channel Interference

Hyungseok Yu

149 Pages

Directed by Professor Gordon L. Stüber

The cooperative relaying scheme is a promising technique for increasing the capacity and reliability of wireless communication. Even though extensive research has performed in information theoretical aspect, there are still many unresolved practical problems of cooperative relaying system. This dissertation analyzes the performance of cooperative decode-and-forward (DF) relaying systems in the presence of multiple interferers and improve network throughput for these systems. We propose and summarize various systems in the view of network topology, transmission structure, and slot allocation. We present closed-form expressions for the end-to-end outage probability, average symbol-error-probability, average packet-error-probability, and network throughput of the proposed systems. This dissertation shows that the robustness of the destination against interference is more important than robustness of the relay against interference from an interference management perspective, and increasing the number of branches yields better outage and error performance improvements against shadowing than increasing the number of hops. In cellular networks, the cooperative diversity systems can outperform the dual-Rx antenna system, but only when the relay is located in a relatively small portion of the total cell area with respect the the destination mobile terminal. The results also show that since the effective regions of the uplink and the downlink do not overlap, different relays should be utilized for cell sectorization in the uplink and the downlink. Finally, the proposed variable-slot selection DF scheme can reduce the system complexity and make the maximum throughput point in the low and moderate signal-to-interference-plus-noise ratio region.